Dynamic Cell Polarization through Recycling of Cdc42

TINA FREISINGER

DISSERTATION

an der Fakultät für Biologie
der Ludwig-Maximilians-Universität München

Dynamic Cell Polarization through Recycling of Cdc42

TINA FREISINGER

Dissertation

an der Fakultät für Biologie

der Ludwig-Maximilians-Universität München

vorgelegt von

Tina Freisinger

aus München

München, den 12. März 2012

Erstgutachter: Prof. Dr. Stefan Jentsch

Zweitgutachter: Prof. Dr. Angelika Böttger

Tag der mündlichen Prüfung: 14.6.2012

Für meine Eltern & meine Großmutter

Contents

List of Figures

List of Tables

Summary

The ability to polarize is a fundamental property of most eukaryotic cells. For example, essential cellular processes, such as proliferation and migration, require establishment of a single axis. Studies in both unicellular and multicellular organisms have helped to elucidate the underlying principles of how cells break symmetry in the presence and absence of spatial cues. In *Saccharomyces cerevisiae*, cell polarization is initiated through spontaneous clustering of the Rho GTPase Cdc42 at the cellular cortex and subsequent stabilization through feedback loops when spatial cues are missing.

The aim of this dissertation is to determine how polarity establishment is achieved with spatial and temporal precision. Several key findings from a combination of genetic tools, live-cell imaging and mathematical modelling have shown the following.

Dynamic recycling of Cdc42 at the site of polarization relies on two parallel pathways. While one pathway is mediated by the only yeast RhoGDI Rdi1, the other pathway is dependent on actin-mediated transport. Fluorescence recovery after photobleaching (FRAP) experiments showed that the two pathways act on different time scales with the GDI pathway being 4-5 times faster than the actin pathway.

In vitro and *in vivo* assays revealed that the fast GDI-mediated pathway relies on a functional GTPase cycle. Moreover, changes in GTP hydrolysis as well as GDP exchange activity were found to alter Cdc42 dynamics and also challenge singularity of polarization.

Furthermore, fast cable dynamics mediated by the formin Bni1 contribute to a unique polarization site when only the actin-pathway is present.

A detailed mathematical model was able to recapitulate measured parameters of the individual pathways and predict defects associated with changes in Cdc42 activation, recycling and hydrolysis.

These results suggest that Cdc42 recycling relies on two pathways with distinct characteristics. The fast GDI-mediated Cdc42 recycling pathway is not always able to establish polarization but restricts it to a single site; The slower actin-mediated pathway ensures robust cell polarization but sometimes induces multiple polarization sites. Both pathways are coordinated by the GTPase cycle and only the combination of both pathways provides fidelity and robustness of cell polarization.

SUMMARY

While the role of Cdc42 in polarity establishment and maintenance has been extensively studied, details about the timing of Cdc42 and its regulators at the onset of polarity were relatively unknown. These details included the appearance order and behaviour of polarity regulators at the polarization site. While the dynamics of the polarity proteins Cdc42, the GEF Cdc24, the GAP Bem2 and the regulator Bem1 are very similar, comparing polarization kinetics revealed differences in the timing of appearance at the polarization site. Single-cell time-lapse microscopy of polarity regulators showed that formation of the polarization site is a continuous three-step process comprised of cap formation, cap condensation and bud formation. In the absence of Bem2, formation of the polarization site lacks the condensation step. Furthermore, cell cycle regulated GEF activation and GAP inactivation determine timing and speed of Cdc42 polarization.

Together, these findings provide vital evidence for how polarity establishment occurs with spatial and temporal precision.

1 Introduction

In order to differentiate and also to generate shape, cells rely on the ability to establish an internal asymmetry. For example, epithelial cells polarize into an apical and a basolateral surface (Drubin & Nelson 1996; Fig. 1.1 B). Migrating cells, such as fibroblasts, display polarized actin structures, which promote extension of the leading edge and retraction of the rear end of the cell (Chung & Funamoto 2001; Fig. 1.1 B). In a *C. elegans* zygote asymmetric distribution of proteins determines the anterior-posterior axis (Fig. 1.1 C). Not only highly specialized cells of higher eukaryotes require the ability to polarize. Also unicellular organisms, such as *S. cerevisiae*, have to generate asymmetry in order to proliferate (Fig. 1.1 D). Recruitment of the bud site selection module and the polarization machinery to a cortical site adjacent to the previous division site (marked by the bud scar) leads to formation of a new bud.

In all these cases external or internal signals trigger signalling cascades, which result in effector activation and subsequent asymmetric orientation of the actin or microtubule cytoskeleton towards the respective stimuli.

Defects in cell polarization can lead to impaired embryogenesis or development of cancer in adult organisms. Therefore, it has been - and still is - an important task to understand the underlying principles required to establish and maintain cell polarity. Cell polarization has been studied in various different cellular systems and major progress in understanding the individual involved protein complexes and signalling pathways has been made. Yet, it is poorly understood how the individual pathways are coordinated to establish cell polarization. *S. cerevisiae* is an eminently suitable model organism to study cell polarity because of its highly conserved polarity regulators. Moreover, budding yeast has a short lifecycle and is simple to cultivate. In addition, *S. cerevisiae* is easily accessible to genetic manipulation and biochemical assays.

1.1 General principles of pattern formation

Theoretical concepts of how a symmetric structure can turn into an asymmetric one have been subject of extensive research. In 1952, Alan Turing has described a system with an asymmetric distribution pattern that resulted from two components with different diffusion

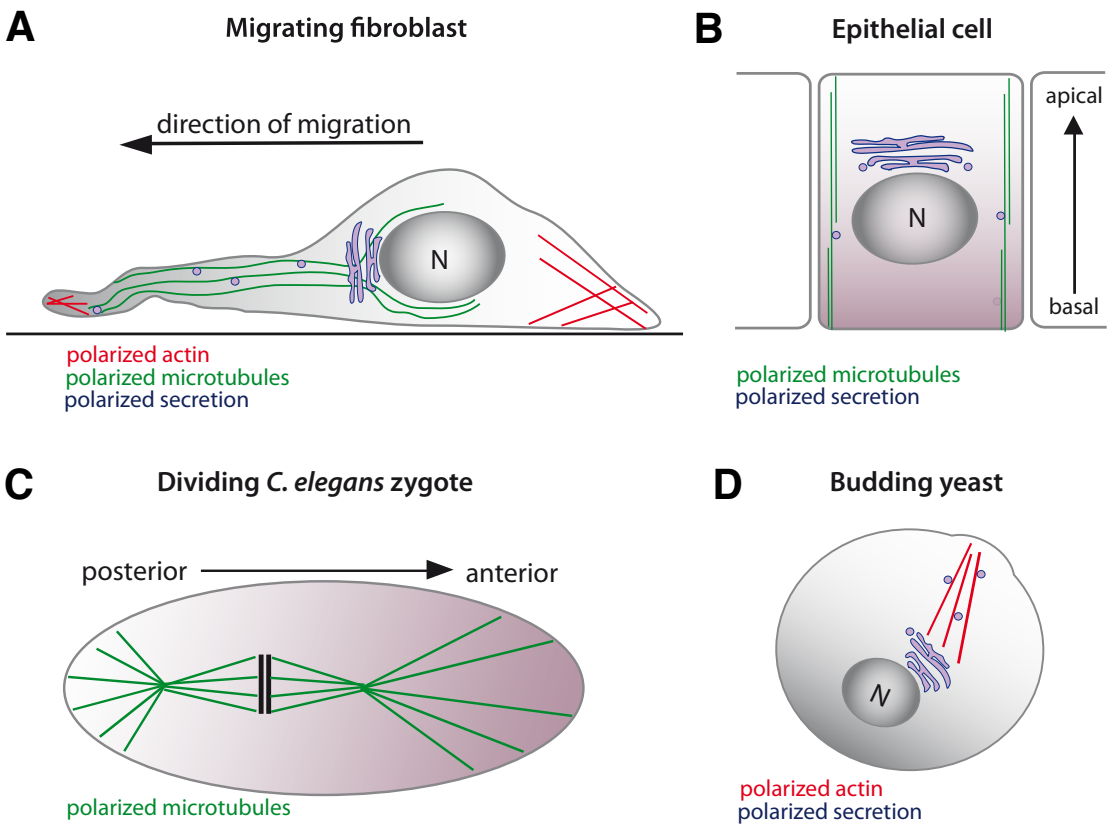

Figure 1.1: Cell polarization in different cell types and organisms. **(A)** Polarized actin structures in the front and rear end of the cell promote migration in fibroblasts. **(B)** Epithelial cells structures require polarized microtubules and secretion. The polarized cell orientation promotes segregation of apical and basolateral proteins (red gradient represents asymmetric protein distribution). **(C)** Polarized microtubules promote cell division and asymmetric protein distribution (red gradient) in a C. *elegans* zygote. **(D)** In budding yeast, formation of a daughter cell requires a polarized actin cytoskeleton and polarized secretion. Parts of the figure were adapted and modified from Etienne-Manneville 2004.

rates (Turing 1952). This theory was extended to explain biological pattern formation relying on a local, slowly diffusing activator and a globally diffusing inhibitor (Meinhardt 1972; Meinhardt 2000).

An asymmetric pattern is the result of internal or external cues, whereby underlying principles are shared between organisms. One example is the ability of cells to build asymmetry in response to an external chemical stimulus. Mating yeast cells grow towards a pheromone gradient released by a mating partner, whereas the slime mold *Dictyostelium* and human neutrophils can move along a chemical gradient to either form a multicellular aggregate or to react to acute inflammation (Parent 2004). When this external stimulus

is uniformly distributed, cells still migrate although in random directions. Other systems that can spontaneously polarize in the absence external stimuli are zygotes of the Algae *Fucus* (Brownlee 1998) or fertilized *Xenopus laevis* eggs (Gerhart et al. 1989).

In *S. cerevisiae* wild-type cells, the polarization site is determined by intrinsic spatial cues - the bud scar and the bud site selection machinery. However, when the genes responsible for bud site selection are missing, bud formation is still initiated although at a random site (Chant 1991).

Major progress has been made in unravelling the underlying molecular mechanisms for spontaneous symmetry breaking. In contrast to traditional models of cell polarization, which follow hierarchical principles, spontaneous cell polarization relies on efficient feedback loops that lead to amplification of stochastic fluctuations. In migrating neutrophils, a feedback loop is established through the polarized accumulation of Phosphatidylinositol-(3,4)-bisphosphate (PIP2) and Phosphatidylinositol-(3,4,5)-triphosphate (PIP3). PIP3 polarization is then stabilized through activation of the small GTPases Rac1, Cdc42 and their downstream targets, which trigger actin polymerization and the Phosphatidyl-3-Kinase (PI3 Kinase). In order to generate an asymmetric distribution, PIP3 needs to be inactivated in other parts of the cell by its global inhibitor PTEN (Meinhardt 2000; Altschuler et al. 2008; Weiner et al. 2002). This example of global inhibition and local activation can explain the spontaneous and also robust polarization in neutrophils but can also be applied on other polarizing systems such as *S. cerevisiae*. Recent studies in yeast suggest that actin-mediated transport plays a major role in establishing and stabilizing positive feedback loops (Wedlich-Soldner et al. 2003). Furthermore, it has been shown that this mechanism is sufficient to break symmetry in G1 arrested cells expressing a constitutively active Cdc42 mutant (Wedlich-Soldner et al. 2003).

1.2 Spatial regulation

Cell polarization results from highly conserved signalling mechanisms triggered by internal or external spatial cues. In neutrophils and *Dictyostelium*, exposure to a chemoattractant triggers signalling through G protein-coupled receptors at the cell membrane. Activated G proteins interact with downstream effectors such as small GTPases or phospholipid kinases and subsequent rearrangement of the cytoskeleton towards sites of po-

larized growth (Chung & Funamoto 2001; Firtel & Meili 2000). Mating yeast cells react to a chemical signal through receptor accumulation at the shmoo tip and activation of the small GTPases Cdc42 and Rac (Arkowitz 1999). During vegetative growth, cell polar-

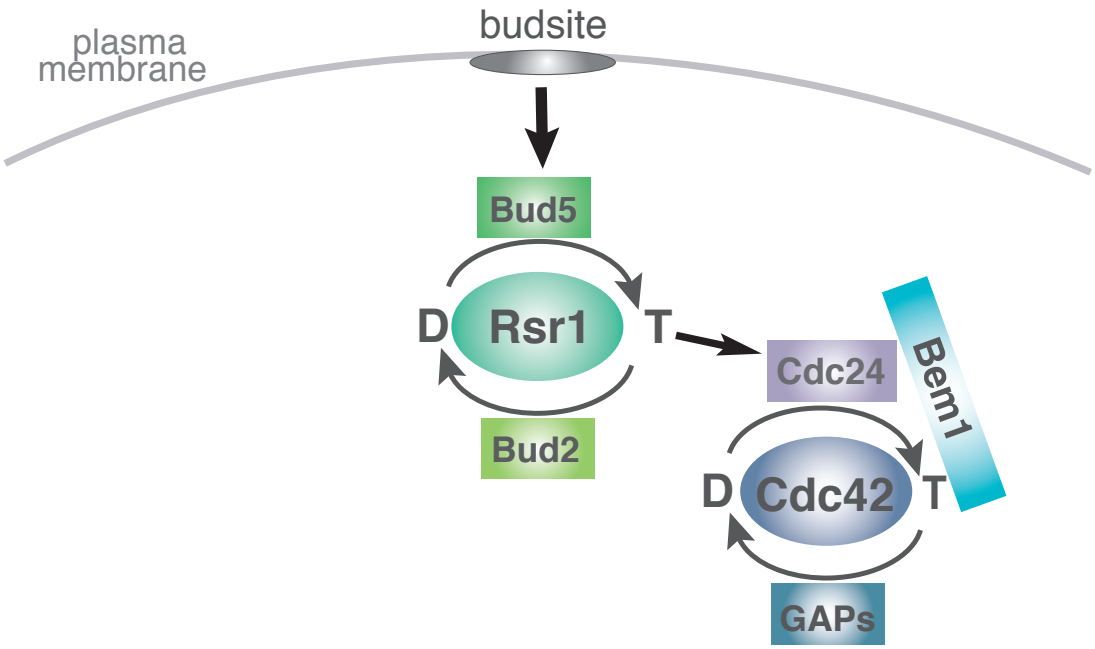

Figure 1.2: Connection of bud site selection and cell polarization machinery. Landmark proteins recruit the Rsr1 machinery through interactions with the Rsr1-GEF Bud5 to the polarization site. Rsr1 bound to GTP has been implicated to interact with polarity regulators Cdc24, Bem1 and Cdc42.

ization in *S. cerevisiae* follows a distinct budding pattern. In haploid cells the new bud grows adjacent to the bud scar, which marks the previous devision site (axial budding pattern), whereas in diploid cells budding is initiated either adjacent or opposite of the bud scar (bipolar budding), depending on their genetic heritage (Chant 1991; Chant 1995). Cortical bipolar or axial landmark proteins recruit the bud site selection module to the respective polarization site. Furthermore, the landmark proteins have been implied to regulate the Rsr1 (Ras-related protein) GTPase module through its Guanine exchange factor (GEF) Bud5 and GTPase-activating protein (GAP) Bud2 (Kang et al. 2001; Fig. 1.1). Genetic studies revealed knockout of *RSR1, BUD5 or BUD2* lead to randomized polarization patterns, indicating that these proteins are required for bud site selection but are not essential for budding *per se* (Bender 1993; Chant 1991; Chant 1995; Park et al. 1993). The

Rsr1 GTPase signalling module is coupled to the polarization machinery through genetic and physical interactions between Rsr1 and Cdc24, Cdc42 and Bem1 (reviewed in Park & Bi 2007; Fig. 1.2). Rsr1 recruits Cdc24 to the site of polarization, inducing a conformational change that is thought to activate Cdc24 (Shimada & Gulli 2000).

1.3 Temporal control - the role of the cell cycle

In *S. cerevisiae* it is crucial that budding is initiated at the right time and only once per cell cycle. Therefore, cell polarization is dependent on cell cycle signals triggered by the

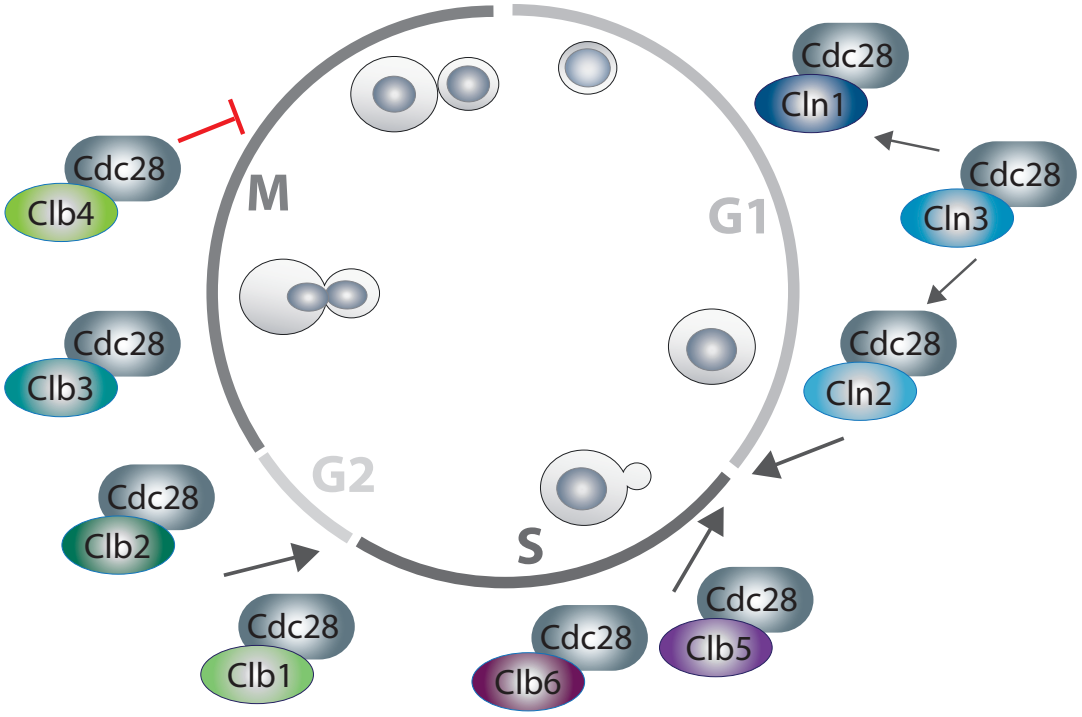

Figure 1.3: Cyclin/CDK complexes regulate the yeast cell cycle. The G1 cyclins (Cln1, Cln2 and Cln3) regulate events in the G1 phase and at the G1/S transition. The S phase cyclins Clb5 and Clb6 promote DNA replication, whereas the mitotic cyclins (Clb1, Clb2, Clb3 and Clb4) initiate processes in Mitosis. B-type cyclins prevent exit from mitosis.

cyclin-dependent kinase1 (CDK1) Cdc28 and its cyclin partners (reviewed in Enserink & Kolodner 2010). In yeast, three G1 (Cln1, Cln2, Cln3) and six B-type cyclins (Clb1-6) have been identified (Fig. 1.3). Although only one G1 cyclin is sufficient for viability, they all have slightly different functions. While Cln3 controls Cln1 and Cln2 transcription, Cln1/Cdc28

and Cln2/Cdc28 are important for spindle body duplication and initiation of bud formation (Fig. 1.3). The B-type cyclins Clb5 and Clb6 in complex with Cdc28 are required for S phase initiation, whereas Clb3 and Clb4 are expressed from S phase until anaphase to regulate DNA replication, spindle assembly and G2/M transition (Fig. 1.3). Clb1/Cdc28 and Clb2/Cdc28 are involved in the regulation of mitotic events but also control processes required for bud morphogenesis such as the switch from polar to isotropic growth. Clb1-4 prevent exit from mitosis (Fig. 1.3) and in order to complete the cell cycle, their activity has to be downregulated (Bloom & Cross 2007).

Bud initiation and formation are tightly coordinated with the cell cycle. In late G1 activation of Cdc28 by Cln1 or Cln2 controls actin orientation to the polarization site, whereas activation of the B-type cyclins Clb1and Clb2 in G2 phase leads to a change from apical to isotropic growth and subsequent depolarization (Lew 1993). Furthermore, regulation of the GEF Cdc24 through cell cycle signals appears to play an important role for polarity establishment. Cdc24 is sequestered in the nucleus by binding to Far1 in late M and early G1 phase. Activation of Cdc28 by Cln2 at the G1/S transition triggers degradation of Far1 and Cdc24 is relocated to the polarization site (Shimada & Gulli 2000). Binding of Rsr1 and Bem1 to the pleckstrin homology domain (PH) and PB1 domain of Cdc24 have been suggested to release Cdc24 from its autoinhibitory state leading to its activation (Shimada et al. 2004). However, whether Rsr1 or Bem1 directly activate Cdc24 has not been tested. Although Cdc28 activity is suggested to be required for localization of Cdc24 to the incipient bud site (Gulli et al. 2000; Shimada & Gulli 2000; Moffat & Andrews 2004) and Cdc24 phosphorylation by Cdc28 has been confirmed *in vitro* (McCusker et al. 2007), mutation of predicted CDK1 phosphorylation sites did not affect its function *in vivo* (Gulli et al. 2000; Wai & Gerber 2009).

Furthermore, Cdc24 is phosphorylated by the p21-activated kinase (PAK) Cla4, which is a downstream effector of Cdc42. Studies on the function of Cdc24 phosphorylation by Cla4 have lead to controversial results. On the one hand, it has been proposed that Cdc24 phosphorylation by Cla4 disrupts Cdc24 binding to Bem1 (Gulli et al. 2000), on the other hand, no change in Cdc24-Bem1 interaction has been found (Bose et al. 2001). Regulation of Cdc24 activity might play an important role in restricting polarization to a single polarization site. Studies on Cdc42 mutants that can bypass Cdc24 activity, suggest

that Cdc24 is important for the timing of the budding event (Caviston et al. 2002; Richman & Johnson 2000).

Not only the Cdc42 GEF is an attractive target for CDK1 phosphorylation but also Cdc42 GAPs have been shown to be CDK1 substrates. Cdc28 phosphorylates Rga2 both *in vitro* and *in vivo* (McCusker et al. 2007; Sopko et al. 2007; X. Zheng et al. 2007) and the lack of phosphorylation leads to impaired Rga2 localization and defects in polarized growth (Sopko et al. 2007). Furthermore, Bem2 and Bem3 have been shown to become hyperphosphorylated and inactivated at bud emergence in a Cdc28-dependent manner, suggesting that they help to restrict Cdc42 activity to bud emergence (Knaus et al. 2007). Bem1 might be a further potential candidate for linking cell polarization to the cell cycle. Bem1 was found to be phosphorylated by Cdc28 *in vitro* (Ubersax et al. 2003) and *in vivo* (Han et al. 2005). While *in vivo* analysis of Bem1 phosphorylation mutants revealed impaired vacuole biogenesis, no obvious defects in bud emergence have been observed so far (Han et al. 2005).

1.4 Polarity regulators

Establishment of cell polarization requires a set of proteins that is recruited to the cell cortex at the G1/S transition of the cell cycle in order to rearrange the cytoskeleton towards the site of polarized growth.

Cdc42, a member of the Rho GTPase family, was found to be a key player in orchestrating cell polarization in many eukaryotic cells (Johnson, 1999). In 1971 Hartwell carried out a genetic screen in *S. cerevisiae*, resulting in the isolation of mutants that arrested as unbudded cells (Hartwell 1971). One of the identified mutants was *cdc24ts*, which later led to the discovery of Cdc42 (Adams et al, 1990). Both proteins were implied to play a role in polarization since cells with inactive Cdc24 or Cdc42 arrested as unbudded cells with multiple nuclei and an unpolarized actin cytoskeleton (Adams et al. 1990; Johnson & Pringle 1990). Cdc42 is highly conserved from yeast to mammals (Fig. 1.4) and strikingly, expression of the human Cdc42 can rescue Cdc42 function in *S. cerevisiae* (Munemitsu et al. 1990).

Cdc42 coordinates many cellular processes that require polarization such as cell motility, morphology and proliferation (Etienne-Manneville & Hall 2002). In yeast, Cdc42 is involved

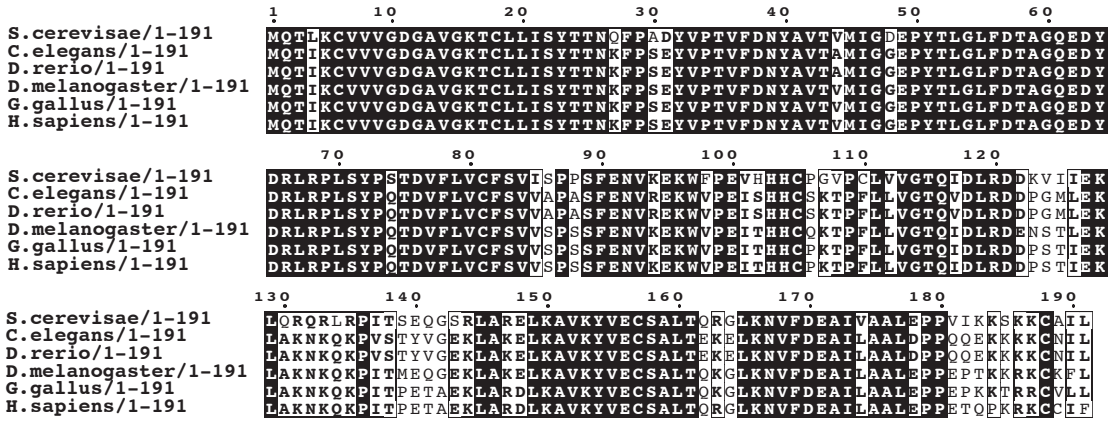

Figure 1.4: Alignment of Cdc42 in different organisms. Alignment of Cdc42 proteins of *S. cerevisiae* (AAB67416.1), *C. elegans* (AAC05600.1), *D. rerio* (NP_956926.1), *D. melanogaster* (AAF49007.1), *G. gallus* (AAC00027.1) and *H. sapiens* (AAM21109.1). Highly conserved regions are highlighted in black. Alignment was done with ClustalW Software (http://www.ebi.ac.uk/Tools/msa/clustalw2/).

in the budding process but is also required for mating and pseudohyphal growth (Johnson, 1999). Effectors containing a Cdc42/Rac-interactive binding (CRIB) domain bind to the switch I domain, which is located at the N-terminus of the Cdc42 protein (Fig. 1.5). The switch II domain and Rho insert domain, which is unique to Rho-GTPases, are also implied in effector binding (Fig. 1.5). At the C-terminus of the Cdc42 protein reside the PB (polybasic region) followed by the CAAX box where postranslational modifications such as isoprenylation facilitate the binding to membranes (reviewed in (Park & Bi 2007; Fig. 1.5).

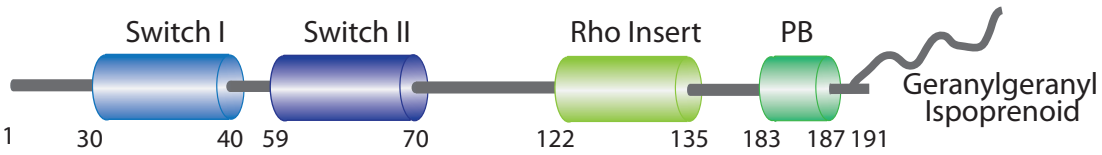

Figure 1.5: Cdc42 protein domains. The Cdc42 protein contains a Switch I domain, Switch II domain, Rho Insert domain, Polybasic (PB) region and CAAX box (AA 188-191), which is modified by isoprenylation (wavy line). Numbers indicate amino acid positions. Figure was adapted and modified from Park & Bi 2007.

At the G1/S transition of the cell cycle, Cdc42 localizes to the polarization site and later to the tip of small buds. When the new bud switches from apical to isotropic growth, Cdc42 redistributes from its cortical location to the cytoplasm, before it localizes to the septin ring in late anaphase (Lew 1993; Fig. 1.6).

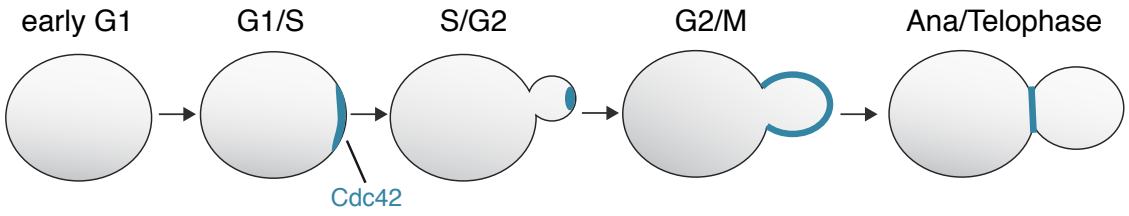

Figure 1.6: Cdc42 localization throughout the cell cycle. Cdc42 localizes to the cellular cortex in a wide cap at the G1/S transition. At the transition from S phase to G2, Cdc42 localizes to the tip of small buds. At the switch from apical to isotropic growth, Cdc42 localization distributes along the bud cortex before it relocalizes to the bud neck in late Anaphase. Figure was adapted and modified from Park & Bi 2007.

Like all Rho GTPases, Cdc42 cycles between an inactive GDP-bound and an active GTP-bound state (Section 1.6.5). GDP/GTP exchange is catalyzed by the GEF Cdc24 (Zheng & Cerione 1994; Section 1.6.5), whereas GTP hydrolysis is mediated by four GAPs Rga1, Rga2, Bem2 and Bem3 (Stevenson et al. 1995; Smith et al. 2002; Marquitz et al. 2002; Zheng & Cerione 1994; Section 1.6.5). Active Cdc42-GTP can bind and activate downstream effectors (Section 1.5). Furthermore, the multi-domain protein Bem1 has been implied as an important Cdc42 regulator because of its ability to promote complex formation of Cdc42-GTP, Cdc24 and the PAK kinase Cla4 at the polarization site (Bose et al. 2001; Gulli et al. 2000; Peterson et al. 1994; Zheng & Cerione 1994; Section 1.6.2). Rdi1, the only RhoGDI described in yeast (Masuda et al. 1994), has been shown to extract Cdc42 from internal membranes (Eitzen et al. 2001) and the plasma membrane (PM) (Richman et al. 2004; Tcheperegine et al. 2005; Section 1.6.4).

1.5 Cdc42 signalling - Effectors

The binding of Cdc42 to downstream effectors results in the activation of various cellular events, such as the rearrangement of the cytoskeleton and cell growth (Bokoch 2003). In *S. cerevisiae* three classes of effectors have been identified. The formin Bni1, which is part of the polarisome, the PAKs Ste20, Cla4 and Skm1 and the yeast specific proteins Gic1 and Gic2 (Park & Bi 2007). Rearrangement of the cytoskeleton relies on two different actin nucleators, the Arp2/3 complex and the formins. Arp2/3 is regulated by the Wiscott-Aldrich Syndrome protein (WASp) homolog, Bee1 and the type I myosins. The

formins Bni1 and Bnr1 are required for actin cable formation in *S. cerevisiae* (Evangelista et al, 2002; Sagot et al. 2001). Cla4, Ste20 and Skm1 belong to the family of p21-activated kinases (PAKs). PAKs are important signalling proteins that regulate a wide range of cellular functions, such as regulating polarization events, cytoskeletal dynamics and MAP kinase pathways, not only in yeast but many other organisms (Bokoch 2003). Cdc42-GTP interacts with PAKs via the CRIB domain, which releases PAKs from their autoinhibited state (Zenke et al. 1999). Skm1 is thought to be involved in the down regulation of sterol-uptake (Lin et al. 2009), whereas Ste20 and Cla4 play a role in actin organization during bud formation. Moreover, Ste20 is involved in activating MAPK pathways during mating (Eby et al. 1998; Holly 1999) and Cla4 appears to play a role during polarity establishment. Cla4 has been shown to form a complex with the polarity regulators Bem1, Cdc24 and Cdc42-GTP, although its function in this complex has been under debate (Gulli et al. 2000; Bose et al. 2001). Furthermore, the redundant CRIB domain containing proteins Gic1 and Gic2 have been identified to act as Cdc42 effectors. While their molecular function remains elusive, genetic analysis implies that these proteins are involved in regulating cell polarization processes (Brown et al. 1997; Chen & Kim 1997).

1.6 Establishment of cell polarization

Wild-type yeast cells establish cell polarity in response to internal or external spatial cues such as the bud scar or a pheromone gradient. Yet, in the absence of directional cues, cells are still able to polarize without displaying any defects in polarity establishment, maintenance or cell morphology. However, their budding pattern appears to be randomized (Chant 1995). In the absence of any spatial cues, active Cdc42 has been suggested to cluster spontaneously and transiently at the site of polarized growth, where it becomes stabilized through effector interactions and two independent positive feedback loops (Butty et al. 2002; Irazoqui et al. 2003; Wedlich-Soldner et al. 2003; Wedlich-Soldner et al. 2004) . While one feedback loop relies on complex formation mediated by Bem1 (Irazoqui et al. 2003), a second feedback loop depends on actin-mediated vesicle transport (Wedlich-Soldner et al. 2003). Furthermore, two mechanisms have been implicated in Cdc42 recycling for polarity maintenance (Slaughter et al. 2009). In the following subsections the pathways involved in polarity establishment will be introduced

in close detail.

1.6.1 The role of the actin cytoskeleton

The cytoskeleton not only maintains cell polarity and morphology but also enables cellular movement, force transmission and growth. Actin and microtubules are major components of the eukaryotic cytoskeleton. In order to carry out their cellular functions, they assemble from monomers to filaments and more complex structures. While in higher eukaryotes both actin and microtubules are important for polarity establishment and maintenance only actin is required for polarity in *S. cerevisiae* (Jacobs et al. 1988).
Three different actin structures fulfill a variety of functions in yeast. Actin patches mark sites of endocytosis, actin cables are required for vesicle transport and actin rings help to constrict the mother/bud neck (reviewed in Moseley 2006). Actin patches consist of short-branched filaments that are nucleated by the Arp2/3 complex (Rodal et al. 2005; Pollard 2003), whereas actin cables function as intracellular transport tracks to promote Myo2-dependent vesicle transport (Bretscher 2003). Actin cables are nucleated by the two budding yeast formins Bnr1 and Bni1 (Evangelista et al. 2002; Sagot & Klee 2001). We have recently shown that actin cable dynamics change during cell polarization. In unpolarized cells, fast polymerization of actin cables is mediated by Bni1, whereas slower polymerization is regulated by both formins Bnr1 and Bni1 in polarized cells (Yu et al. 2011). The actin ring is formed during anaphase and constricts the bud from the mother cell with the help of Myo1 to promote cytokinesis (Bi et al. 1998; Lippincott 1998). Furthermore, actin has been suggested to play an important role in generating a positive feedback loop required for polarity establishment (Wedlich-Soldner et al. 2003; Wedlich-Soldner et al. 2004; Section 1.6.3).

1.6.2 The role of Bem1

It has been suggested that Bem1 forms a complex with Cdc42-GTP, Cdc24 and Cla4 (Bose et al. 2001; Gulli et al. 2000; Peterson et al. 1994; Zheng & Cerione 1994), thereby promoting accumulation of active Cdc42 at the polarization site (Gulli et al, 2000, Bose et al, 2001, Butty et al, 2002). This Bem1-mediated feedback loop is able to break sym-

metry even in the absence of spatial cues and actin. While cells lacking Bem1 are still viable, these cells appear to be temperature-sensitive (Bender 1993). Although Bem1 has been implicated to act as a scaffold protein for the other complex members, it displays rather fast protein dynamics, suggesting that it is comprised of highly dynamic molecules (Wedlich-Soldner et al. 2004).

1.6.3 The role of feedback loops

Feedback loops have been implicated in the fundamental process of pattern formation (Section 1.1). During the last decade, the role of feedback loops in establishing and maintaining cell polarity in yeast has been subject of extensive research. Bem1 has been proposed to mediate complex formation between the PAK Cla4, Cdc24 and Cdc42-GTP, initiating a positive feedback loop by increasing the local concentration of active Cdc42 at the polarization site (Gulli et al, 2000; Bose et al, 2001; Butty et al, 2002; Fig. 1.7).

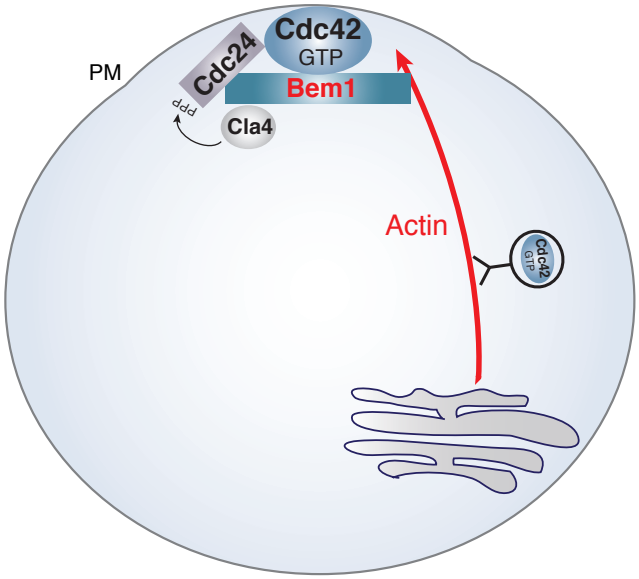

Figure 1.7: Polarity establishment requires Bem1- and actin-mediated positive feedback loops Cdc42 has been suggested to become stabilized through complex formation with Bem1, Cdc24 and Cla4. Actin-dependent vesicle transport leads to a further accumulation of Cdc42 at the polarization site. PM:Plasma membrane.

Whether subsequent Cdc24 phosphorylation by Cla4 leads to disruption of the Cdc24-Bem1 binding and hence termination of polarized growth, remains under debate (Gulli

et al, 2000; Bose et al, 2001). Furthermore, it has been suggested that Bem1 promotes symmetry breaking by physically linking the GEF and PAK. A GEF-PAK chimera was able to rescue an otherwise lethal *rsr1*Δ *bem1*Δ double mutant (Kozubowski et al, 2008).
Actin-dependent transport has been implicated in a second positive feedback loop for symmetry breaking. While actin cable nucleation requires activated Cdc42-GTP, accumulation and stabilization of activated Cdc42 at the polarization site in turn also relies on actin-dependent vesicle transport and endocytosis (Wedlich-Soldner et al. 2003; Marco et al. 2007; Fig. 1.6). This actin-mediated feedback loop was able to break symmetry in G1 arrested cells expressing a constitutively active $Cdc42^{Q61L}$ mutant (Butty et al. 2002; Wedlich-Soldner et al. 2003). Further studies revealed that *bem1*Δ cells treated with the actin-depolymerizing drug Latrunculin A (LatA), completely failed to polarize, suggesting that coupling of a Bem1- and a actin-mediated feedback loop is required to establish cell polarity (Wedlich-Soldner et al. 2004).

1.6.4 The role of the GDI

RhoGDIs were originally described as rather passive inhibitors of distinct Rho protein functions such as inhibiting the dissociation of GDP from Rho GTPases (Chuang et al. 1993; Leonard et al. 1992) and inhibiting the intrinsic GTPase activity (Hart et al. 1992). After the crystal structure of RhoGDI in complex with Cdc42 had been solved (Hoffman et al. 2000), the idea of GDIs as passive inhibitors had to be adjusted. RhoGDI has been shown to actively extract Rho GTPases from membranes and to retain them in an inactive state in the cytosol (Bustelo & Sauzeau 2007; DerMardirossian & Bokoch 2005; Cole et al. 2009; Johnson et al. 2009). A two-step mechanism for Cdc42 extraction by the RhoGDI has been suggested. First, the N-terminus of the RhoGDI interacts with the switch I and II domains of Cdc42, and second, the geranylgeranyl moiety of the Cdc42 is inserted into the geranylgeranyl binding pocket of the RhoGDI. This interaction is thought to be facilitated by interactions between the polylysine region at the C-terminus of Cdc42 and the acidic patch in the geranylgeranyl binding pocket (Hoffman et al. 2000). A single point mutation (R66E) in the switch II region is sufficient to abolish binding between Cdc42 and RhoGDI (Gibson & Wilson-Delfosse 2001; Fig. 1.8).
Although, the RhoGDI crystal structure revealed no preference for either the GDP- or GTP-

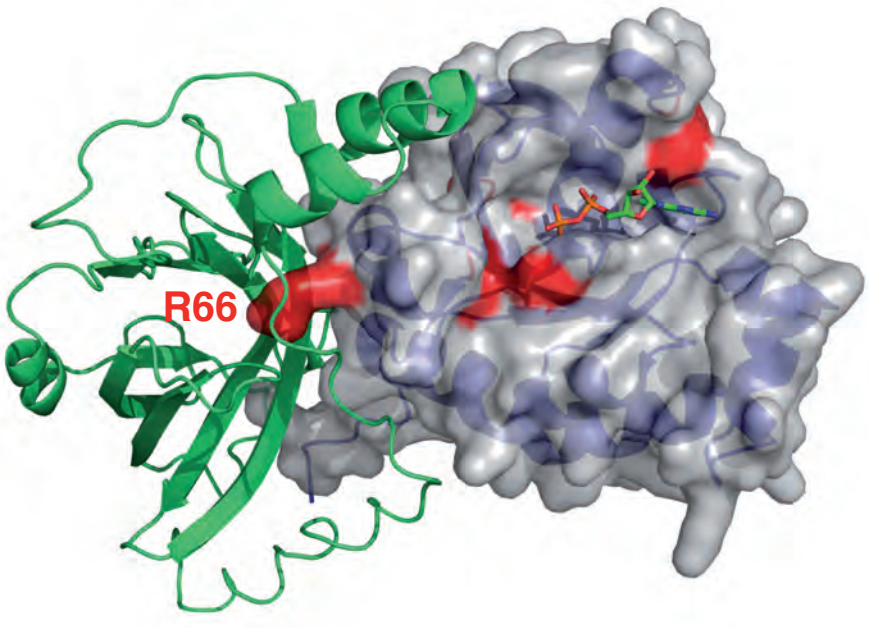

Figure 1.8: Cdc42 GDI structure. 3D structure of Cdc42 (surface structure (grey) overlay with ribbon structure(blue)) in complex with GDI (green). Red region is the mutated R66 residue, which abolishes Cdc42 binding to GDI. Crystal structure of Cdc42 complex with its GDI was solved by Hoffman et al. (Hoffman et al. 2000), PDB accession code 1DOA. The figure was generated with PyMOL software (DeLano W.L. (2008), the PyMOL Molecular Graphics system; DeLano Scientific LLC. Palo Alto, CA, USA.

bound form (Hancock & Hall 1993; Nomanbhoy et al. 1999), controversial observations have been reported. On the one hand, Rho-GTP has been extracted after GDI overexpression (Tiedje et al. 2008), on the other hand, the affinity of the RhoGDI to Cdc42-GDP was found to be 10 fold higher compared to the GTP-bound form (Johnson et al. 2009). The mechanism which leads to dissociation of the RhoGDI-Rho GTPase complex is still unclear. It has been suggested, that lipids change the GDI conformation, thereby facilitating GTPase-activation by a GEF (Faure & Dagher 2001; Robbe et al. 2003). Furthermore, phosphorylation may promote Rho GTPase release from the GDI. In general, while phosphorylation of Rho GTPases increases their affinity for GDIs, phosphorylation of the GDI has the opposite effect (Garcia-Mata et al. 2011). Although GEFs seem obvious candidates to help dissolve the GDI-GTPase complex, little evidence for this hypothesis has been provided so far. Insights on a possible mechanism how GEFs might act on the GDI-GTPase interaction come from studies on a pathogenic protein DrrA, which displays GDF

(GDI displacement factor) and GEF activity towards Rab1 (Murata et al. 2006; Machner 2006; Ingmundson et al. 2007; Wu et al. 2010). Solving the crystal structure of the DrrA-GEF domain in complex with Rab1 and analyses of the kinetic and thermodynamic properties revealed that GDI displacement by DrrA is directly linked to GEF- rather than GDF activity (Schoebel et al. 2009). Rdi1, the only known RhoGDI in yeast (Masuda et al. 1994), has been shown to extract Cdc42 from vacuolar (Eitzen et al. 2001) and internal membranes as well as from the plasma membrane (Richman et al. 2004; Tcheperegine et al. 2005; Tiedje et al. 2008). Controversial results have been reported concerning *RDI1* overexpression. While one group found cells overexpressing *RDI1* to be lethal (Masuda et al. 1994) , a different group merely observed a rounder cell morphology (Tcheperegine et al. 2005). The different phenotypes could be explained by dose-dependent expression of *RDI1* (Tiedje et al. 2008). So far, no obvious phenotype for *rdi1*Δ has been reported, although deletion of *RDI1* lead to suppression of mitotic exit defects in *lte1*Δ cells (Tiedje et al. 2008). Furthermore, Rdi1 has been implicated to play an essential role in the actin-independent recycling during polarity maintenance (Slaughter et al. 2009).

1.6.5 The role of the GTPase cycle

The ability to cycle between an inactive GDP- and an active GTP-bound state is a central feature of all GTPases. Since the affinity of small G proteins for GDP/GTP molecules is high the dissociation rate of nucleotides is very low, hence exchange of GTP for GDP requires GEFs to accelerate the process (Vetter 2001; Bos et al. 2007). In *S. cerevisiae*, only one GEF - Cdc24 is known, which is also essential for viability (Zheng & Cerione 1994). Furthermore, the GTP/GDP exchange step requires proteins that accelerate the hydrolysis reaction (Bos et al. 2007). Several mutations (G12V, Q61L, D118A) (Fig. 1.9) in the putative GTP binding and hydrolysis domains of Cdc42 lead to dominant dosage-dependent lethality, suggesting that GTP hydrolysis is essential for its normal function (Ziman et al. 1991) The hydrolysis reaction is mediated by the four potential GAPs Bem2, Bem3, Rga1 and Rga2 (Stevenson et al. 1995; Smith et al. 2002; Marquitz et al. 2002; Zheng & Cerione 1994). Interestingly, a triple knockout mutant bearing deletions of Rga1, Rga2 and Bem3 is still viable, merely displaying elongated buds, which is consistent with an implied higher activity of Cdc42. *bem2*Δ mutants display Cdc42 activation to multiple sites, suggesting that Bem2 func-

tion is required to restrict Cdc42 activation to a single site (Knaus et al. 2007). Cdc42 mutants bearing a single nucleotide exchange at residue 60 (G60A and G60D; Fig. 1.9) in the putative binding and hydrolysis domain rendered Cdc42 hyperactive, which also lead to polarization at multiple sites in a *CDC42* deletion mutant background (Caviston et al. 2002).

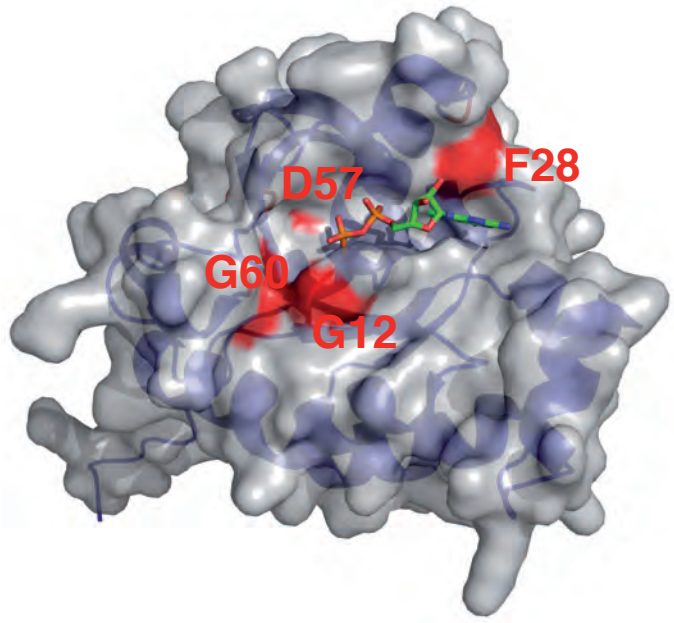

Figure 1.9: Cdc42 structure. 3D structure of Cdc42 (ribbon: blue; with surface model: grey) with mutated amino acid residues highlighted in red. GDP is shown as stick model. Crystal structure of Cdc42 complex with its GDI was solved by Hoffman et al. (Hoffman et al. 2000). The figure was generated with PyMOL software (DeLano W.L. (2008), the PyMOL Molecular Graphics system; DeLano Scientific LLC. Palo Alto, CA, USA.

While mutants bearing the amino acid exchange at residue 61 appeared to be locked in the GTP-bound state, mutants at residue 60 were still able to cycle with decreased GTP/GDP exchange. FRAP experiments of the inactive $Cdc42^{D57Y}$ and the constitutively active $Cdc42^{Q61L}$ mutant revealed much slower recovery half-times than wild-type Cdc42 (Wedlich-Soldner et al. 2004). These results suggest that the ability of Cdc42 to cycle between the active and inactive state plays an important role in the high exchange rate of Cdc42 between the polarization site and the cytosol. These findings are supported by the reduced complex formation of $Cdc42^{D57Y}$ and $Cdc42^{Q61L}$ with Rdi1 *in vivo* (Slaugh-

ter et al. 2009). Furthermore, the interaction between $Cdc42^{Q61L}$ and Cdc42 effectors is stabilized and hence the constitutively mutant is protected from endocytosis (Slaughter et al. 2009). This suggests that the GTPase cycle controls both Cdc42 recycling pathways by assisting complex formation with Rdi1 and releasing Cdc42 from its effectors thereby promoting endocytosis.

A recent computational model predicted that proteins controlling GTPase cycling have to be tightly regulated in order to simultaneously maintain high activity of Cdc42 and fast turnover (Goryachev & Pokhilko 2006). In fact, a mutation in the highly conserved residue Phe28 of Ras related proteins, was shown to increase the GDP association state and activate the protein *in vivo* (Reinstein et al. 1991; Fig. 1.9). The same mutation in the human Cdc42H protein leads to accelerated GDP/GTP exchange rate. Remarkably, expression of this mutated Cdc42 in fibroblasts led to giant, multinucleate cells, a phenotype similar to the expression of the oncogenic Dbl (Lin et al. 1997).

1.7 Uniqueness of polarization

It is crucial that cell polarization occurs only once per cell cycle. When Cdc42 is no longer under the control of Cdc28/G1 CDK-cyclin complex, such as in an overexpressed constitutive mutant of Cdc42 ($Cdc42^{Q61L}$, $Cdc42^{G12V}$) in combination with the absence of all G1 cyclins, polarization can still be initiated at multiple sites (Gulli et al. 2000; Wedlich-Soldner et al. 2003). The importance of the cell cycle in singularity of polarization is also supported by the fact that the Cdc42 GAPs are highly cell cycle regulated. Bem2 and Bem3 have been shown to function as global inhibitors of Cdc42 activation during the G1 phase and their subsequent inactivation by Cdc28/Cln-mediated hyperphosphorylation leads to site-specific activation of Cdc42 at bud emergence (Knaus et al. 2007). In line with these results, it has been shown that slow hydrolyzing Cdc42 mutants bearing point mutations at residue 60 displayed polarization at multiple cortical sites (Caviston et al. 2002). Studies on artificially rewired cells and mathematical modelling suggest that fast competition between polarization clusters is required to restrict polarization to a single site (Howell et al. 2009; Goryachev & Pokhilko 2008). Also, the amount of activated Cdc42 and the activity of Cdc42 itself may play an important role in ensuring a single polarization site. Expression of an increased concentration of constitutively active $Cdc42^{Q61L}$ at the

plasma membrane led to an increased number of cells initiating polarization at two or more polarization sites (Wedlich-Soldner et al. 2003).

1.8 The role of mathematical modelling

While theoretical approaches have been very valuable in understanding symmetry breaking for decades (Turing 1952; Meinhardt 1972; Meinhardt 2000; Section 1.1), recently, mathematical models have helped to advance the understanding of underlying general principles of cell polarization in various organisms and cell types in the presence and absence of spatial cues (reviewed in Jilkine 2011 and Onsum & Rao 2009). Very few mathematical models are developed in a bottom-up approach, whereby predictions are made from known biochemical reactions (Goryachev & Pokhilko 2008). Most simulations generate predictions in a top-down approach that in turn could be experimentally tested, or often, both approaches are combined (Onsum & Rao 2009). Budding yeast has been an attractive model to understand the underlying principles of spontaneous cell polarization not only in experiments, but also to employ theoretical approaches. In a series of top-down modelling studies, various attempts were made to understand the involvement of actin-dependent feedback loops in symmetry breaking. While Wedlich-Söldner et al in 2003 suggested an actin-dependent positive feedback loop, which amplified and stabilized initial stochastic fluctuations of the polarity regulator Cdc42 (Wedlich-Soldner et al. 2003), a negative-actin-dependent feedback loop was considered to remove Cdc42 from the membrane in the absence of the Rsr1 landmark protein (Ozbudak et al. 2005). In 2008 Goryachev & Pokhilko developed a bottom-up model to explain yeast cell polarization (Goryachev & Pokhilko 2008). The authors suggested a turing-like mechanism to explain why the cell only polarizes once per cell cycle (Goryachev & Pokhilko 2008). This model was then extended to explain experimental observations of two competing clusters in artificially rewired cells that sometimes grow two buds (Howell et al. 2009). A simple stochastic model developed by Altschuler et al. in 2008 suggested that one positive feedback alone is sufficient to establish cell polarization and that polarization frequency depends on low expression of Cdc42 (Altschuler et al. 2008). Although an actin-dependent positive feedback loop was implied in various theoretical studies, Layton et al were the first to consider vesicle membranes in their simulations (Layton et al.

2011).

2 Results

2.1 Cdc42 copy number does not influence polarization behaviour and protein dynamics

The focus of our study lies on understanding events during polarity establishment, which take place at the G1/S transition of the cell cycle. Hence, an enrichment for cells in the respective cell cycle stage is desirable. To that end, we used an *S. cerevisiae* strain that could be synchronized in a cell cycle dependent manner. The strain bears deletions

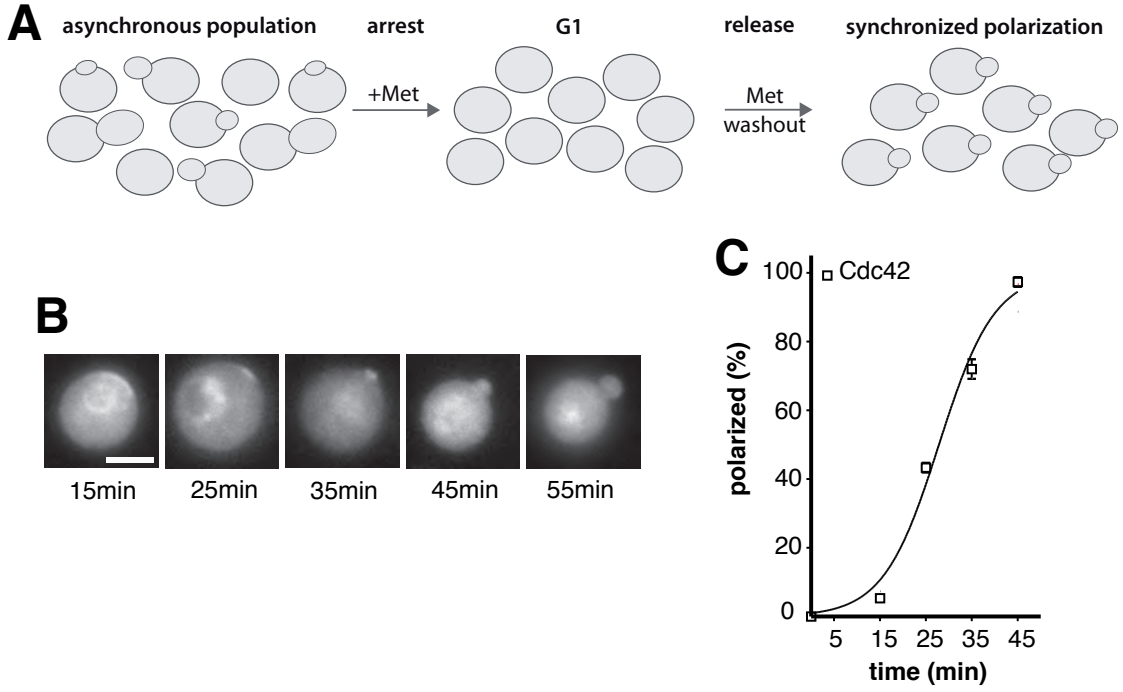

Figure 2.1: Assay for determining polarization kinetics. (A) Schematic depiction of the polarization assay. Yeast cells can be arrested in G1 by methionine (Met) addition to the growth medium. Subsequent methionine washout releases cells from G1 in a synchronized manner **(B)** Visualization of GFP-tagged Cdc42 during polarity establishment and bud development. Scale bars: 4 µm. **(C)** Polarization kinetics of ectopically expressed GFP-Cdc42 (2x42). Data for each time point (mean ± SD) are based on the analysis of three individual experiments with 50 cells each.

of *CLN1*, *CLN2*, and *CLN3*. *CLN2* is expressed under the control of a repressible Met3 promoter (Amon et al. 1994), which allows to arrest cells in the G1 phase of the cell cycle by adding methionine to the growth medium, resulting in repression of *CLN2* expression. Subsequent methionine washout releases cells from G1 arrest in a synchronized manner

(Fig. 2.1 A).

In this study, all experiments were carried out with an ectopically expressed, N-terminally GFP-tagged Cdc42 unless otherwise stated. Furthermore, the construct contains a myc tag, which is not used in this study and therefore, the construct will be referred to as GFP-Cdc42/Cdc42 hereafter. Information about polarization kinetics was obtained by determining the number of cells displaying a GFP-Cdc42 signal at the cell cortex (cap) or in the bud at different time points. On a single-cell level, Cdc42 localizes into wide caps, which narrow gradually before forming the bud (Fig. 2.1 B). The majority of control cells (98 %) have formed a polarization cap or bud 55 min after release from G1 arrest (Fig. 2.1 C).

Protein dynamics were obtained by performing FRAP experiments on the polarization site (Fig. 2.2 A). Therefore, we bleached the cap and monitored its fluorescence recovery

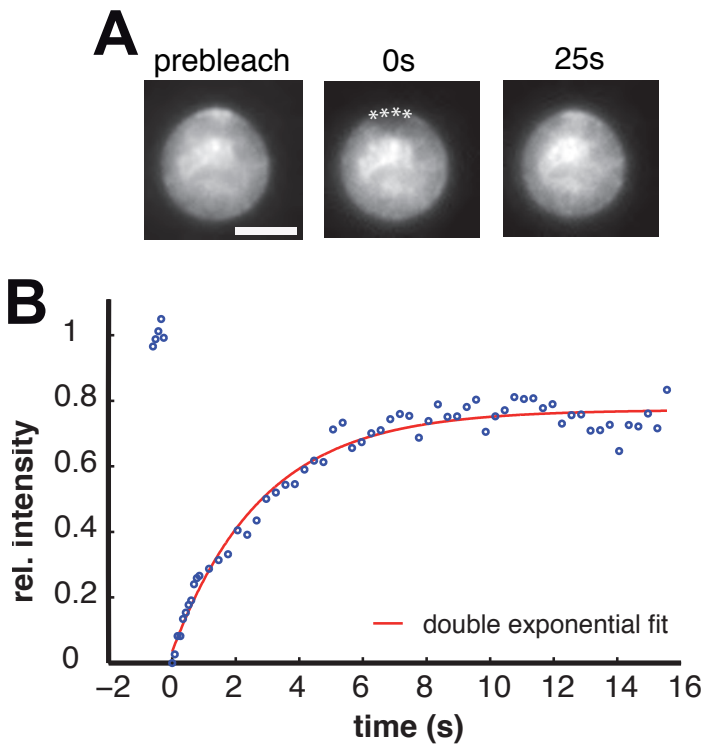

Figure 2.2: Protein dynamics were determined by FRAP experiments. (A) Representative FRAP experiment. Depicted is a control cell before, at and 25 min after the bleach event. Asterisks mark the site of the FRAP event. **(B)** Representative recovery curve of a control cell. The curve was generated by double exponential fitting. Scale bars: 4 µm.

over time. The recovery curve was obtained by fitting the recovered signal at different time points with a double exponential curve, which represented two different processes involved in the recovery. Initial rapid recovery resulted from diffusion, whereas the slower recovery was dependent on transport events (Fig. 2.2 B). Since we were only interested in transport-dependent recovery, only half-times that represented this pathway were considered.

To verify that the amount of expressed Cdc42 did not affect cell behaviour, we tagged Cdc42 at the endogenous locus (1x42) and compared polarization efficiency and protein dynamics of endogenously (1x) and ectopically (2x42) expressed GFP-Cdc42.

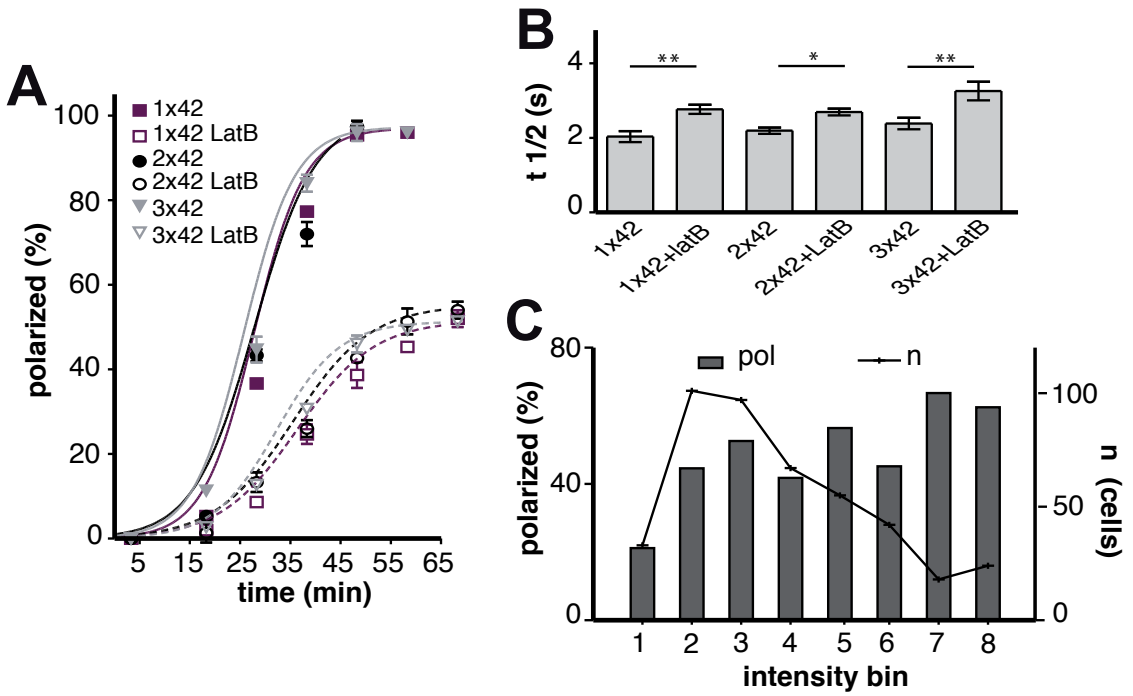

Figure 2.3: Cdc42 expression level does not affect protein dynamics. (A) Comparison of polarization kinetics of endogenously tagged GFP-Cdc42 (1x42). ectopically expressed GFP-Cdc42 (2x42) or two ectopically expressed copies of GFP-Cdc42 (3x42) in the absence and presence of LatB. Data for each time point (mean $\pm$ SD) are based on the analysis of three individual experiments with 50 cells each. **(B)** Comparison of half-life (t 1/2) of endogenously tagged GFP-Cdc42 (1x42), ectopically expressed GFP-Cdc42 (2x42) or two ectopically expressed copies of GFP-Cdc42 (3x42) in the absence and presence of LatB. Bar graphs correspond to the mean $\pm$ SEM. N $\geq$ 10. $*$ indicates that the difference is statistically significant (p < 0.05, t-test). $**$ indicates that the difference is statistically very significant (p < 0.01, t-test). **(C)** Absence of correlation between GFP-Cdc42 expression levels (intensities) and probability of polarization.

Furthermore, we generated a strain ectopically expressing two GFP-Cdc42 constructs in

addition to the endogenous, untagged version (3x42). Neither polarization kinetics nor proteins dynamics were affected by copy number of Cdc42 in both control and actin-depleted (LatB-treated) cells (Fig. 2.3 A, B). In addition, we investigated whether the polarization probability depends on Cdc42 expression levels. Therefore, we expressed Cdc42 under the endogenous or a galactose-inducable promoter and induced cells for 30 min, 60 min, 90 min and 120 min. We counted the number of polarized cells in dependence of their fluorescence intensity and found no significant correlation (Fig. 2.3 C), indicating that expression levels had no effect on polarization probability.

2.2 Actin and Rdi1 extraction act in parallel

2.2.1 Synthetic lethal screen reveals genetic interactions between polarity regulators and actin-dependent transport components

To systematically evaluate the proposed redundancy between polarity regulators and actin-dependent transport components during polarity establishment, we performed a synthetic lethal screen with Cdc42 and its direct regulators, the GEF Cdc24, the GAPs (Bem2, Bem3, Rga1 and Rga2), the GDI Rdi1, the adaptor protein Bem1 and the Cdc42 effector Cla4 (Tab. A.3). The majority of the genes tested is not required for cell viability. In a synthetic interaction screen, two (or more) single mutants were crossed and analyzed for growth defects (Fig. 2.4 A). Analysis of synthetic lethal or synthetic sick double mutants allowed the identification of genes involved in redundant rather than in the same pathways. We included a collection of conditional alleles in our screen, in order to assay essential genes such as Cdc42, Cdc24 and many actin associated proteins. The heat map displayed in Fig. 2.4 B compares genetic (blue) (Tab. A.3) and physical (orange) (Tab. A.4) interactions between polarity regulators and actin-dependent transport components. While many genetic interactions were found (Fig. 2.4 B, blue heat map), physical interactions were rare (Fig. 2.4 B, orange heat map), indicating that components of cell polarization and actin-related processes function in parallel rather than in the same pathways.

In contrast to only one GEF, there are four potential GAPs, Bem2, Bem3, Rga1 and Rga2,

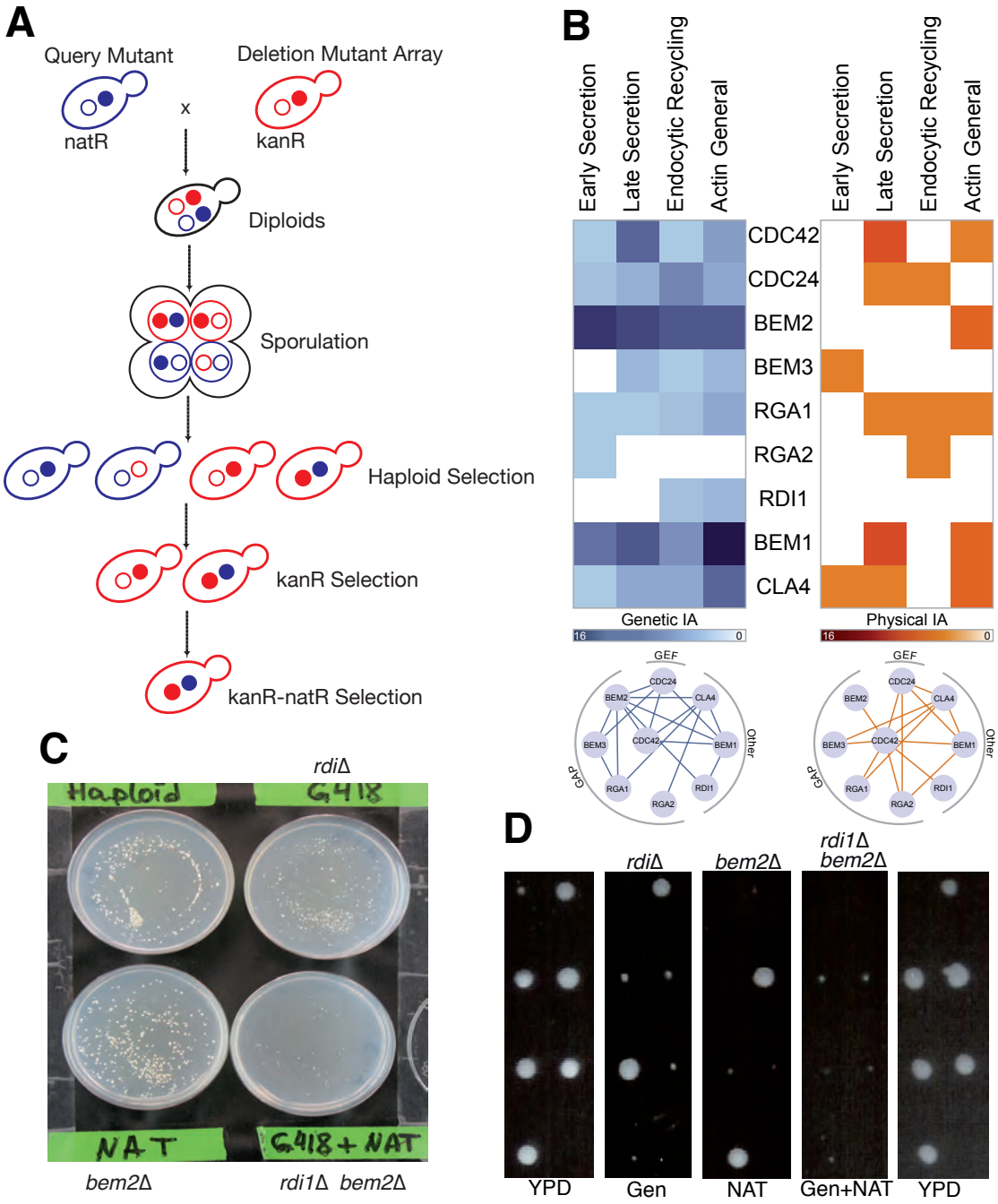

Figure 2.4: Synthetic lethal screen. (A) Schematic depiction of a work flow for a systematic synthetic lethal screen. **(B)** Comparison of genetic and physical interactions between polarization and transport components. Above: The number of genetic (blue) and physical (orange) interactions of the polarization proteins to proteins of the transport components were colour-coded in a heat map. Below: the interactions between the polarization proteins are depicted in a graph. Random spore analysis **(C)** and tetrad analysis **(D)** verify the synthetic lethal interaction between *BEM2* and *RDI1*.

for Cdc42 in *S. cerevisiae* (Zheng et al. 1994; Gladfelter et al. 2002. Smith et al. 2002; Marquitz et al. 2002). Interestingly, Bem2 showed the largest number of genetic interactions with actin related processes. Furthermore, Bem2 was found to be synthetic lethal with Rdi1 (Fig. 2.4 B, C; Tab. A.3), the only RhoGDI known in yeast. These data suggest that Bem2 might have an important role in polarity establishment, while the other GAPs might be involved in later events of cell polarization (Perez 2010; Caviston & Longtine 2003). Furthermore, the polarity regulator Rdi1 displayed interactions with actin-dependent components supporting the redundancy of the two Cd42 recycling pathways (Fig. 2.4 B; Tab. A.3).

2.2.2 Cdc42 polarization depends on recycling through Rdi1 and actin

In order to investigate the role of Rdi1 during polarity establishment we deleted *RDI1* in GFP-Cdc42 expressing control cells. In contrast to control cells, which displayed a high cytosolic pool of Cdc42, we observed Cdc42 accumulation in internal and plasma membranes in *rdi1*Δ cells (Fig. 2.5; Fig. 2.6 A).

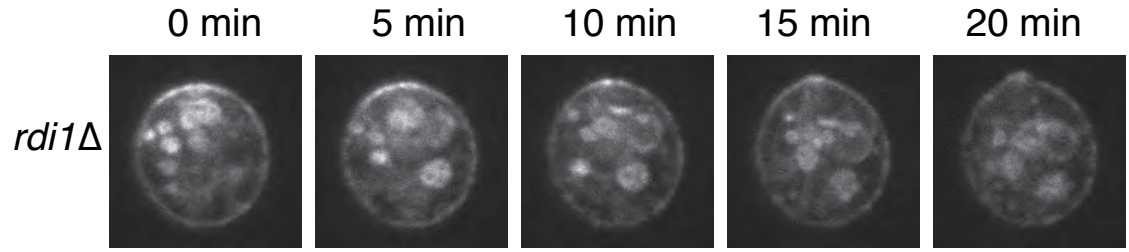

Figure 2.5: Cap and bud formation in *rdi1*Δ cells. Single pictures of a time-lapse movie of GFP-Cdc42 caps in *rdi1*Δ cells. The time-lapse movie was started at the beginning of cap formation (t=0 min). Framerate: 1 min, every 5th frame is depicted in this figure.

In addition, we generated a Cdc42 mutant, deficient of Rdi1 binding ($Cdc42^{R66E}$), which displayed the same phenotype (Fig. 2.6 A). Despite the increased membrane association of Cdc42 in *rdi1*Δ and $Cdc42^{R66E}$ cells , polarization kinetics of GFP-Cdc42 in control, *rdi1*Δ cells and cells expressing $Cdc42^{R66E}$ were similar (Fig. 2.6 A). Next, we disrupted the actin pathway in control, *rdi1*Δ and $Cdc42^{R66E}$ cells to investigate the suggested redundancy more carefully. Polarization was completely inhibited when *rdi1*Δ or $Cdc42^{R66E}$ cells

were treated with the actin-depolymerizing drug LatB, whereas polarization efficiency of Cdc42 was only slightly reduced in control cells (Fig. 2.6 B; Wedlich-Soldner et al. 2004). To rule out side-effects of the LatB treatment, we also monitored polarization efficiency in a temperature-sensitive secretion mutant of the type V myosin Myo2 (*myo2-16*). While *myo2-16* polarized to 80 %, the *myo2-16 rdi1*Δ double mutant completely failed to polarize at the restrictive temperature (35 °C), (Fig. 2.6 C). In addition, reduction of endocytic

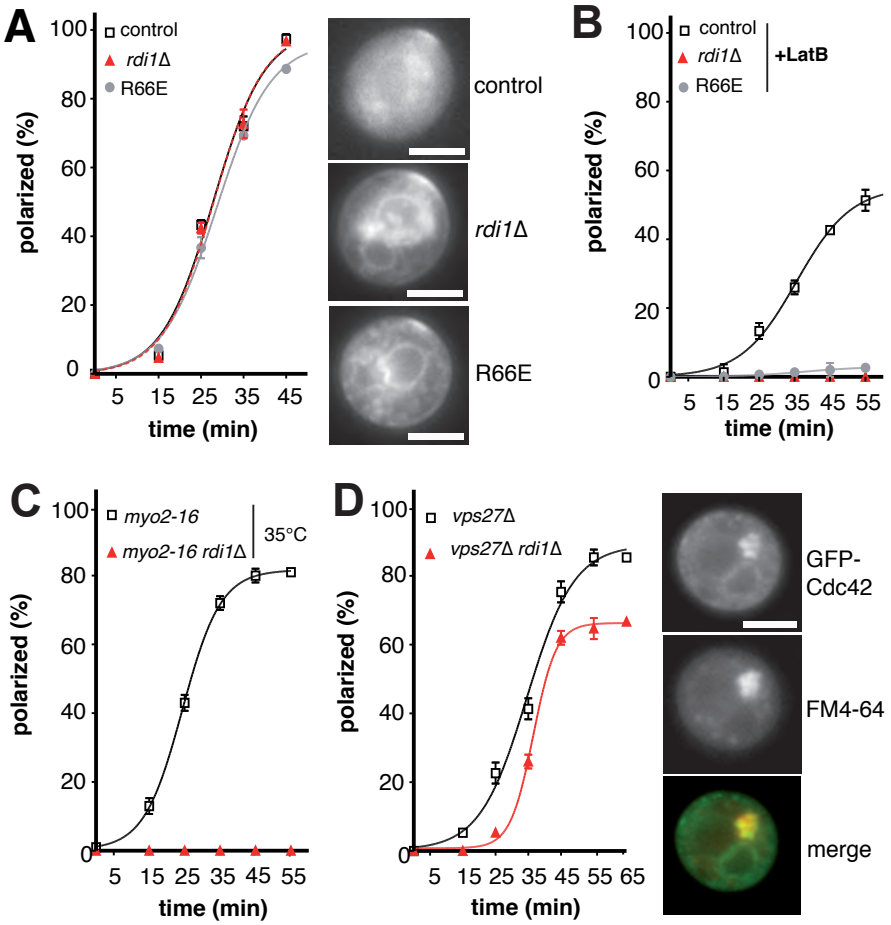

Figure 2.6: Polarization kinetics of Rdi1 and actin-dependent transport. (A) Polarization efficiency of GFP-Cdc42 in control cells, *rdi1*Δ and the mutant Cdc42^{R66E}. GFP-Cdc42 localizes to polarization caps after release from G1 arrest. **(B)** Polarization curves of LatB-treated control, *rdi1*Δ and Cdc42^{R66E} cells. **(C)** Polarization curves of Cdc42 in the endocytic mutant *vps27*Δ and *vps27*Δ *rdi1*Δ. Colocalization of GFP-Cdc42 and the membrane dye FM4-64 shows Cdc42 accumulation in class E compartments in *vps27*Δ and *vps27*Δ *rdi1*Δ mutants. **(D)** Polarization curves of Cdc42 in the temperature-sensitive transport mutants *myo2-16* and *myo2-16 rdi1*Δ at 35 °C. Data for each time point (mean ± SD) are based on the analysis of three individual experiments with 50 cells each. Scale bar: 4 µm.

recycling by deleting the ESCRTIII component Vps27 (Katzmann et al. 2003) led to a slowdown in polarization (Fig. 2.6 D). Colocalization experiments of GFP-Cdc42 with FM4-64 stained endosome membranes in *vps27*Δ cells revealed that Cdc42 accumulated in class E compartments (Fig. 2.6 D). This finding indicates that Cdc42 is actively recycled through the endocytic system.

2.2.3 Cdc42 dynamics depend on recycling through Rdi1

We determined protein dynamics of Cdc42 caps using FRAP (Fig. 2.2) in control cells and cells either compromised in actin- or Rdi1-dependent recycling.

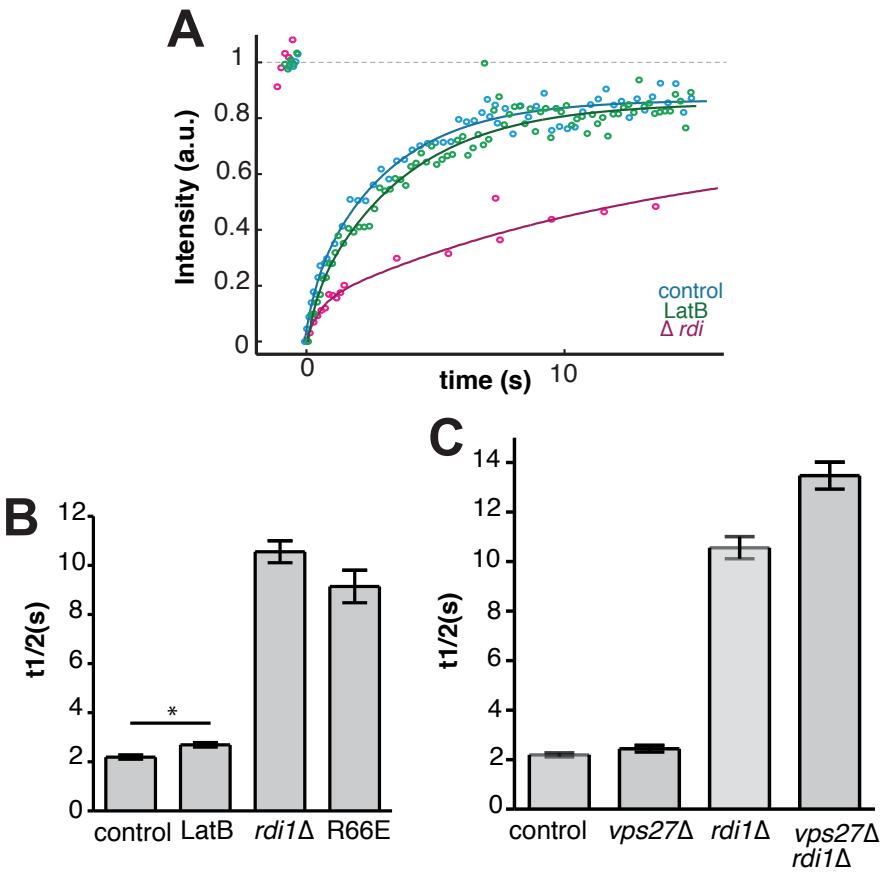

Figure 2.7: Protein dynamics of Cdc42 in the actin-dependent and Rdi1-dependent pathway. (A) Recovery curve for Cdc42 in control, LatB and *rdi1*Δ cells. **(B)** Average half-life (t 1/2) of GFP-Cdc42 fluorescence recovery after photobleaching in control, LatB-treated, *rdi1*Δ cells and the mutant Cdc42^{R66E}. **(C)** Average half-life (t 1/2) of GFP-Cdc42 fluorescence recovery after photobleaching in control, *vps27*Δ, *rdi1*Δ and *vps27*Δ *rdi1*Δ cells. Bar graphs correspond to the mean ± SEM. N ≥ 10. ∗ indicates that the difference is statistically significant ($p < 0.05$, t-test).

Cdc42 caps in control cells recovered rapidly with 2.2 s half-time (Fig. 2.7 B; Tab. A.1). Protein dynamics were only slightly reduced to 2.5 s when control cells were treated with LatB (Fig. 2.7 B; Tab. A.1), whereas recovery of *rdi1*Δ and Cdc42^{R66E} cells was much slower (10 s; Fig. 2.7 B; Tab. A.1).

This difference implies that Rdi1-mediated recycling acts four times faster than the actin-dependent pathway. We also performed FRAP experiments on *vps27*Δ cells and found half-times in the range of LatB-treated cells (Fig. 2.7 C; Tab. A.1). Protein dynamics in *vps27*Δ *rdi1*Δ were significantly slower than *rdi1*Δ single mutants (Fig. 2.7 C; Tab. A.1), further confirming the proposed redundancy between actin-dependent and Rdi1-mediated recycling of Cdc42.

2.3 GTPase cycling is required for Rdi1-mediated Cdc42 recycling

Cycling of Cdc42 between the GDP and GTP bound state is essential for viability of cells (Park & Bi 2007). Cdc42 alleles containing point mutations in the putative GTP-binding and hydrolysis domains (Cdc42^{G12V} Cdc42^{Q61L} Cdc42^{D118A}) resulted in dominant-lethal or dose-dependent dominant-lethal phenotypes (Ziman et al. 1991). FRAP analysis of the Cdc42^{Q61L} (expressed from a galactose-inducable promoter with the wild-type Cdc42 copy present) revealed slow half-times of 60 s (Slaughter et al. 2009; Wedlich-Soldner et al. 2004). Similar values were found in an inactive Cdc42^{D57Y} mutant (expressed from a galactose-inducable promoter with the wild-type Cdc42 copy present) (Slaughter et al. 2009; Wedlich-Soldner et al. 2004), indicating that the GTPase cycle plays a prominent role for Cdc42 dynamics. To elucidate the role of the GTPase cycle in GDI-dependent extraction, we altered the previous approaches and performed experiments in our strain background.

2.3.1 GTPase cycling is required for fast Cdc42 dynamics

The experiments mentioned in the previous paragraph were conducted in a strain background (cln1::hisG *cln2*Δ cln3::LEU2 pMET-CLN2::TRP1) that differed from the strain background used in this study (cln1::HisG cln2 *cln3*Δ::HisG yipLac204-MET-CLN2::TRP1). In or-

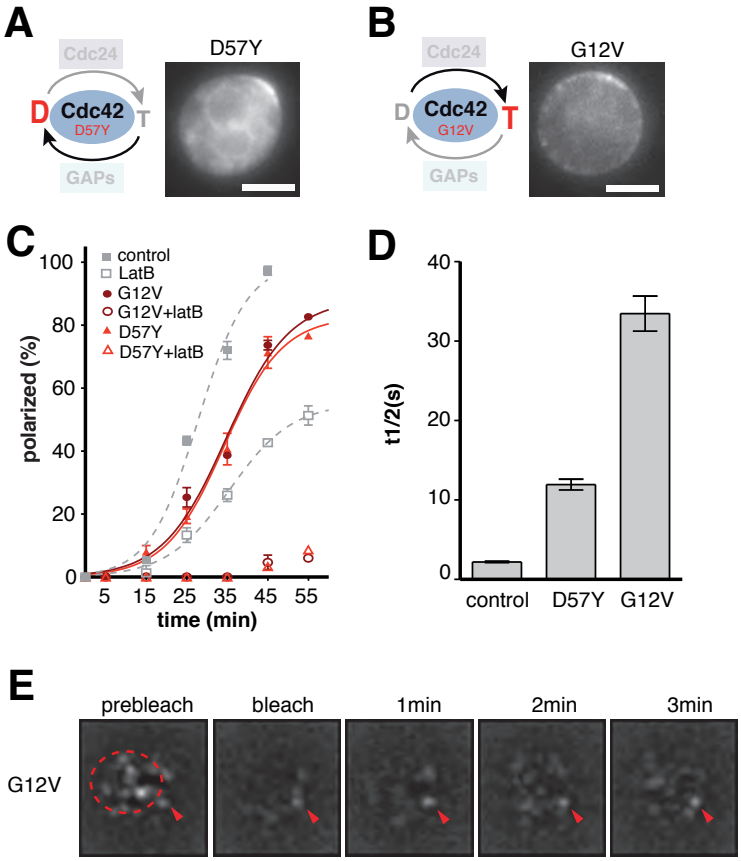

Figure 2.8: The role of the GTPase cycle. **(A)** Schematic depiction and localization of the GFP-Cdc42^{D57Y} mutant. **(B)** Schematic depiction and localization of the GFP-Cdc42^{G12V} mutant. **(C)** Polarization efficiency of Cdc42^{D57Y} and Cdc42^{G12V} in the presence and absence of LatB compared to control cells treated with and without LatB. Data for each time point (mean $\pm$ SD) are based on the analysis of three individual experiments with 50 cells each; **(D)** Average half-life (t 1/2) of control cells, Cdc42^{D57Y} and Cdc42^{G12V}. Bar graphs correspond to the mean $\pm$ SEM, N $\geq$ 10. **(E)** Recovery of GFP- Cdc42^{G12V} after partial FRAP in total internal reflection fluorescence (TIRF) microscopy. The red arrow marks a stable unbleached Cdc42^{G12V} patch. Scale bars: 4 µm.

der to preserve consistency, we repeated experiments in our strain background. Furthermore, to avoid strong protein overexpression, we used the endogenous Cdc42 promoter instead of the galactose-inducable promoter to express the constitutively active and inactive mutant of Cdc42. However, we failed to generate a Cdc42^{Q61L} mutant that was able to polarize and instead expressed the constitutively active Cdc42^{G12V} mutant. Expression of Cdc42^{D57Y} under the endogenous promoter was successful. Cdc42^{D57Y} mutants (with the untagged wild-type Cdc42 present) displayed a high cytosolic pool (Fig. 2.8 B), whereas Cdc42^{G12V} (with the untagged wild-type Cdc42 present) appeared

to accumulate in small patches in the plasma membrane (Fig. 2.8 B). Polarization kinetics and efficiency of both cycling mutants were decreased compared to control cells (Fig. 2.8 C). Furthermore, polarization of Cdc42^{D57Y} and Cdc42^{G12V} was strongly actin-dependent (Fig. 2.8 C). We could confirm previously measured (Wedlich-Soldner et al. 2004; Slaughter et al. 2009) slow recovery half-times of 12 s and 30 s, for Cdc42^{D57Y} and Cdc42^{G12V} , respectively (Fig. 2.8 D; Tab. A.1). These recovery times were consistent with values retained from FRAP experiments in *rdi1*Δ cells, where Cdc42 polarization was solely actin-dependent (Fig. 2.8 D; Tab. A.1). As mentioned in the previous paragraph, we observed Cdc42^{G12V} localization in a patch-like pattern at the cell cortex. We used total internal reflection microcopy (TIRFM) to visualize and bleach Cdc42^{G12V} patches, which recovered slowly and patches in the unbleached area remained stable over time (Fig. 2.8 D).

2.3.2 GTP hydrolysis is required for Cdc42 extraction

After we demonstrated that efficient recycling of Cdc42 strongly depends on its ability to cycle between the GDP- and GTP-bound state, we decided to investigate the involvement of the GTPase cycle in GDI-dependent recycling in mechanistic detail. Spectroscopic assays were performed to determine the nucleotide-dependent dissociation kinetics of Mant (methylanthaniloyl-modified)-labelled Cdc42 from purified HAF (hexdecanoylaminofluorescein)-labelled liposomes in the presence of RhoGDI. We measured the increase of Mant-fluorescence recovery as a result of Cdc42 dissociation from liposomes (Fig. 2.9 A). Interestingly, Cdc42-GDP dissociated more than 10x faster than Cdc42-GTP, confirming that RhoGDI preferentially extracts Cdc42-GDP (Fig. 2.9 B; Johnson et al 2009). Furthermore, in the presence of a GAP domain, Cdc42-GTP dissociated with approximately the same rate as Cdc42-GDP (Fig. 2.9 B), indicating that Cdc42-GTP hydrolysis is the rate-limiting step for its dissociation from liposomes. This observation was supported by the fact that nonhydrolyzable Cdc42GMPPNP hardly showed any fluorescence recovery (Fig. 2.9 B). These experiments were contributed by Jared Johnson, Cornell University.

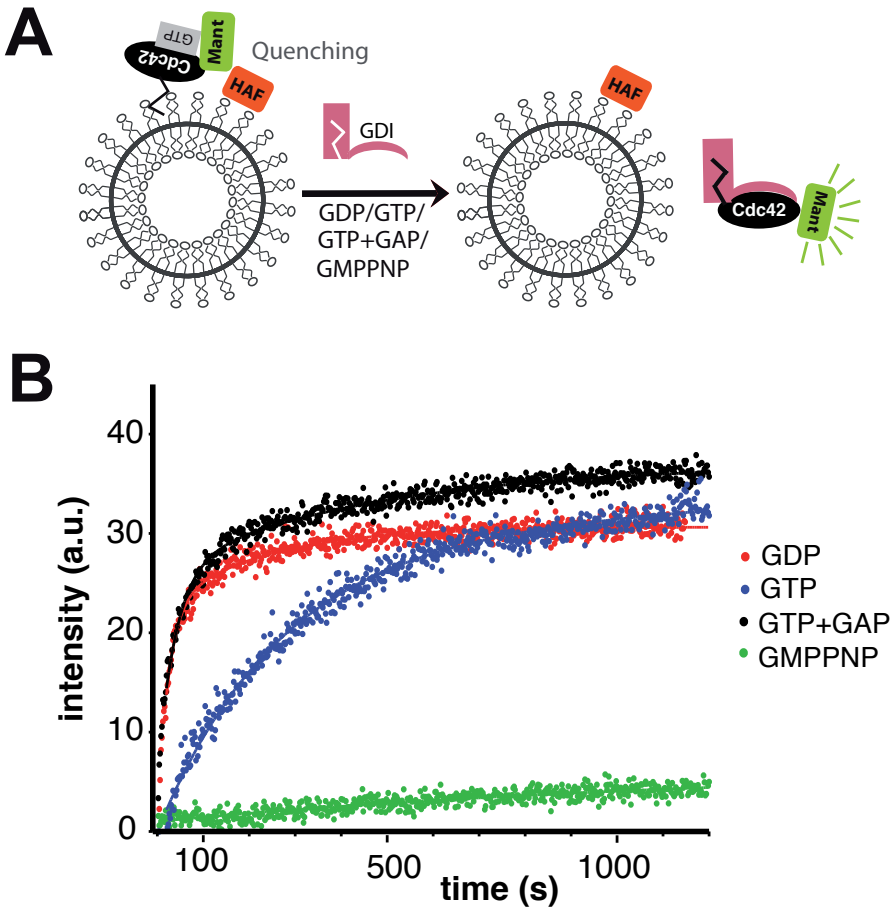

Figure 2.9: GDI-dependent extraction of Cdc42 from liposomes. (A) Schematic depiction of spectroscopic extraction assay from liposomes. **(B)** Dissociation rate of Mant-labelled Cdc42 from HAF-labelled liposomes upon GDI addition in the presence of GDP (red curve), GTP (blue curve), GTP and GAP (black curve) or GMPPNP (green curve).

Next, we investigated Cdc42 hydrolysis *in vivo* by deleting the GAPs *BEM2*, *BEM3* and *RGA2*. However, we failed to generate a knockout of the fourth GAP, *RGA1*. In contrast to *bem2*Δ cells, which displayed a round morphology and wide caps (Fig. 2.10 A), *bem3*Δ and *rga2*Δ cells exhibited an oval cell shape and smaller caps (Fig. 2.10 A). Polarization efficiency was over 80 % in all GAP mutants (Fig. 2.10 B, C). Interestingly, only few *bem2*Δ cells (15 %) were able to polarize in the absence of actin (Fig. 2.10 C), indicating a critical role for GTP hydrolysis in GDI dependent recycling of Cdc42. While protein dynamics of Cdc42 in *bem3*Δ and *rga2*Δ were similar to control cells, 2.8 s and 3.3 s, respectively (Fig. 2.10 E; Tab. A.1), recovery half-times of Cdc42 in *bem2*Δ were significantly reduced

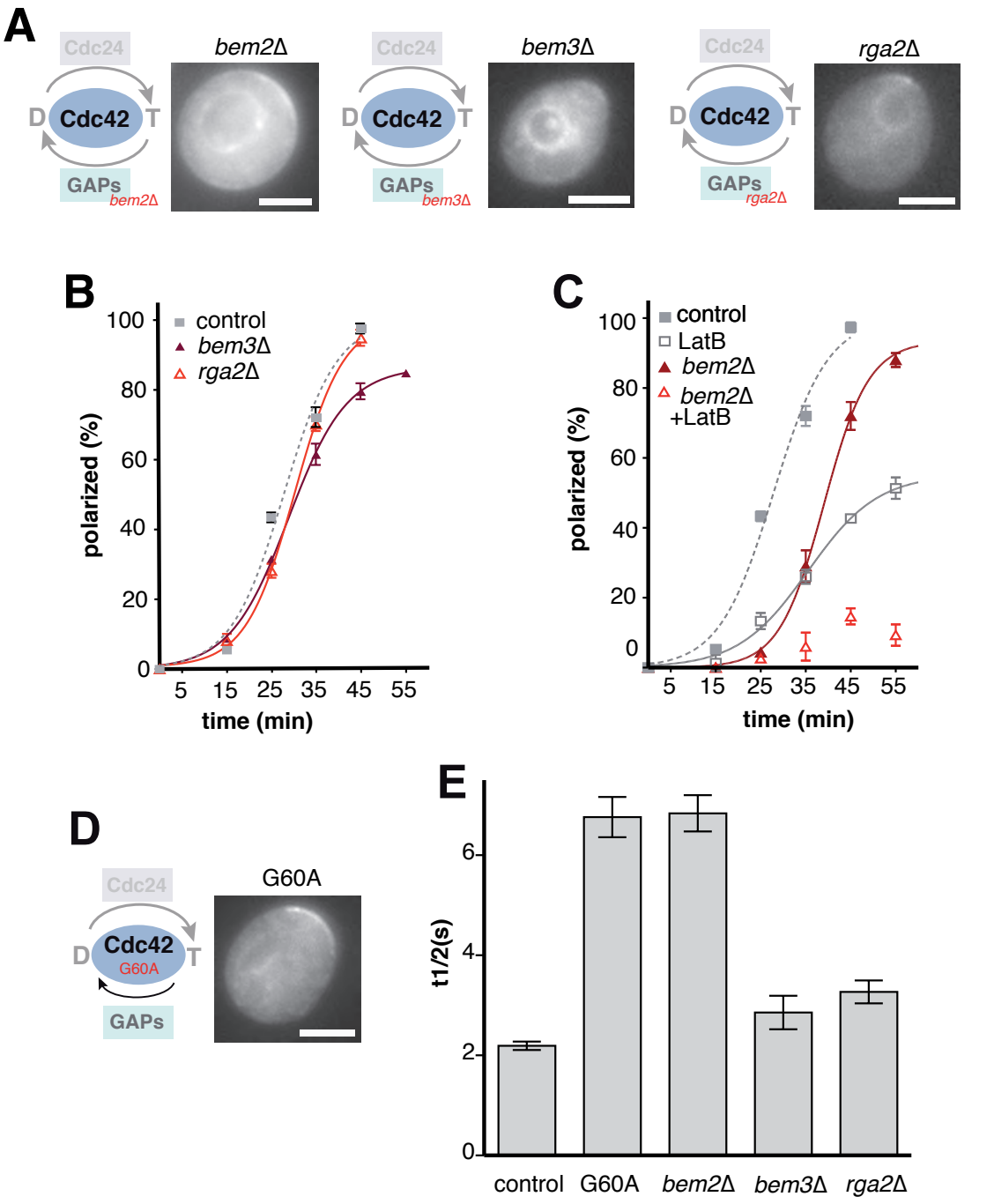

Figure 2.10: The role of hydrolysis. **(A)** Schematic depiction and localization of GFP-Cdc42 in *bem2*Δ, *bem3*Δ and *rga2*Δ cells. **(B)** Polarization efficiency of Cdc42 in control, *bem3*Δ and *rga2*Δ cells. **(C)** Polarization efficiency of Cdc42 in *bem2*Δ cells in the presence and absence of LatB. **(B)** and **(C)** Data for each time point (mean ± SD) are based on the analysis of three individual experiments with 50 cells each. **(D)** Schematic depiction and localization of the GFP-Cdc42^{G60A} mutant. Average half-life (t 1/2) of control cells, Cdc42^{G60A}, *bem2*Δ, *bem3*Δ and *rga2*Δ. Bar graphs correspond to the mean ± SEM. N ≥ 10. Scale bars: 4 µm.

to 6.8 s (Fig. 2.10 E; Tab. A.1). The same recovery half-time of 6.8 s was found in a slow hydrolyzing $Cdc42^{G60A}$ mutant (with the untagged wild-type Cdc42 present) (Flg. 2.10 E; Tab. A.1).

2.3.3 Increase of GDP exchange activity speeds up protein dynamics

We have shown in the previous paragraph that GTP hydrolysis contributes to efficient Cdc42 recycling (see 2.3.2). This result infers that the inactivation as well as the activation part of the GTPase cycle plays a critical role in Cdc42 recycling. Hence, we decided to investigate the effect of GDP exchange activity on GDI-mediated membrane extraction of Rho GTPases.Therefore, we performed liposome binding assays with the small GTPase Rac1 and its GDI (Fig. 2.11 A).

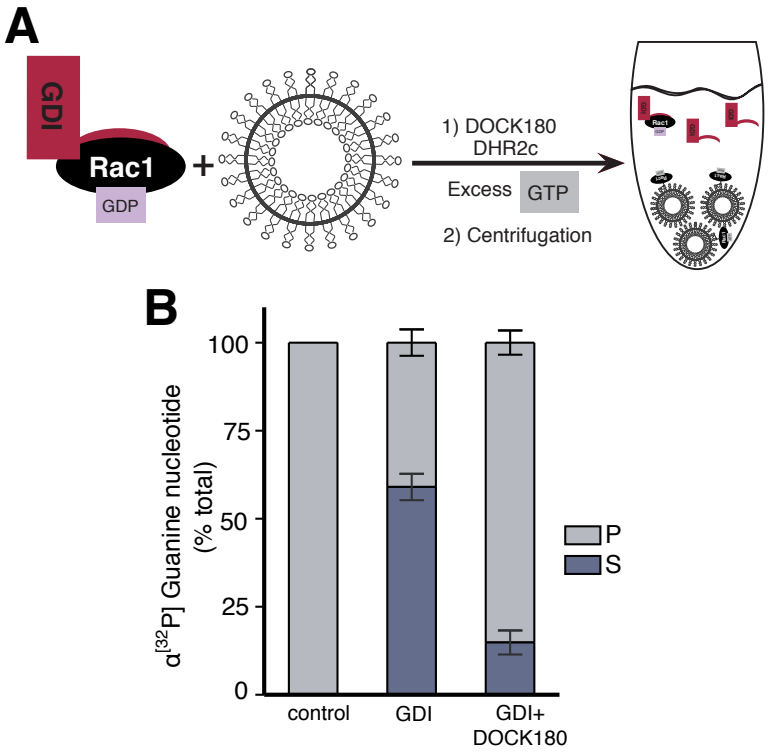

Figure 2.11: GEF influences GTPaseGDI complex. (A) Schematic depiction of the liposome binding assay. **(B)** Amounts of radioactively labelled Rac1 were measured in pellet (P) and soluble (S) fractions after addition of GDI with or without the GEF domain of Dock180 (DHR2C).

The GDI was not able to efficiently extract Rac1 after its association with liposomes in the presence of the GEF domain (DHR2C) and nonhydrolyzable GTP analog (Fig. 2.11 B). Inversely, nucleotide exchange by the GEF was reduced in the presence of GDI (Fig. 2.12 A, B), consistent with the proposed competition between GEF and GDI for binding at the switch II region of Rho GTPases (Schoebel et al. 2009; Ugolev et al. 2008). Increased GEF activity is therefore expected to interfere with GDI binding and should consequently increase Cdc42 concentration on the membrane.
(These experiments were contributed by Jared Johnson, Cornell University.)

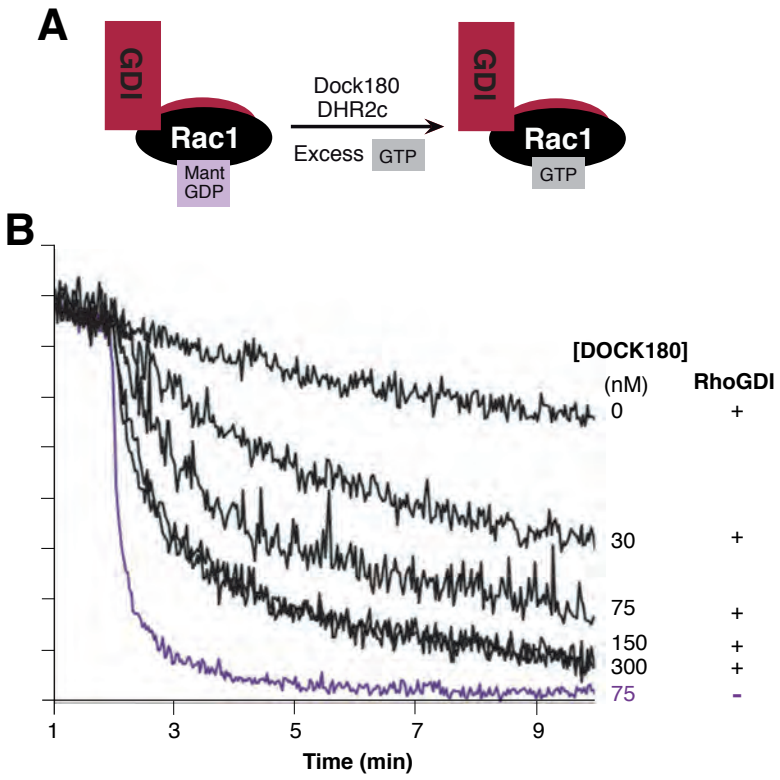

Figure 2.12: GEF influences GTPaseGDI complex (A) Schematic depiction of liposome extraction assay. **(B)** Rac1 was preloaded with Mant-GDP in the presence of liposomes, unlabelled GTP and GDI. Loss of Mant-fluorescence due to exchange was monitored after addition of the DHR2C GEF domain at 2 min. The exchange curve without added GDI is shown in purple.

To evaluate the role of GEF activity on GDI-mediated Cdc42 recycling *in vivo*, we ectopically overexpressed Cdc24 by integrating a second copy fused to either GFP (Fig. 2.13) or RFP (Fig. 2.14). We confirmed that Cdc24 overexpression did not alter the Cdc24 cap/cytosol intensity ratio in control and *bem2*Δ cells (Fig. 2.13 A). Also, polarization ef-

ficiency of Cdc24 was not affected by copy number in the presence and absence of LatB (Fig. 2.13 B). Further, we tested whether Cdc24 overexpression had any effect on Cdc24 dynamics in control, LatB-treated and *bem2*Δ cells. FRAP experiments revealed that Cdc24 overexpression in the presence or absence of LatB or in *bem2*Δ cells did not change recovery half-times of around 2.1 s (Fig. 2.13 C; Tab. A.1).

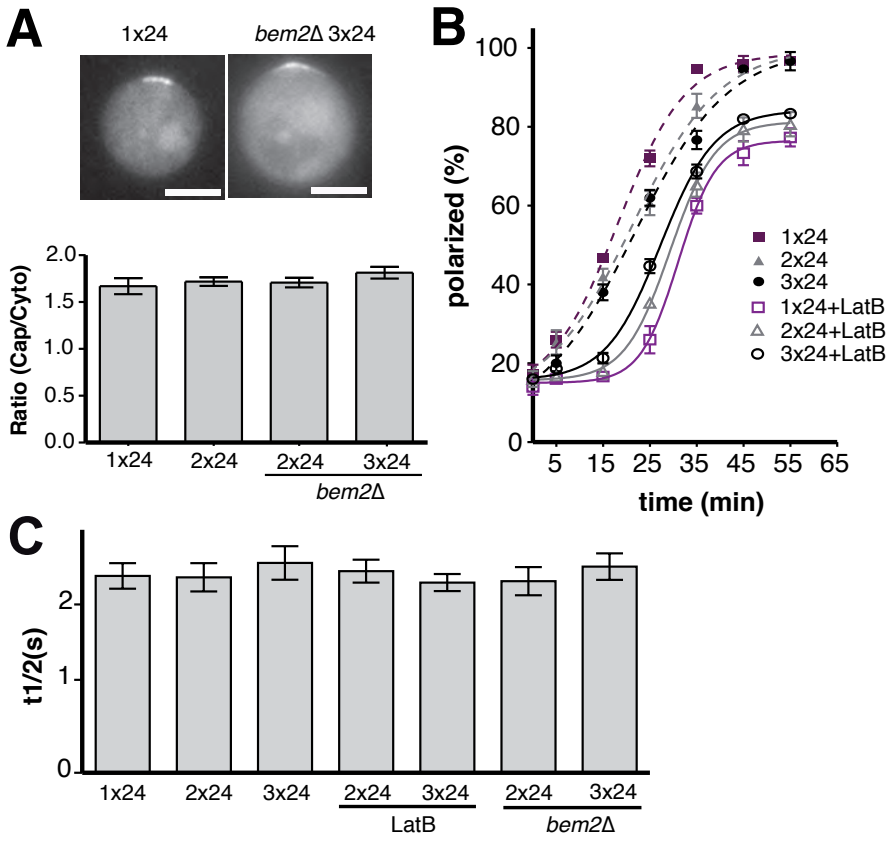

Figure 2.13: Cdc24 expression level does not influence Cap/Cell intensity ratio, polarization efficiency or protein dynamics (A) Cdc24 cap in cells expressing endogenously GFP-tagged Cdc24 (1x24) and *bem2*Δ cells expressing two copies of GFP-Cdc24 plasmids. Scale bars: 4 µm. Bar graphs depict cap/cell ratio of endogenously tagged GFP-Cdc24 (1x24) and ectopically expressed GFP-Cdc24 (2x24) in control cells as well as ectopically expressed (2x24) and two copies of ectopically expressed GFP-Cdc24 (3x24) in *bem2*Δ cells. **(B)** Polarization kinetics of endogenously tagged GFP-Cdc24 (1x24) and ectopically expressed GFP-Cdc24 (2x24) and two copies of ectopically expressed GFP-Cdc24 (3x24) in the presence or absence of LatB. Data for each time point (mean ± SD) are based on the analysis of three individual experiments with 50 cells each. **(C)** Average half-life (t 1/2) of endogenously tagged GFP-Cdc24 (1x24) and ectopically expressed GFP-Cdc24 (2x24), two copies of ectopically expressed GFP-Cdc24 (3x24), endogenously tagged GFP-Cdc24 (1x24), ectopically expressed GFP-Cdc24 (2x24) in the presence of LatB and one (1x24) and two copies (2x24) of ectopically expressed GFP-Cdc24 in *bem2*Δ cells. **(A)** und **(B)** Bar graphs correspond to the mean ± SEM. N ≥ 10.

We expressed Cdc24-RFP in strains with slower Cdc42 recycling to test whether Cdc24 overexpression changed polarization behaviour and protein dynamics. Colocalization of GFP-Cdc42 and Cdc24-RFP showed that Cdc42 and Cdc24 were properly expressed and colocalized in the polarization cap (Fig. 2.14 A). Polarization kinetics of Cdc42 (Fig. 2.14 B) as well as protein dynamics were not altered by Cdc24 overexpression in the presence or absence of actin (Fig. 2.14 C; Tab. A.1).

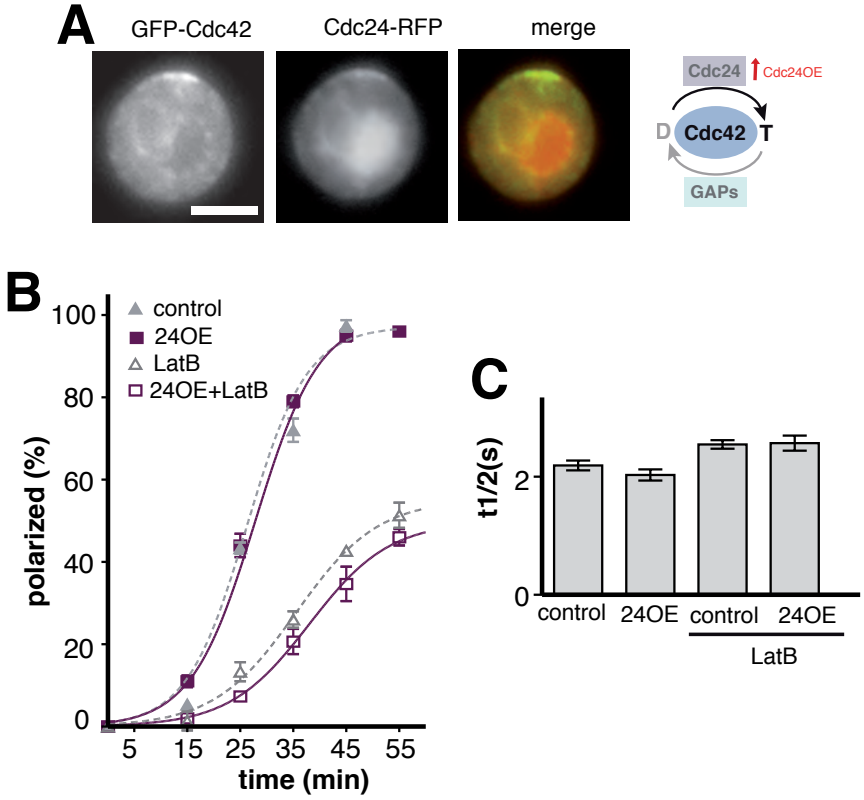

Figure 2.14: Polarization kinetics and protein dynamics of control cells overexpressing Cdc24 (A) Control cell expressing GFP-Cdc42 and Cdc24-RFP. Depicted are single channels and overlay. Scale bar: 4 µm. Schematic depiction of Cdc24 overexpression. **(B)** Polarization kinetics of control cells and cells overexpressing Cdc24 (24OE) in the presence and absence of LatB. Data for each time point (mean ± SD) are based on the analysis of three individual experiments with 50 cells each. **(C)** Average half-life (t 1/2) of control cells and cells overexpressing Cdc24 (24OE) in the presence and absence of LatB. Bar graphs correspond to the mean ± SEM. N ≥ 10.

Next, we tested wether Cdc24 overexpression altered protein kinetics or behaviour in cells with decreased Cdc42 hydrolysis. Although Cdc24 overexpression in *bem2*Δ did not lead to changes in polarization kinetics with or without actin (Fig. 2.15 B), Cdc42 protein dynamics were significantly decreased (Fig. 2.15 C; Tab. A.1).

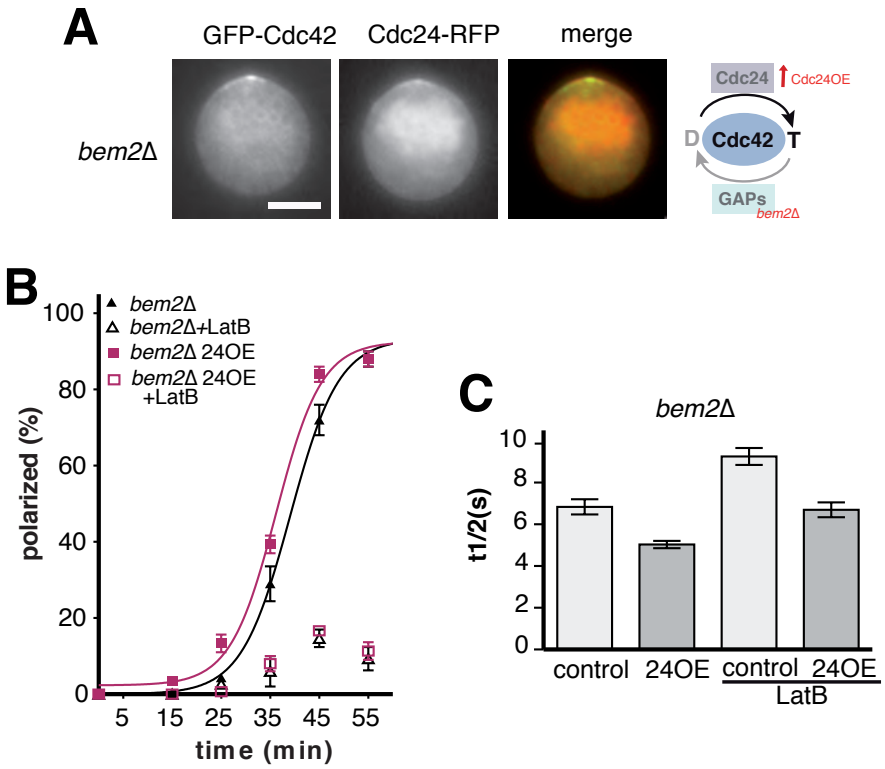

Figure 2.15: Polarization kinetics and protein dynamics of *bem2*Δ cells overexpressing Cdc24. **(A)** *bem2*Δ cell expressing GFP-Cdc42 and Cdc24-RFP. Depicted are single channels and overlay. Scale bar: 4 µm. Schematic depiction of Cdc24 overexpression in *bem2*Δ cells. **(B)** Polarization kinetics of *bem2*Δ cells and *bem2*Δ cells overexpressing Cdc24 (24OE) in the presence and absence of LatB. Data for each time point (mean ± SD) are based on the analysis of three individual experiments with 50 cells each. **(C)** Average half-life (t 1/2) of control cells and cells overexpressing Cdc24 (24OE) in the presence and absence of LatB. Bar graphs correspond to the mean ± SEM. N ≥ 10.

This effect was independent of actin (Fig. 2.15 C; Tab. A.1) and was also seen in the slow hydrolyzing Cdc42^{G60A} mutant (Fig. 2.16 C; Tab. A.1). Importantly, increase of Cdc42 dynamics after Cdc24 overexpression required Rdi1 binding, since faster FRAP dynamics were not measured in Cdc42^{R66E} cells (Fig. 2.16 D; Tab. A.1).

We generated a Cdc42 mutant (Cdc42^{F28L}), which displayed high global intrinsic GDP exchange activity (Reinstein et al. 1991; Lin et al. 1997) to explain the increase of protein dynamics in slow-hydrolyzing mutants upon increased GDP exchange activity. We expressed Cdc42^{F28L} in control (Fig. 2.17 A) and *bem2*Δ (Fig. 2.17 B) cells. Cdc42^{F28L} caps were smaller compared to Cdc42 caps, consistent with an increased recruitment to membranes outside the polarization site. Polarization kinetics and efficiency of Cdc42^{F28L}

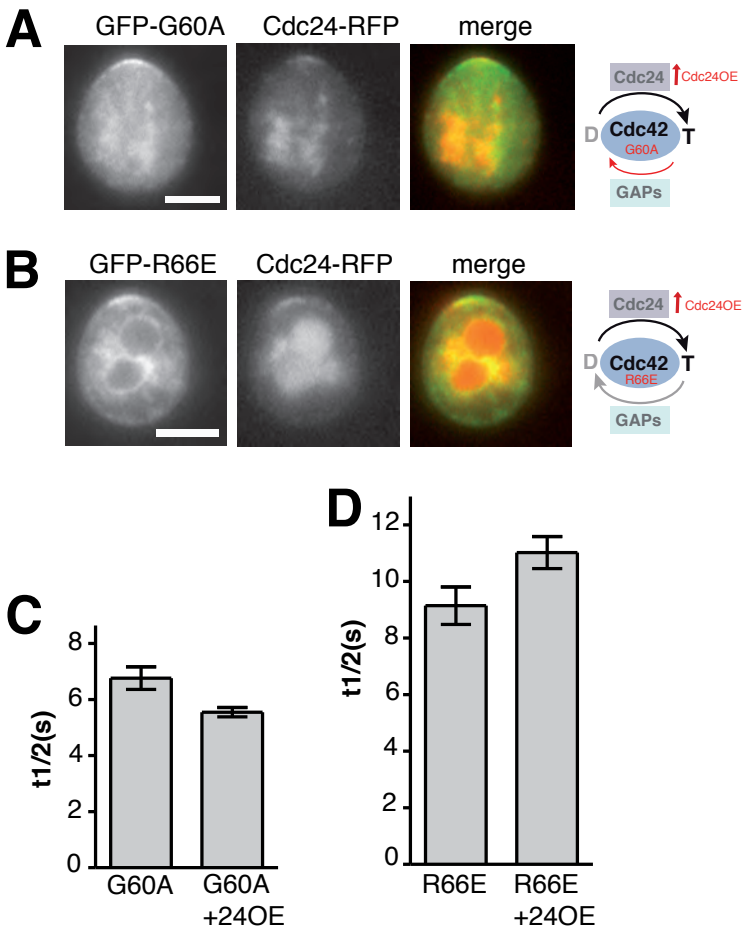

Figure 2.16: Protein dynamics of Cdc42 mutants overexpressing Cdc24 (A) Cdc42^{G60A} expressing Cdc24-RFP. Depicted are single channels and overlay. Scale bar: 4 µm. Schematic depiction of Cdc24 overexpression in Cdc42^{G60A} cells. **(B)** Cdc42^{R66E} expressing Cdc24-RFP. Depicted are single channels and overlay. Scale bar: 4 µm. Schematic depiction of Cdc24 overexpression in Cdc42^{R66E} cells **(C)** Average half-life (t 1/2) of Cdc42^{G60A} overexpressing Cdc24 (24OE) **(D)** Average half-life (t 1/2) of Cdc42^{R66E} and Cdc42^{R66E} overexpressing Cdc24 (24OE). **(C)** and **(D)** Bar graphs correspond to the mean ± SEM. N ≥ 10.

in control cells were comparable to Cdc42 cells but polarization of the Cdc42^{F28L} mutant strongly depended on actin (Fig. 2.17 C). Polarization of Cdc42^{F28L} in *bem2*Δ cells was 10 min delayed and less efficient compared to Cdc42 polarization in *bem2*Δ cells (Fig. 2.17 C). Polarization of Cdc42^{F28L} in *bem2*Δ was also highly actin dependent (Fig. 2.17 D). Since Cdc42^{F28L} displayed high intrinsic GDP exchange activity, it was expected to have the same effect on protein dynamics as Cdc24 overexpression. While protein dynamics of Cdc42^{F28L} were in the same range as in control cells (Fig. 2.17 E; Tab. A.1), Cdc42^{F28L} in

*bem2*Δ exhibited significantly increased protein dynamics (Fig. 2.17 E; Tab. A.1).

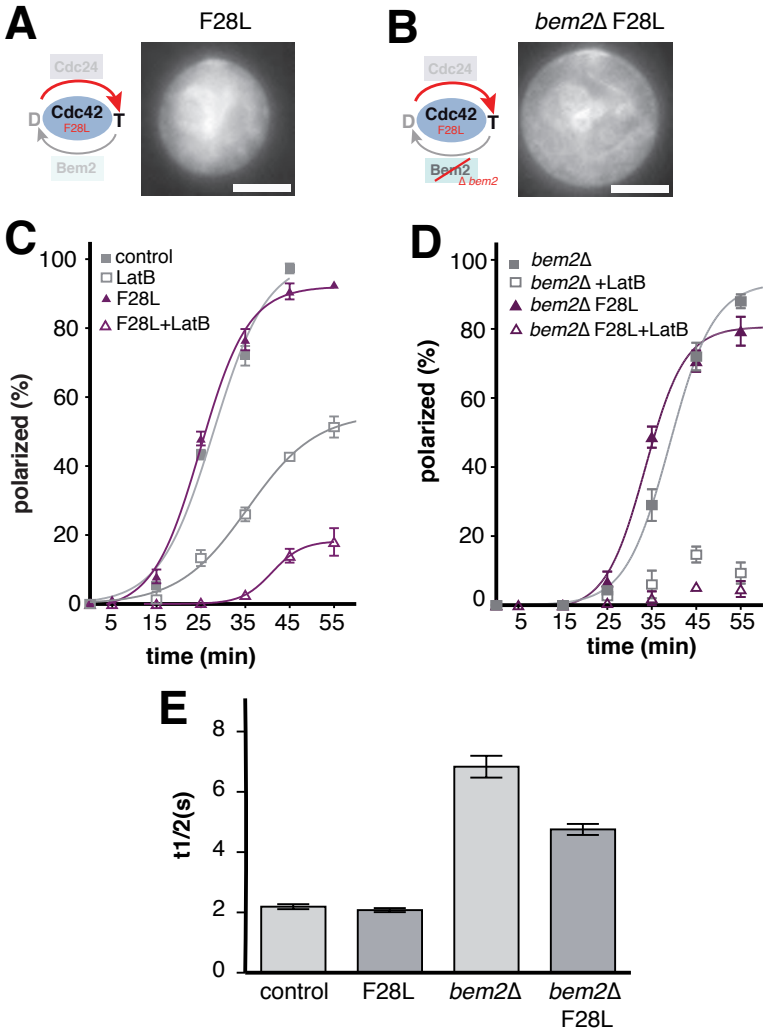

Figure 2.17: Polarization kinetics and protein dynamics of Cdc42^{F28L} in control and *bem2*Δ cells **(A)** Schematic depiction and localization of GFP-Cdc42^{F28L} in control cells. Scale bar: 4 µm. **(B)** Schematic depiction and localization of GFP-Cdc42^{F28L} in *bem2*Δ cells. Scale bar: 4 µm. **(C)** Polarization kinetics of Cdc42 and Cdc42^{F28L} in control cells in the presence and absence of LatB. **(D)** Polarization kinetics of Cdc42 and Cdc42^{F28L} in *bem2*Δ cells in the presence and absence of LatB. **(E)** Average half-life (t 1/2) of Cdc42 and Cdc42^{F28L} in control cells and Cdc42 and Cdc42^{F28L} in *bem2*Δ cells. Bar graphs correspond to the mean ± SEM. N ≥ 10. **(C)** and **(D)** Data for each time point (mean ± SD) are based on the analysis of three individual experiments with 50 cells each.

2.4 Uniqueness of budding relies on fast cycling and low activity of Cdc42

It is crucial that polarity establishment in *S.cerevisiae* is initiated only once per cell cycle. Interestingly, we observed a small percentage (2.3 %) of *rdi1*Δ cells, which initiated polarization at two different cortical sites (Fig. 2.19 A). In *bem2*Δ cells an even higher number of cells displaying two polarization sites was observed (8.7 %, Fig. 2.18 A).

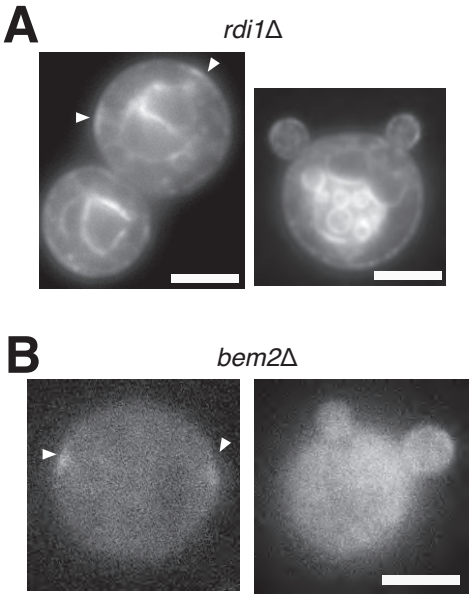

Figure 2.18: *rdi1*Δ cells and *bem2*Δ cells display Cdc42 at two polarization sites. (A) *rdi1*Δ cells with two caps (arrows) and two buds. Scale bar: 4 µm. **(B)** *bem2*Δ cells with two caps (arrows) and two buds. Scale bar: 4 µm.

We found a strong effect of increased GDP exchange activity on protein dynamics (see 2.3.3) and asked whether this activity increase also influences budding frequency. To that end, we performed washout experiments utilizing the naturally occurring activation of Cdc42 after G1/S transition, which is mediated by activation of its GEF (Arkowitz 1999) and inactivation of its GAPs (Knaus et al. 2007). Cells were released from G1/S arrest in the presence of LatB to prevent immediate polarization. The drug was washed out after 20 min or 40 min, resulting in varying increased GDP exchange activities (Fig. 2.19 A).

While only 2.3 % Δ *rdi1* cells with normal GDP exchange activity grew double buds (Fig. 2.19 B, C), this number was significantly raised to 13 % and 23 %, when GDP exchange activ-

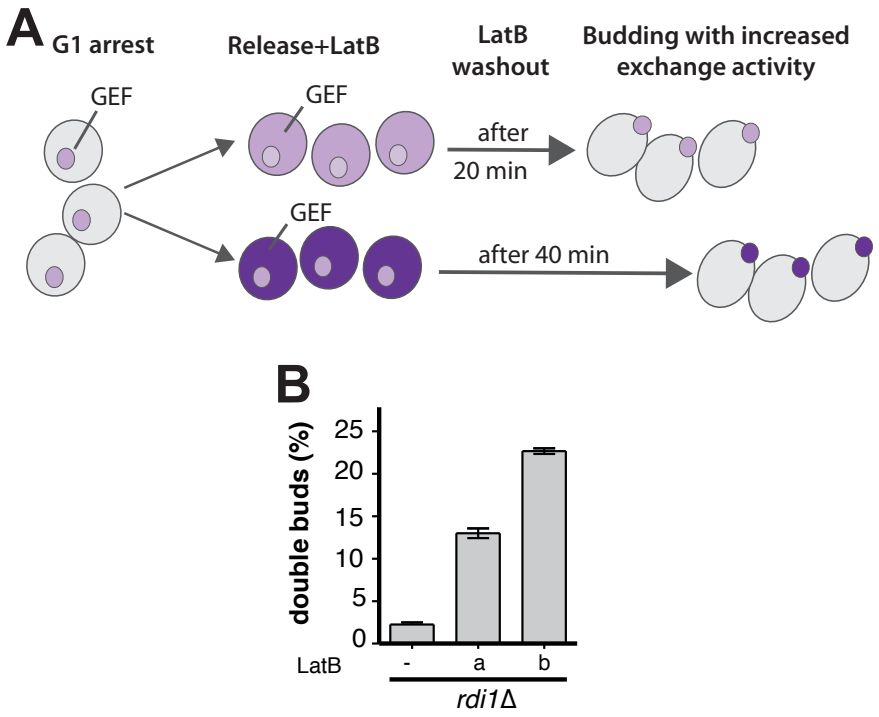

Figure 2.19: Washout experiment with *rdi1*Δ cells. (A) Workflow of the washout experiment. **(B)** Percentage of cells with two buds without (-), after 20 min (a) or after 40 min (b) of LatB treatment and subsequent washout. Bar graphs correspond to the mean ± SD. Data is based on the analysis of three individual experiments with N ≥ 100 cells each.

ity was increased after 20 min or 40 min LatB treatment and subsequent washout, respectively (Fig. 2.20 C). Next, we investigated the effect of increased GDP exchange activity on budding frequency in *bem2*Δ cells. We increased GDP exchange activity by either performing washout experiments (Fig. 2.19 A), overexpressing Cdc24 by integrating a Cdc24-RFP plasmid (Fig. 2.20 A) or combining both approaches. In GFP-Cdc42 *bem2*Δ cells, washout experiments increased the percentage of cells with two buds from 9 % to 13 % and 25 % (Fig. 2.20 C). Overexpression of Cdc24 in *bem2*Δ cells raised the number of double buds from 9 % to 12 % (Fig. 2.20 C). This number was further increased to 17 % and 25 % of cells displaying double buds after 20 min and 40 min LatB treatment, respectively (Fig. 2.20 C). Additionally, we performed washout experiments with *bem2*Δ cells expressing the fast exchanging Cdc42^{F28L} mutant (Fig. 2.20 B), which displayed 25 % cells with double buds (Fig. 2.20 C). Strikingly, washout after 20 min or 40 min of LatB treatment raised the number even further to 55 % and 63 % (Fig. 2.20 C). Importantly,

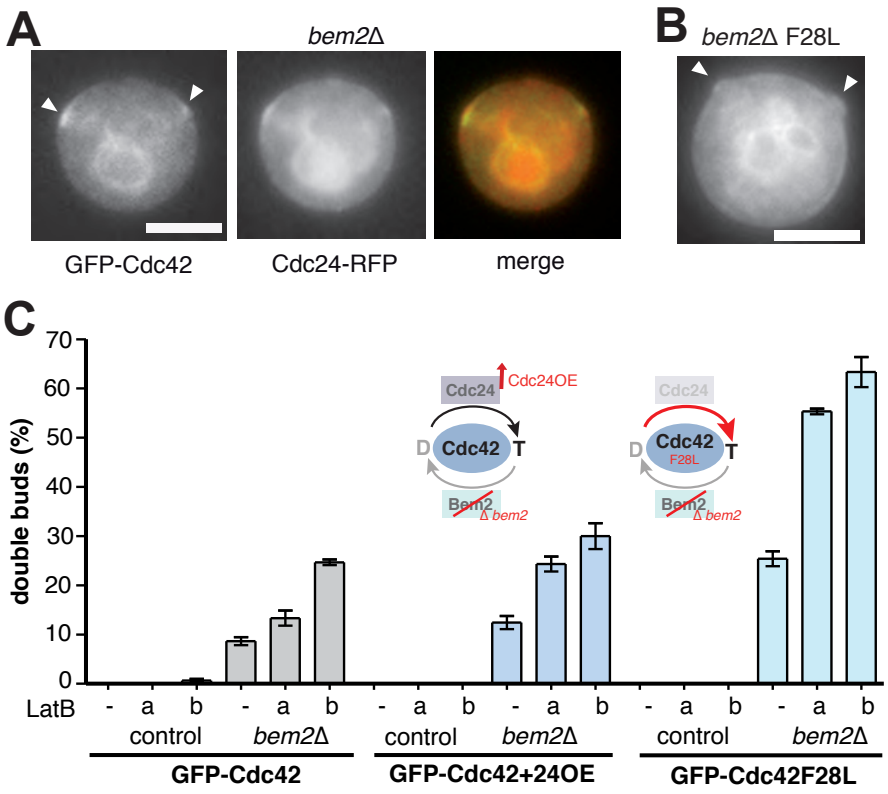

Figure 2.20: Increased GDP/GTP activity in *bem2*Δ cells. (A) Example for two polarization sites (arrows) in *bem2*Δ cells overexpressing Cdc24. Depicted are single channels and overlay. Scale bar: 4 µm. **(B)** Example for formation of two buds (arrows) in *bem2*Δ cells expressing Cdc42^{F28L}. Scale bar: 4 µm. **(C)** control and *bem2*Δ cells expressing GFP-Cdc42. GFP-Cdc42 and Cdc24-RFP or Cdc42^{F28L} were treated without (-) and with LatB for 20 min (a) or or 40 min (b). Bar graphs correspond to the mean ±SD of the percentage of cells with two buds. Data is based on the analysis of three individual experiments with N ≥ 100 cells each.

washout experiments on control cells expressing GFP-Cdc42, overexpressing Cdc24-RFP or expressing Cdc42^{F28L} did not have a significant effect on budding frequency (Fig. 2.20). This indicates that the activation and inactivation part of the GTPase cycle have to be tightly regulated in order to ensure a single polarization site. Next, we tested whether the increased number of cells with double buds was indeed a result of Cdc24 overexpression and increased GDP exchange activity rather than an artifact of Cdc24-RFP expression. GDP exchange activity in *bem2*Δ cells was augmented by either expressing one Cdc24-GFP or two copies of Cdc24-GFP (2xCdc24-GFP) and subsequent washout experiments were performed. The number of cells displaying two buds was increased from 10 % to 18 % in *bem2*Δ cells expressing two copies of Cdc24-GFP (2xCdc24-GFP; Fig. 2.21 A).

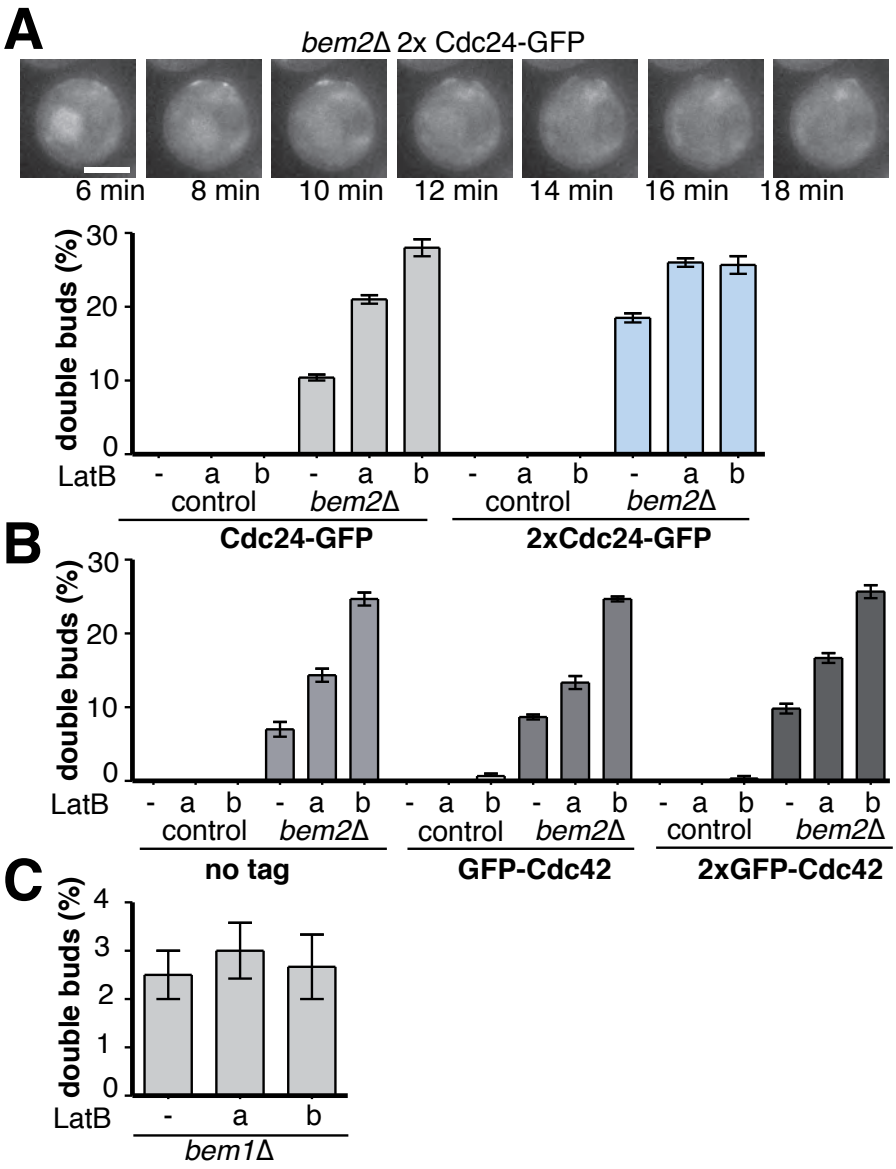

Figure 2.21: Influence of Cdc24 and Cdc42 expression levels on double bud formation (A) Formation of two caps and buds in *bem2*Δ cells ectopically expressing two copies of GFP-Cdc24 (3x24). Depicted are single snapshots (every second frame) of a time-lapse movie with 1 min frame rate. Maximum projection of 3 frames with 0.4 µm increment. Scale bar: 4 µm. Control and *bem2*Δ cells ectopically expressing one copy of Cdc24-GFP or two copies of Cdc24-GFP (2xCdc24-GFP) were treated without (-) and with LatB for 20 min (a) or or 40 min (b). **(B)** Control and *bem2*Δ cells without GFP- tagged Cdc42, expressing one ectopically integrated GFP-Cdc42 or two ectopically integrated GFP-Cdc42 (2xGFP-Cdc42) were treated without (-) and with LatB for 20 min (a) or or 40 min (b). **(C)** GFP-Cdc42 in *bem1*Δ cells were treated without (-) and with LatB for 20 min (a) or or 40 min (b). **(A)-(C)** Bar graphs correspond to the mean ±SD of the percentage of cells with two buds. Data is based on the analysis of three individual experiments with N $\geq$ 100 cells each.

Overexpression of Cdc24 in addition to washout experiments raised the number of cells with two buds (Fig. 2.21 A).

In contrast, expression levels of Cdc42 in *bem2*Δ did not have an effect on budding frequency, since the percentage of double budded cells did not change with the number of expressed GFP-Cdc42 copies (Fig. 2.21 B). To verify that the effect of GDP exchange activity was specific to extraction and hydrolysis mutants, we performed washout experiments on *bem1*Δ cells and found no change in the number of cells growing two buds (Fig. 2.21 C).

2.5 Role of actin dynamics in cell polarization

Actin cable nucleation in *S. cerevisiae* depends on the formins Bnr1 and Bni1. Cable formation towards the polarization site is essential for directed transport and bud growth. Cable nucleation is mainly mediated by Bni1 in unbudded cells, whereas in large budded cells both formins regulate actin cable formation (Yu et al. 2011). To investigate the role of Bni1 during cell polarity establishment, we performed polarization assays with Cdc42 in Δ*bni1* cells (Fig. 2.22 A). Since we were specifically interested in actin-dependent recy-

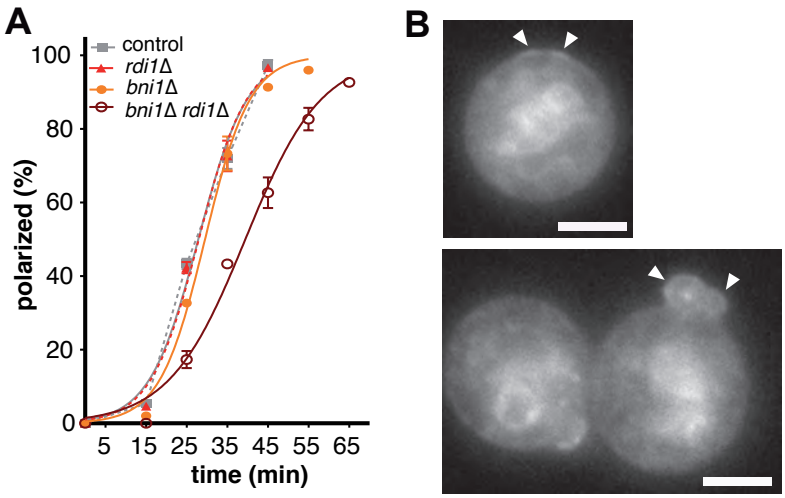

Figure 2.22: Role of Bni1 and Rdi1 in cell polarization. (A) Polarization kinetics of Cdc42 in control cells, *rdi1*Δ, Δ*bni1* and Δ*bni1 rdi1*Δ mutants. Data for each time point (mean ± SD) are based on the analysis of three individual experiments with 50 cells each. **(B)** Example for split-cap (top) and split-bud formation (bottom) in Δ*bni1 rdi1*Δ cells. Scale bar: 4 µm.

cling, we additionally deleted *RDI1* and monitored polarization kinetics (Fig. 2.22 A). While

Cdc42 in *bni1*Δ cells polarized with almost the same kinetics and efficiency as in control and *rdi1*Δ cells, polarization in the *bni1*Δ *rdi1*Δ double mutant was slower (Fig. 2.22 A). Moreover, 5 % of *bni1*Δ*rdi1*Δ cells exhibited a split-bud phenotype (Fig. 2.22 B, bottom), indicating that fast actin cable dynamics mediated by the formin Bni1 are required to focus Cdc42 into a single polarization site. (These results were published in Yu et al. 2011)

2.6 A stochastic model for Cdc42 recycling

The stochastic model was developed and contributed by Ben Klünder, Department of Physics, LMU. Munich.

The combination of multiple feedback loops and recycling mechanisms render it difficult to predict effects of specific changes in our system of Cdc42 polarization. We generated a stochastic particle-based model explicitly describing the dynamics of Cdc42 polarization in yeast cells to verify whether the experimentally determined interactions were able to create a robust and unique symmetry axis. We assumed instant equilibration of Cdc42

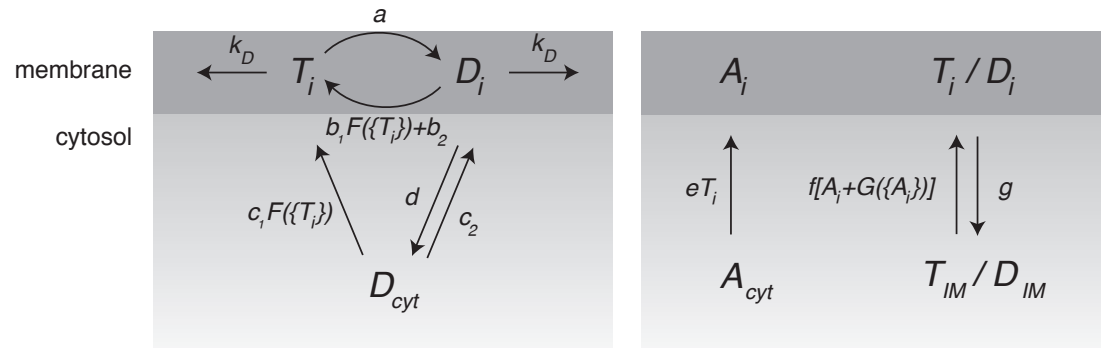

Figure 2.23: Schematic depiction of model reactions. Schematic depiction of the model reactions describing the GDI-mediated recycling pathway, the Cdc42 GTPase cycle (left) and the actin-mediated recycling pathway (right).

in the cytosol and lateral diffusion in the plasma membrane with a diffusion constant D = 0.036 $\mu m_2/s$ (Marco et al. 2007). Nucleotide-exchange could occur spontaneously or catalyzed by Cdc24 and was subject to a thresholded positive feedback loop involving Bem1 (Irazoqui et al. 2003; Wedlich-Soldner et al. 2004). GTP hydrolysis depended on GAP activity and we implemented selective Cdc42-GDP extraction from the plasma membrane by Rdi1. Membrane recruitment from the cytosolic Rdi1/Cdc42-GDP pool was

implemented as a second positive feedback loop to represent competition between GEF and GDI. Finally, a coarse grained description of actin-dependent endocytosis and directed exocytosis was used based on our previous approach (Wedlich-Soldner et al. 2003), where sites of focused exocytosis were randomly generated with a rate depending on the concentration of Cdc42-GTP. Endocytosis was modelled with a constant extraction rate. All model parameters were taken from the literature, our own measurements, or fitted to reproduce characteristic experimental observations of cap shape, polarization efficiency and FRAP rates (Fig. 2.23). We initially adjusted the model to reproduce characteristics of the individual recycling pathways (LatB-treated or *rdi1*Δ cells).

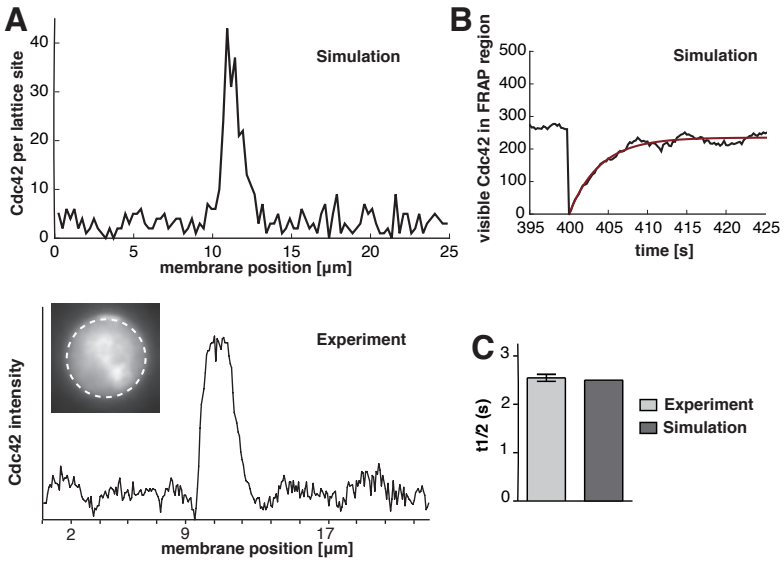

Figure 2.24: Simulation of the Rdi1 pathway. (A) Simulated (top) and experimental (bottom) cap profiles (linescan along dotted lines) of LatB-treated cells. **(B)** Representative simulated FRAP recovery curve of LatB-treated cells. **(C)** Comparison of half-life († 1/2) of experiment (light grey) and simulation (dark grey) of LatB-treated cells. Experimental bar graph corresponds to the mean $\pm$ SEM. N $\geq$ 10.

Our mathematical model was able to separately produce Rdi1-dependent (Fig. 2.24) or actin-dependent (Fig. 2.25) polarization of Cdc42. The model could generate polarized caps with realistic shape (Fig. 2.24 A, B; Fig. 2.25 A, B) and FRAP dynamics (Fig. 2.24 C, D; Fig. 2.25 C, D).

The model accurately generated control cells with cap shape (Fig. 2.26 A, B) and protein dynamics (Fig. 2.26 C, D) comparable to experimental data when both pathways

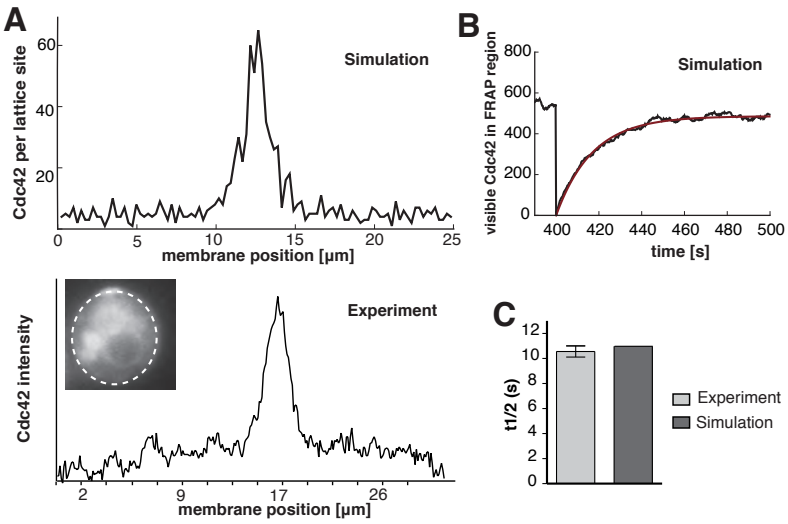

Figure 2.25: Simulation of the actin pathway. (A) Simulated (top) and experimental (bottom) cap profiles (linescan along dotted lines) of *rdi1*Δ cells. **(B)** Representative simulated FRAP recovery curve of *rdi1*Δ cells. **(C)** Comparison of half-life (t 1/2) of experiment (light grey) and simulation (dark grey) of *rdi1*Δ cells. Experimental bar graph corresponds to the mean $\pm$ SEM. N $\geq$ 10.

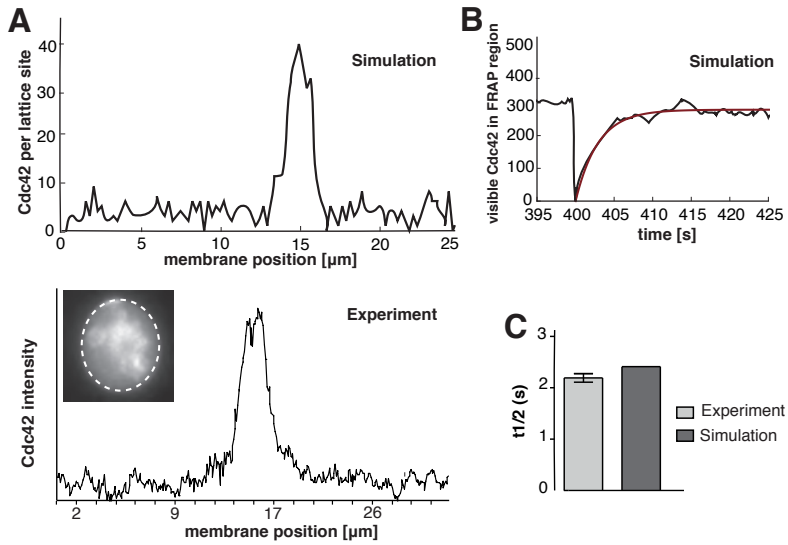

Figure 2.26: Simulation of control cells. (A) Simulated (top) and experimental (bottom) cap profiles (linescan along dotted lines) of control cells. **(B)** Representative simulated FRAP recovery curve of control cells. **(C)** Comparison of half-life (t 1/2) of experiment (light grey) and simulation (dark grey) of control cells. Experimental bar graph corresponds to the mean $\pm$ SEM. N $\geq$ 10.

were combined . The model predicted a reduction in polarization efficiency (Fig. 2.27 A) and FRAP dynamics (Fig. 2.27 B) upon decreased GTP hydrolysis rates as GDI-mediated extraction was restricted to Cdc42-GDP. These predictions were consistent with out experimental results, which showed slower protein dynamics in hydrolysis mutants (Fig. 2.10). Temporal and cell-to-cell variations in the hydrolysis rate could also explain the reduced polarization efficiency (Fig. 2.6 B) and unstable caps (Wedlich-Soldner et al. 2004) observed in LatB-treated cells.

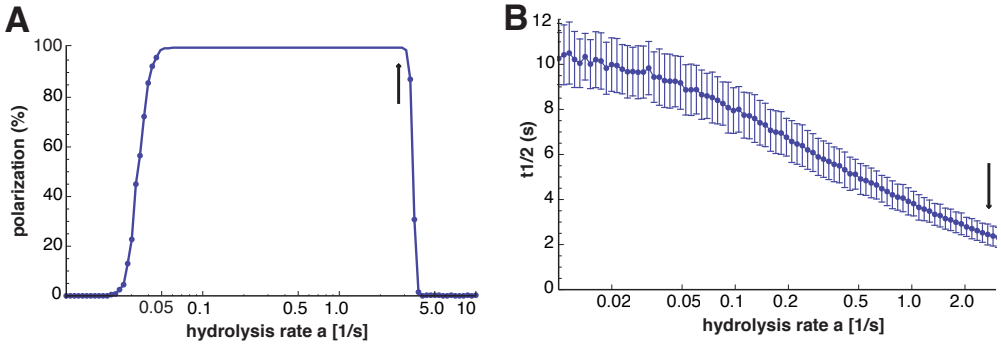

Figure 2.27: Model predictions on polarization efficiency and FRAP recovery half-life. (A) Plot of predicted polarization efficiency in the presence of LatB in dependence of the GTP hydrolysis rate. The arrow represents the estimated hydrolysis rate for control cells. **(B)** Plot of predicted Cdc42 FRAP half-life in dependence of the GTP hydrolysis rate. Error bars correspond to one SD. The arrow represents the estimated hydrolysis rate for control cells.

The GDI recycling pathway alone never generated more than one stable polarization site, consistent with our observations of LatB-treated cells. However, yeast cells are certainly capable of simultaneously polarizing in two or more sites. For example after deletion of *BEM2* (Knaus et al. 2007), deletion or overexpression of *BEM1* (Kozubowski et al. 2008; Howell et al. 2009) or overexpression of constitutively active $Cdc42^{Q61L}$ (Wedlich-Soldner 2003). Formation of multiple polarization sites in the above mentioned examples depended on actin and increased Cdc42 activity. We found that 2.3 % of *rdi1*Δ cells formed two polarization sites and later two buds (Fig. 2.19 B, C). We used these results to fit free parameters in the actin-mediated recycling part of our model, creating multiple polarization sites (Fig. 2.28 A).

With these parameters the model generated two predictions. First, increased Cdc42 activation should increase the percentage of *rdi1*Δ cells forming multiple polarization sites (2.28 B, black curve). Second, even cells with functional GDI should form multiple

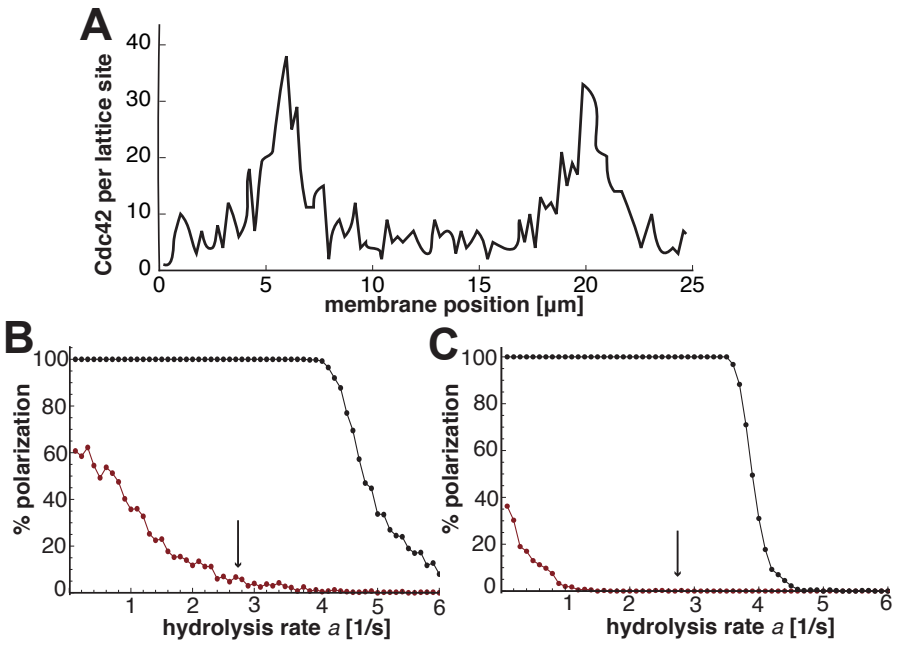

Figure 2.28: Model predictions on double buds. (A) Formation of two caps in the simulation of a *rdi1*Δ cell. **(B)** Effects of varying rates of GTP hydrolysis on total polarization (black) and formation of two (red) polarization sites in simulations of *rdi1*Δ cells. **(C)** Effects of varying rates of GTP hydrolysis on total polarization (black) and formation of two (red) polarization sites in simulations of control cells. Arrows: hydrolysis rate predicted for control cells.

caps if GTP hydrolysis was sufficiently reduced (2.28 B, red curve). Our experiments could confirm these predictions (Fig. 2.19; Fig. 2.20).

2.7 Timing aspects of cell polarization

Timing of cell polarization is tightly regulated with the cell cycle and requires precise activation and inactivation of polarity regulators by cell cycle signals. So far, it is unknown in which timely order Cdc42 and its regulators cluster at the polarization site and how the cap is formed on a single-cell level.

2.7.1 Polarity regulators polarize on different time scales

To investigate the order of appearance of polarity regulators, we performed polarization assays on endogenously GFP-tagged Cdc42, Cdc24, Bem1 and Bem2. We found that 10-12 % of the cells expressing Cdc24 and Bem1 were polarized during G1/S arrest, whereas no Bem2 or Cdc42 signal was visible at that time point (Fig. 2.29 A). While the majority (over 90 %) of Bem1 and Cdc24 cells were polarized after 35 min, cells expressing Cdc42 or Bem2 polarized with 10 min delay (Fig. 2.29 A). Interestingly, although polarization kinetics and timing appear to vary among polarity regulators, protein dynamics were approximately the same (Fig. 2.29 B).

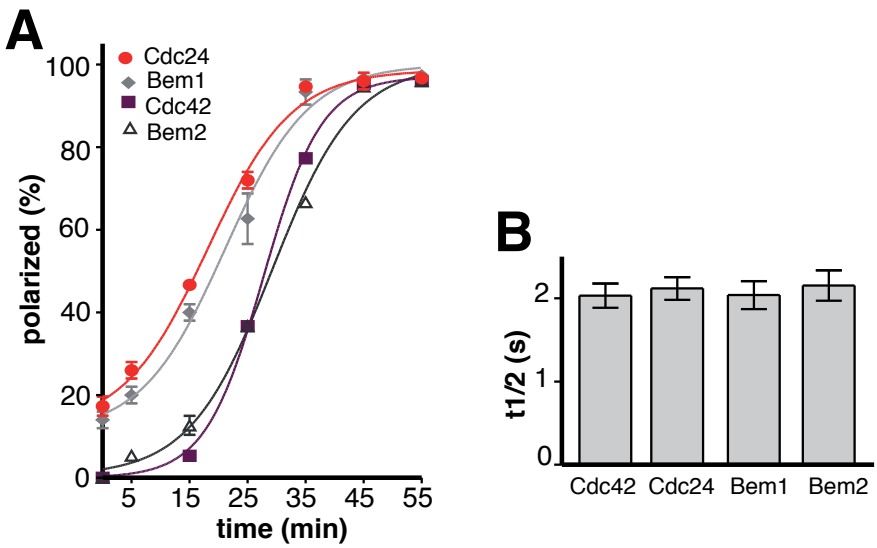

Figure 2.29: Polarization kinetics and protein dynamics of polarity regulators. (A) Polarization kinetics of endogenously GFP-tagged Cdc24, Cdc42, Bem1 and Bem2. Data for each time point (mean ± SD) are based on the analysis of three individual experiments with 50 cells each. **(B)** Average half-life (t 1/2) of endogenously GFP-tagged Cdc24, Cdc42, Bem1 and Bem2. Bar graph corresponds to the mean ± SEM. N ≥ 10.

2.7.2 Cap formation of polarity regulators

The polarization assay is a valuable method to elucidate protein kinetics and compare polarization behaviour between different strain populations. Yet, no information on cap and bud formation can be obtained with this method. To gain insights on the process of cap and bud formation on a single-cell level, we arrested cells as previously described, but transferred them onto glass bottom dishes one hour prior to release of G1 arrest. Then we performed time-lapse microscopy on Cdc42 and its regulators Bem1, Cdc24 and Bem2.

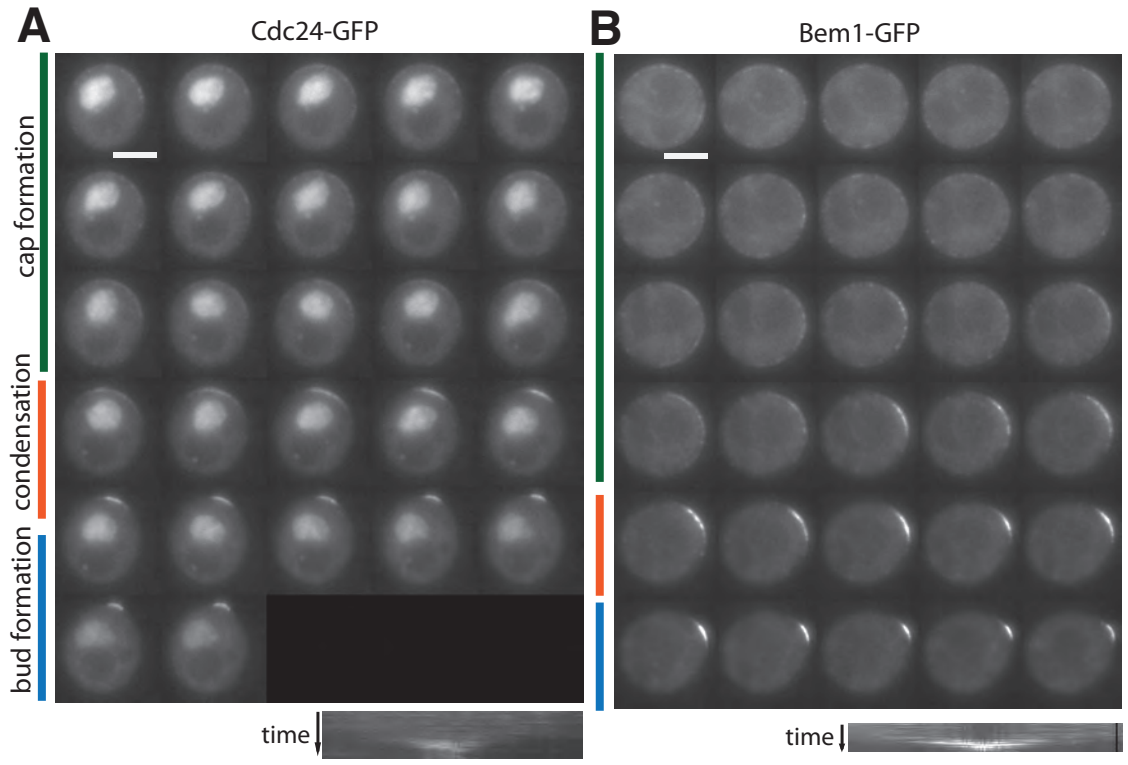

Figure 2.30: Cdc24 and Bem1 cap formation. (A) Montage of time-lapse acquisition of Cdc24 (expression of two copies of Cdc24-GFP) cap formation. Kymograph indicates cap condensation over time. **(B)** Montage of time-lapse acquisition of Bem1 (expression of ectopically integrated Bem1-GFP) cap formation. Kymograph indicates cap condensation over time. **(A)** and **(B)** Time-lapse acquisition was started shortly after release from G1/S arrest. Maximum projection of 2 individual planes with 0.4 µm increment. Framerate: 1 min. Scale bar: 4 µm.

Cdc24 and Bem1 were subjected to time-lapse microscopy right after release from G1. Interestingly, pre-polarized cells displayed wide caps in a patch-like pattern for 12-15 min until caps started to condense with an intensifying signal before the bud started to form

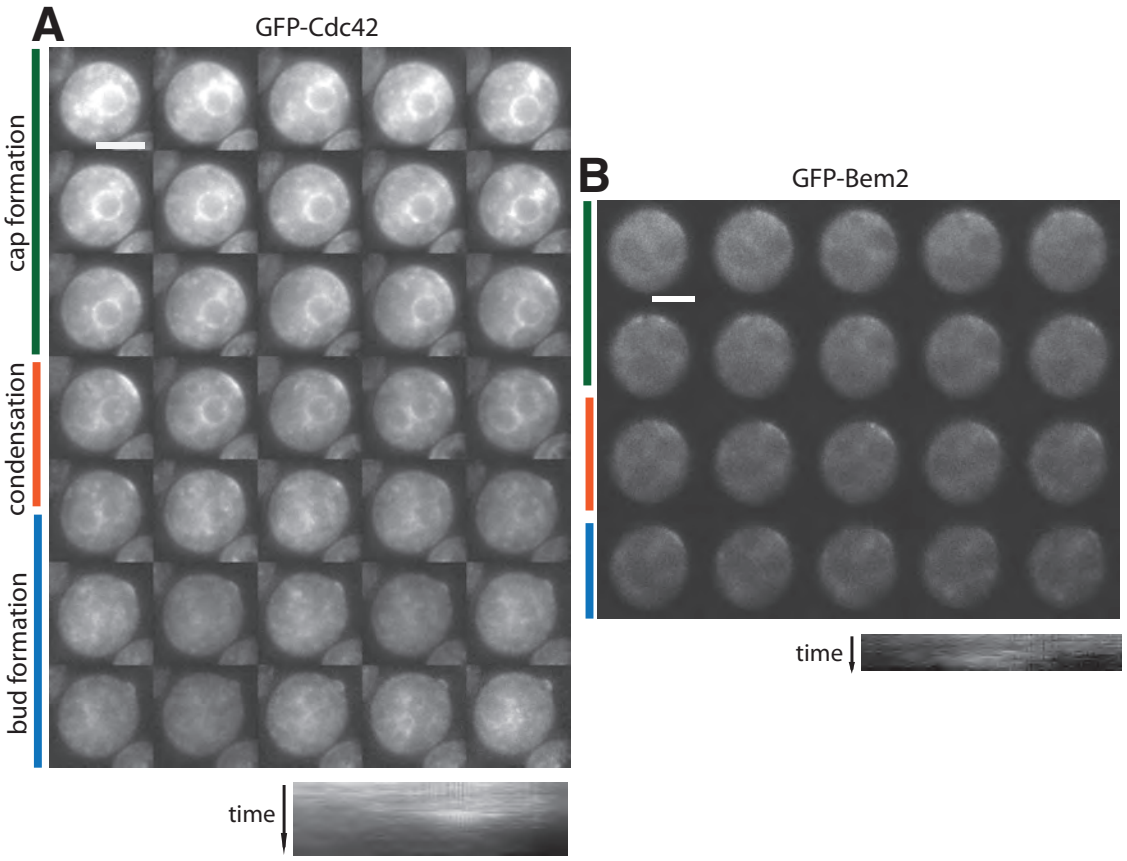

Figure 2.31: Cdc42 and Bem2 cap formation. **(A)** Montage of time-lapse acquisition of Cdc42 (expression of ectopically expressed GFP-Cdc42) cap formation. Kymograph indicates cap condensation over time. Maximum projection of three planes with 0.4 µm increment. **(B)** Montage of time-lapse acquisition of Bem2 (expression of endogenously tagged GFP-Bem2) cap formation. Kymograph indicates cap condensation over time. Maximum projection of four planes with 0.4 µm increment. **(A)** and **(B)** Time-lapse acquisition was started 15 min after release from G1/S arrest. Framerate: 1 min. Scale bar: 4 µm.

(Fig. 2.30 A, B). Cap formation behaviour was very similar in Cdc24 and Bem1 expressing cells, following a continuous three step process with cap formation, cap condensation and bud formation (Fig. 2.30 A, B). Once the caps had formed, they were very bright, with little cytosolic signal in both strains (Fig. 2.30 A, B). In Cdc24 expressing cells, a decreasing GFP-Cdc24 signal in the nucleus indicated relocation to the polarization site (Fig. 2.30 A). Polarization assays revealed delayed Bem2 and Cdc42 polarization compared to Cdc24 and Bem1 (Fig. 2.29). Hence, we started time-lapse acquisition of Bem2 and Cdc42 cells 15 min after release in order to avoid unnecessary photobleaching. Cdc42 caps were difficult to observe at early time points because of the high cytosolic pool and high sig-

nal on internal membranes (Fig. 2.31 A). Similar to Cdc24 and Bem1 cells, the cap remained wide for 14-15 min before it started to condense and subsequently formed a bud (Fig. 2.31 A). Hence, Cdc42 also polarized in three steps comprised of cap formation, condensation and bud formation. Bem2 localization in the cap appeared much more diffuse and less intense compared to Cdc24 and Bem1 cells (Fig. 2.31 B). Nevertheless, cap establishment followed the three-step process that was also observed in Cdc24, Bem1 and Cdc42 cells (Fig. 2.30; Fig. 2.31).

2.7.3 Rapid polarization of Cdc24 and Cdc42 depends on Bem1 and Bem2

Polarization assays of Cdc24 and Cdc42 in *bem1*Δ and *bem2*Δ cells revealed that polarization was significantly delayed compared to control cells (Fig. 2.32 A, B). Furthermore, no pre-polarization of Cdc24 and Bem1 was observed in *bem2*Δ cells (Fig. 2.32 B).

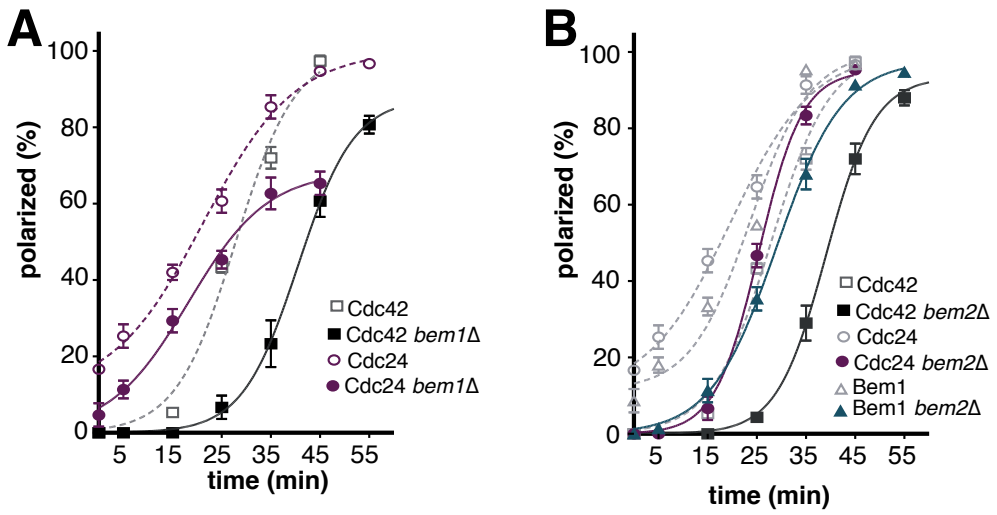

Figure 2.32: Polarization kinetics in *bem1*Δ and *bem2*Δ cells. **(A)** Polarization kinetics of Cdc24 and Cdc42 in control and *bem1*Δ cells. **(B)** Polarization kinetics of Cdc24, Cdc42 and Bem1 in *bem2*Δ cells. **(A)** and **(B)** Data for each time point (mean ± SD) are based on the analysis of three individual experiments with 50 cells each.

We observed wide caps localizing in a patch-like pattern in *bem2*Δ cells expressing Cdc24 25 min after G1/S release using time-lapse microscopy. In contrast to control cells, Cdc24 caps in *bem2*Δ cells remained wide with shoulders until bud formation (Fig. 2.33). These results indicate that Bem2 is required for Cdc24 cap condensation.

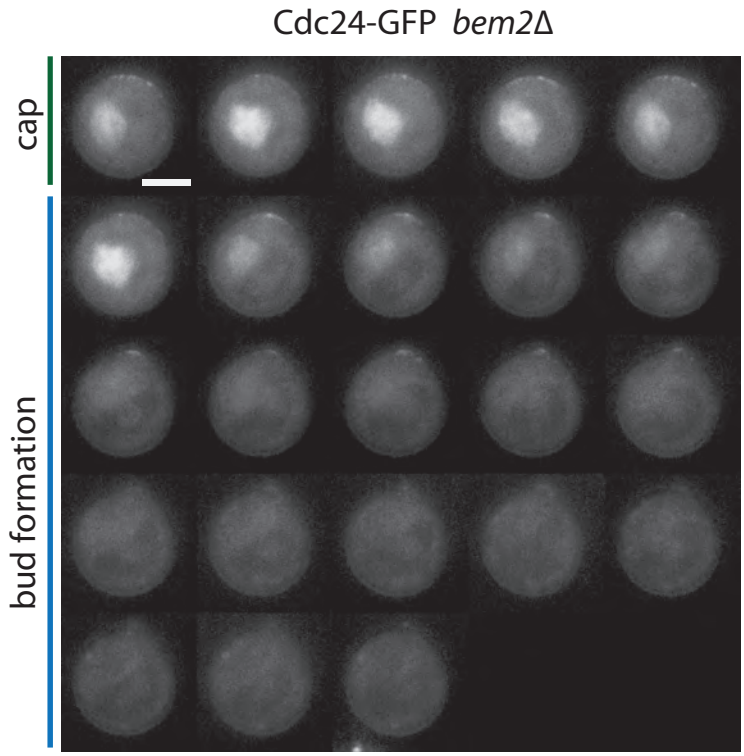

Figure 2.33: Cdc24 cap formation in *bem2*Δ cells. Montage of time-lapse acquisition of Cdc24 (expression of two ectopically integrated copies of Cdc24-GFP) cap formation. Time-lapse acquisition was started 20 min after release from G1/S arrest. Maximum projection of three planes with 0.4 µm increment. Framerate: 1 min. Scale bar: 4 µm

2.7.4 Polarization initiation depends on cell cycle signals

To investigate the nature of GAP activity on polarization kinetics we performed washout experiments (Fig. 2.19 A), exploiting the naturally occurring cell cycle dependent activation of Cdc42 at G1/S transition. This requires activation of the GEF (Arkowitz 1999) and inactivation of the GAPs (Knaus et al. 2007). We expected polarization kinetics to be higher in washout experiments because during LatB treatment, Cdc24 has already been released from the nucleus (Arkowitz 1999) and Bem2 is already hyperphosphorylated (Knaus et al. 2007). In order to accurately measure polarization kinetics, we used *rdi1*Δ cells as they completely failed to polarize when treated with LatB (Fig. 2.6 B). After washout of LatB, Cdc42 polarization in *rdi1*Δ was initiated earlier and was also faster compared to polarization in a normal polarization assay (Fig. 2.34). These results confirmed that Cdc24 and Bem2 regulation, possibly through cell cycle signals, is involved in

the timing and speed of Cdc42 polarization.

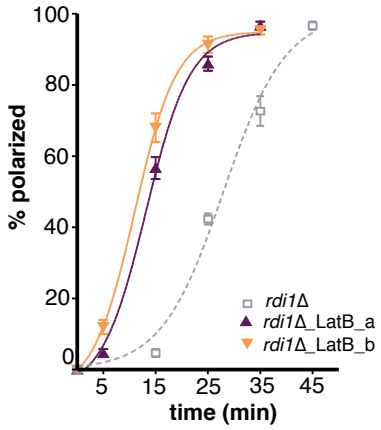

Figure 2.34: Polarization kinetics in washout experiments. Polarization kinetics of Cdc42 in *rdi1*Δ cells during washout experiments. Cells were treated for 20 min (LatB a) or 40 min (LatB b) before washout of the drug. Data for each time point (mean ± SD) are based on the analysis of three individual experiments with 50 cells each.

3 Discussion

Major progress has been previously made in identifying and characterizing the key players and individual pathways involved in cell polarization. The results presented in this study give new insights in the interplay of different feedback loops involved in Cdc42 recycling in the context of polarity establishment (Fig. 3.1). We found that actin-dependent transport and GDI-dependent recycling act redundantly to exchange Cdc42 at the sites of polarized growth. Furthermore, we have shown that the GTPase cycle influences Cdc42 extraction mediated by Rdi1. Uniqueness of polarization is compromised in extraction and hydrolysis mutants. Moreover, we found that efficient GTPase cycling with tightly regulated GDP exchange and GAP activity is essential to focus Cdc42 into a single polarization site. A stochastic particle-based model was able to recapitulate measured parameters and predict changes in protein dynamics and polarization efficiency in cells with reduced hydrolysis.

We compared the polarization behaviour and kinetics of major polarity regulators and found that they appear at different time points at the polarization site. Single-cell time-lapse microscopy of those regulators revealed that formation of a polarization site and the subsequent bud follows a continuous three-step process comprised of cap formation, cap condensation and bud formation. Interestingly, this process is altered in cells lacking Bem2. Furthermore, we found the timing and kinetics of polarity establishment strongly depend on the cell cycle dependent regulation of Cdc24 and Bem2.

3.1 Actin and GDI: Two pathways for Cdc42 recycling

The role of actin in polarity establishment in the absence of spatial cues has been controversially debated. In contrast to actin-independent, Bem1-mediated polarity establishment in *rsr1*Δ cells (Irazoqui et al. 2003), symmetry breaking mediated by the constitutively active Cdc42^{Q61L} in G1 arrested cells strongly depends on actin (Wedlich-Soldner et al. 2003). A more recent publication suggested that only the combination of an actin-mediated and a Bem1-mediated feedback loop promotes spatial and temporal robustness (Wedlich-Soldner et al. 2004).

We now found an additional redundant pathway for cell polarization by performing a

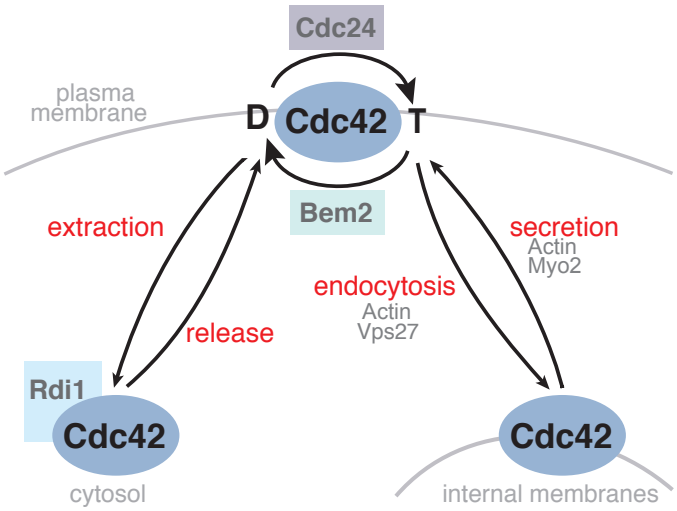

Figure 3.1: Model for polarity establishment. Schematic depiction of involved pathways and proteins required for polarity establishment. D and T indicate GDP and GTP-bound form of Cdc42. Arrows between D and T indicate GTPase cycling, which is facilitated by the GEF Cdc24 and the GAPs (only Bem2 is depicted). Arrows between Rdi1-bound Cdc42, membrane-bound Cdc42 and Cdc42 at the plasma membrane represent physical recycling pathways.

synthetic lethal screen. Polarity regulators displayed many genetic interactions with actin-dependent transport components, supporting the essential role of actin in polarity establishment. The genetic interaction between the RhoGDI Rdi1 and actin-dependent transport suggested the existence of redundant pathways for the physical recycling of Cdc42. Analysis of polarization efficiency revealed that Cdc42 polarization became completely actin dependent in the absence of Rdi1. A major criticism in treating the cells with the actin-depolymerizing drug LatB was the complete block of actin and possible resulting artifacts. Hence, we used a temperature-sensitive mutant (*myo2-16*) of the vesicle-transport adaptor Myo2 in order to further confirm the proposed redundancy and, at the same time, avoid the radical block of actin-polymerization. This mutant, in combination with Rdi1 depleted cells, also resulted in the complete loss of polarization. Although we were not able to identify a mutant that selectively blocked endocytosis, we observed reduced polarization efficiency and protein dynamics in a mutant compromised in late endocytic recycling. Furthermore, GFP-Cdc42 expressed in this mutant accumulated in aberrant endocytic compartments, indicating that endocytosis is indeed involved in active Cdc42

recycling. The observed effects were stronger in combination with *rdi1*Δ, further supporting the suggested redundancy and reinforcing actin's important contribution to polarity establishment.

While many studies have shown that GDI extracts Cdc42 from membranes *in vitro* and *in vivo* (Hoffman et al. 2000; Cole & McLaughlin 2007; Koch et al. 1997; Richman et al. 2004; Tiedje et al. 2008; Slaughter et al. 2009), no obvious phenotype for a *RDI1* deletion mutant has been reported so far. Indeed, polarization kinetics and efficiency of Cdc42 in *rdi1*Δ cells resembled those of control cells. This could be explained by the existence of the proposed redundant pathway for Cdc42 recycling. Our FRAP data revealed slow Cdc42 fluorescence recovery in *rdi1*Δ cells, whereas Cdc42 in LatB treated cells recovered within the time range of control cells, suggesting that GDI mediates a fast pathway for Cdc42 recycling. These findings agree with a study on maintenance of cell polarity, which showed that GDI-mediated rapid recycling of Cdc42 acts in parallel to actin-dependent transport in order to maintain polarity and preserve cap morphology (Slaughter et al. 2009). GDIs have long been considered as negative regulators due to their biochemical characteristics such as inhibiting the dissociation of GDP from small GTPases (Chuang et al. 1993) and extracting them from membranes into the cytosol (Nomanbhoy & Cerione 1996). The finding that Rdi1 promotes fast protein dynamics of Cdc42 suggests that GDIs regulate Cdc42 in a positive rather than in a negative manner. We found that Cdc42 extraction through GDI- and actin-dependent transport represent two recycling mechanisms for Cdc42, whereby each pathway displays distinct characteristics. While the GDI pathway alone is responsible for fast Cdc42 recycling, it fails to polarize in 40 % of the cells. The actin pathway alone is much slower regarding Cdc42 protein dynamics, but ensures efficient polarization through vesicle transport along stable actin cables. Yet, this particular robustness of actin cables sometimes leads to the formation of two polarization sites (Section 3.3). Only the combination of actin- and GDI-dependent recycling promotes robust Cdc42 polarization with high fidelity.

3.2 GDI and the GTPase cycle

FRAP experiments on the inactive Cdc42^{D57Y} and the constitutively active Cdc42^{Q61L} mutant revealed slow recovery half-times, indicating that the GTPase cycle influenced the

high exchange rate of Cdc42 at the site of polarization (Wedlich-Soldner et al. 2004). We were able to confirm the slow recovery of inactive and constitutively active mutants. However, we used a different strain background and expressed the mutants under the endogenous Cdc42 promoter in order to avoid overexpression artifacts. Furthermore, we used a different constitutively active point mutant of $Cdc42^{G12V}$ since the $Cdc42^{Q61L}$ mutant was lethal to cells under the control of the endogenous promoter.

Interestingly, we found that $Cdc42^{G12V}$ localized in stable patches at the cell cortex. The stable patches and the slow recovery time of $Cdc42^{G12V}$ might depend on effector interactions, which prevent the protein from being endocytosed (Slaughter et al. 2009). In line with our results, fluorescence cross correlation spectroscopy (FCCS) data showed that the GDI interacts with Cdc42 in the cytoplasm but showed weak interaction with $Cdc42^{D57Y}$ and $Cdc42^{Q61L}$ (Slaughter et al. 2009), indicating that Cdc42 has to cycle in order to get extracted by the GDI.

Controversial results have been published regarding which nucleotide bound form of Cdc42 is extracted by the GDI. While the structure of RhoGDIs indicated no preference for any nucleotide-bound state of the RhoGTPase (Hancock & Hall 1993; Nomanbhoy et al. 1999), the GDP-bound form displayed a 10-fold higher affinity to the RhoGDI than the GTP-bound form (Johnson et al. 2009). However, a different group observed preferential extraction of the constitutively active GTP-bound form of Cdc42 after *RDI1* overexpression (Tiedje et al. 2008). Our *in vitro* extraction assays from liposomes revealed that the GDP-bound form of Cdc42 gets extracted 10 times faster than the GTP-bound form. In addition, we found that Cdc42-GTP in the presence of a GAP domain dissociated with approximately the same speed as the GDP-bound form, indicating that GTP-hydrolysis is the rate-limiting step for GDI-mediated Cdc42 extraction.

3.2.1 GDI and the GTP hydrolysis

We found a genetic interaction between *RDI1* and *BEM2* in our synthetic lethal screen, further supporting the *in vitro* results that GDI-dependent extraction of Cdc42 requires GTP hydrolysis. Interestingly, of the four Cdc42 GAPs, Bem2 displayed the largest number of genetic interactions with actin-related transport components. This suggests that this GAP plays an important role during polarity establishment, whereas the other GAPs might be

involved in later stages of polarized growth such as maintaining cell morphology or organization of the septin ring (Perez 2010; Caviston & Longtine 2003). This would also explain the altered morphology of *bem3*Δ cells and the reduced number of genetic interactions between *RDI1* and the other GAPs. Moreover, Cdc42 dynamics in *rga2*Δ and *bem3*Δ were similar to protein dynamics in control cells, indicating that these GAPs have no influence on the GDI-dependent recycling. Cdc42 polarization in *bem2*Δ cells was strongly actin-dependent, suggesting that GTP hydrolysis is essential for efficient cell polarization of the GDI-pathway. Moreover, the slow protein dynamics of Cdc42 in *bem2*Δ and of the slow hydrolyzing $Cdc42^{G60A}$ mutant represent additional *in vivo* experiments, further supporting the idea that GTP hydrolysis is required for GDI-dependent Cdc42 recycling.

3.2.2 GDI and GEF activity

In vitro liposome binding experiments revealed that the Rac1 GEF domain DHR2C in the presence of non-hydrolysable GTP analogue was able to dissociate the GDI-Rac1 complex, resulting in increased Rac1 binding to liposomes. Correspondently, liposome extraction assays showed that GEF exchange activity was reduced in the presence of the GDI, which is consistent with a GEF-GDI competition for binding to the switch II region of Rho GTPases (Schoebel et al. 2009; Ugolev et al. 2008). These results indicate that GEF activity interferes with binding of GDI to Rho GTPases thereby increasing GTPase binding to membranes. Similar observations were made in the small GTPase Rab1. A Rab1-specific GEF, transferred by the bacterial pathogen *L. pneumophilia* named DrrA, was necessary and sufficient to displace Rab1 from its GDI (Wu et al. 2010). Interestingly, the bacterial DrrA displays both GEF and GDF (GDI-displacement factor) activity towards Rab1 and both activities are required for Rab1 recruitment to membranes (Ingmundson et al. 2007). It remains to be elucidated, whether eukaryotic GEFs of other small GTPases contain specific domains with similar functions.

Our *in vitro* experiments showed that GDI-dependent extraction of Cdc42 from membranes depended on GEF activity. When we analyzed the effect of GEF activity *in vivo*, we found that an increase of GDP exchange activity in control cells did not significantly change polarization efficiencies or recovery times of Cdc42. This might be explained by a possible physical limit of Cdc42 and its regulators at a half-life of 2 s, since Cdc42, Bem1,

Bem2 and also Cdc24 all showed comparable recovery times of 2 s. Surprisingly, increase of GEF activity had a significant effect on protein dynamics in hydrolysis mutants. Protein dynamics were faster compared to *bem2*Δ cells with normal GDP exchange activity. This result was surprising as an increased GEF amount was expected to lead to elevated Cdc42-GTP levels, hence, less extraction of Cdc42-GDP by Rdi1 and slower Cdc42 protein dynamics in the cap.

Cdc24 overexpression was expected to globally decrease Cdc42-GDP amounts, however, recruitment of Cdc24 in the cap is a non-linear process depending on a Cdc42-GTP-, Bem1-mediated feedback loop (Gulli et al. 2000; Butty et al. 2002; Bose et al. 2001). Intensity comparisons of Cdc24 revealed that the amount of Cdc24 was not altered by *BEM2* deletion or Cdc24 overexpression, suggesting that the amount of Cdc24 recruitment to the cap is limited and could not be further increased through higher exchange activity. Nevertheless, Cdc24 overexpression is expected to increase Cdc42-GTP in all other locations except the cap and Cdc42 recruitment to membranes outside the cap would be increased through competition with the GDI. The resulting free GDI-molecules would then be available to extract Cdc42 from the cap, leading to faster protein dynamics. This hypothesis was supported by a Cdc42 mutant with high intrinsic GDP exchange activity ($Cdc42^{F28L}$), which also displayed faster protein dynamics in hydrolysis mutants.

Our *in vitro* and *in vivo* data showed that an active GTPase cycle is required for efficient GDI-mediated Cdc42 recycling. We conclude that both GEF and GAP activity have to be tightly regulated in order to allow rapid exchange between membranes and the cytosol.

3.3 Singularity in polarization

We demonstrated that formation of a single polarization site relies on fast GTPase cycling and GDI-dependent recycling of Cdc42. Formation of two polarization sites was only observed in actin-containing cells, suggesting that orientation and formation of actin cables to two different cortical sites promotes the essential stability to form a bud. Recently, Howell et al. suggested that artificially rewired cells, which depend on actin for symmetry breaking, formed two polarization sites due to slow competition of two polarization clusters (Howell et al. 2009). This was based on theoretical predictions according

to a "winner-takes it all" principle (Goryachev & Pokhilko 2008). This mathematical model differed from our theoretical simulations (Section 3.5) and we never observed two initial foci merging into a single polarization site in our experiments.

We found some *rdi1*Δ cells displayed two Cdc42 caps that later formed two buds, indicating fast recycling is required to focus Cdc42 into a single polarization site. Moreover, 8.7 % of Cdc42 *bem2*Δ displayed two buds, suggesting that also efficient hydrolysis is required for unique polarization. Cdc24 displayed an even higher number (10 %) of cells with two buds in line with previously published data (Knaus et al. 2007), indicating that Bem2 is required to restrict Cdc24 activation to bud emergence. Interestingly, neither *bem3*Δ nor *rga2*Δ cells displayed a significant number of cells with double buds. These results support the hypothesis that those GAPs are not as important for polarity establishment as Bem2, but rather fulfill their functions in later stages of cell polarization.

The role of Cdc42 hydrolysis in budding frequency has been addressed earlier for mutants with an amino acid exchange at the 60 residue analyzed in a *cdc42*Δ background (Caviston et al. 2002). These mutants appeared to be slow hydrolyzing and hyperactive, resulting in a multi budded phenotype. We also analyzed a slow hydrolyzing Cdc42 mutant (G60A). The reason for us not to detect a significant number of cells with two buds might lie in the recessiveness of the mutant. We integrated $Cdc42^{G60A}$ in addition to the wild-type copy, which probably takes over to regulate budding frequency. In contrast to dominant lethal mutants bearing an amino acid exchange at the residue 61, the hyperactive mutants were still able to undergo (reduced) cycling, explaining their viability.

Furthermore, we have shown that GDP exchange activity strongly influences the frequency of double bud formation in cells compromised in GTP hydrolysis or GDI recycling. Cells lacking Rdi1 or Bem2 with increased GDP exchange activity displayed higher numbers of cells with double buds compared to *rdi1*Δ and *bem2*Δ with normal exchange activity. These findings suggest that Cdc42 has to cycle efficiently and rapidly at the same time in order to ensure only one budding event per cell cycle. In line with our results, mathematical modelling predicted that optimally maintained GEF and GAP concentrations ensure maximized GEF activity and rapid turnover at the same time (Goryachev & Pokhilko 2006).

3.4 The role of actin dynamics

A study from our group revealed that Bni1 mediates fast actin dynamics in unpolarized cells, whereas slower cable polymerization in polarized cells depended on both formins Bnr1 and Bni1 (Yu et al. 2011). Polarization assays in a *rdi1*Δ *bni1*Δ double mutant revealed slower and less efficient polarization of Cdc42, further supporting the proposed redundancy between actin-dependent and GDI-dependent recycling. Moreover, some *rdi1*Δ *bni1*Δ cells displayed a split-bud phenotype, which might arise from stabilized actin cables directing Cdc42-containing vesicles to opposite sites of the septin ring, mediated by the other formin Bnr1 (Pruyne et al. 2004). These results indicate that fast reorganization of actin cables in unpolarized cells contributes to focus Cdc42 into a single polarization site.

3.5 Mathematical model

We generated a stochastic particle-based model that was able to realistically recapitulate our measured parameters and made a number of accurate predictions. First, protein dynamics and polarization dynamics in the presence of LatB were decreased when GTP hydrolysis was reduced. Second, changes in the number of polarization sites upon increased Cdc42 activation and decreased extraction or hydrolysis lead to an increased percentage of cells growing two buds. While other models focus on polarity maintenance and cap morphology (Marco et al. 2007; Slaughter et al. 2009), our model recapitulates and predicts events and changes in Cdc42 recycling during polarity establishment. A conceptual model based on a single feedback for Cdc42 recruitment with Cdc42 polarity establishment being the result of stochastic fluctuations, predicted that polarization efficiency depended on Cdc42 expression levels (Altschuler et al. 2008). However, we could not confirm their observations when we repeated the same experiment. A Turing-type model for polarity establishment was able to generate stable GDI-mediated Cdc42 polarization through highly cooperative recruitment of the GEF to Cdc42-GTP on the membrane (Goryachev & Pokhilko 2008). This would predict that the protein dynamics of Cdc24 would depend on Cdc42 activity, a prediction we could not confirm. In summary, our model accurately reflected experimentally made observations regarding

the robust cell polarization mediated by the actin pathway in combination with the high fidelity governed by the GDI-pathway.

3.6 The role of lipids in polarity establishment- a side note

While our study focused mainly on recycling mechanisms for Cdc42 that contribute to establishment of cell polarization, we have not considered the role of lipids. Phosphoinositols such as PtdIns(4,5)P2 and PtdIns(1,4,5)P3 have been shown to regulate small GTPases and cell polarity and Phosphatidylethanolamine (PE) and Phosphatidylserine (PS) have been recently implied to play a role in polarity establishment.

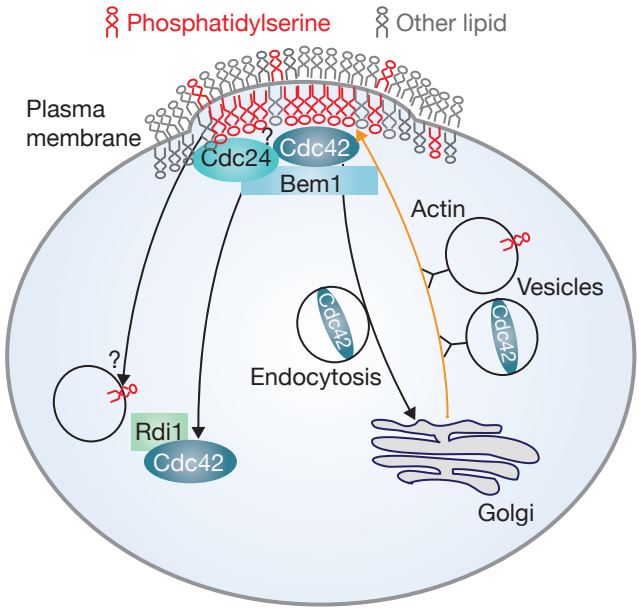

Figure 3.2: Lipids in polarity establishment. Schematic depiction of the role of lipids in polarity establishment. Lipid bilayer with Phosphatidylserine (PS) and other lipids is indicated around the polarization site. PS is concentrated at the inner leaflet of the membranes. Vesicles are represented as black circles. Cdc42 and PS have are transported along actin cables (orange arrow) towards the polarization site. Membrane extraction by its GDI Rdi1 is indicated. The role of PS endocytosis and recycling on its polar localization remain unclear. The extent to which electrostatic interactions between PS and Cdc42, Cdc24 or Bem1 contribute to polarized localization of Cdc42 and PS remains to be determined. This figure is taken from Freisinger and Wedlich-Söldner 2011.

While PE is mainly concentrated in the outer leaflet (Yeung et al, 2008), PS appears to be enriched in the inner leaflet of the plasma membrane (Saito et al. 2007). This asymmetric distribution of lipids depends on the activity of flippases. The flippase complex

Lem3 Dnf1/2 has been suggested to regulate GAP activity by flipping PE from the outer leaflet to the inner leaflet of the PM (Iwamoto et al. 2004; Saito et al. 2007). PE remains on the outer leaflet and Cdc42 remains polarized at the bud tip In the absence of flippase activity, resulting in hyper-polarized growth due to missing GAP activity (Saito et al. 2007). More recently, PS has been implicated in regulating polarity establishment. PS is localized at the incipient bud site similar to the localization of polarity markers (Fairn et al. 2011). Moreover, in the absence of the PS synthase Cho1 the number of budded cells was significantly decreased and Cdc42 and Bem1 were only localized properly in a small percentage of cells (Fairn et al. 2011). PS might play an important role in concentrating Cdc42 directly at the membrane by changing the Cdc42 diffusion rate, mediated by a direct lipid-protein interaction. This interaction could be facilitated by the positively charged geranylgeranyl moiety of Cdc42 and the anionic PS. Active recycling of PS through endocytosis, secretion and possibly GDI, similar to Cdc42, could also contribute to PS polarization (Fig. 3.2) Yet, it is also possible that the PS-mediated localization of Cdc42 is a secondary effect of PS binding to other polarity regulators that contain a PH or PX domain such as Cdc24, Bem1 or Boi1/Boi2. The link between lipids, such as PS and PE to the polarization machinery orchestrated by Cdc42 might be an exciting task for future research (Freisinger & Wedlich-Soldner 2011).

3.7 Timing of cell polarization

Polarization assays and time-lapse microscopy revealed that polarity regulators arrive at the polarization site at different time points. While the scaffold-protein Bem1 and the GEF Cdc24 are pre-polarized, the GAP Bem2 and Cdc42 arrive approximately 15 min later at the polarization site, suggesting that Bem2 and Cdc42 are recruited by Bem1 and Cdc24. It has been previously shown that Cdc24 is relocated from the nucleus to the polarization site, where it binds to Bem1 and Cdc42-GTP (Shimada et al. 2000; Butty 2002). It would make sense for Cdc24 and Bem1 to be at the polarization site prior to Cdc42 in order to provide a platform for the other polarity regulators. The cap remains very broad during those early phases of Bem1 and Cdc24 polarization, displaying a patchy distribution. The increase of cap intensity might correlate with Cdc42 arrival at the polarization site, which leads to stabilization of the polarization site through the proposed feedback loop (Gulli et

al. 2000; Bose et al. 2001; Butty et al. 2002). Bem2 arrives at the polarization site approximately at the same time as Cdc42. In order to more accurately determine the timing of polarity regulators relative to each other, two-colour time-lapse movies would be required. Interestingly, polarity regulators protein dynamics are the same even though their timing is different, suggesting high exchange rates of all polarity regulators are essential for efficient and dynamic polarity establishment.

Although the polarization assay proved to be a valuable method to determine and compare polarization kinetics and behaviour between different strain populations, it does not allow us to draw any conclusions on the process of cap/bud formation on a single-cell level. We performed time-lapse microscopy on the polarity regulators Cdc42, Cdc24, Bem1 and Bem2 to resolve the process of cap/bud formation and observed a continuous three step process for polarization. All polarity regulators displayed initial broad caps (step 1) that started condensing (step 2) before bud formation (step 3). We found this three step process to be altered in cells lacking Bem2. The cap-condensation step is missing and the broad cap directly formed the bud. These results indicate that Bem2-mediated hydrolysis is required for the condensation step.

Polarization assays of Cdc42 in *rdi1*Δ cells after washout revealed earlier and faster polarization, indicating that not only Cdc42 activity but also polarization speed is increased. This effect probably results from overruled cell cycle dependent Cdc24 activation and GAP inactivation at the G1/S transition in washout experiments. Tight regulation of polarity regulators such as Cdc24 and Bem2 through cell cycle signals appears to be eminent for the timing of cell polarization. It has been suggested that the GAPs are phosphorylated by Cdk1 at bud emergence (Sopko et al. 2007; Knaus et al. 2007; Zheng & Cerione 1994). While only Rga2 and Bem3 have been shown to be direct targets of Cdk1 (Sopko et al. 2007; Knaus et al. 2007), it remains to be investigated whether Bem2 is also directly phosphoryated by Cdk1.

3.7.1 Timing-Outlook

The link between the cell cycle and polarity establishment remains an interesting target for future investigations. *In vivo* and *in vitro* phosphorylation targets of Cdk1 have been identified in several studies. For example, Cdc24 is phosphorylated by Cdk1 both *in vitro*

and *in vivo* (McCusker et al. 2007; Gulli et al. 2000; Bose et al. 2001; Wai & Gerber 2009), however no *in vivo* effect has been observed so far. Either, the specific phosphorylation site on Cdc24 has not been identified yet or a different protein represents the link between the cell cycle and polarity establishment. Bem1 is also phosphorylated by Cdk1 *in vitro* and *in vivo*, but mutations of a conserved consensus site only resulted in defective vacuole biogenesis rather than defective bud emergence (Han et al. 2005). A promising candidate might be the PAK kinase Cla4, which forms a complex with Bem1, Cdc24 and Cdc42-GTP (Gulli et al. 2000; Bose et al. 2001; Butty et al. 2002). Cla4 phosphorylation depends on a Clb2-Cdk1 complex during mitosis (Tjandra & Compton 1998), but it remains unclear whether Cla4 might also be phosphorylated by Cdk1 during G1 and whether this phosphorylation would impact polarity establishment. Identification of possible consensus sites, subsequent mutation and phenotypic analysis could help to characterize Cla4 as a possible candidate that links cell polarity establishment to the cell cycle.

4 Materials and Methods

4.1 Materials

4.1.1 Strains

Bacteria

***Echerichia coli* strain** The *E.coli* DH10B (Invitrogen) used for molecular cloning, is a derivative from the original *E.coli* strain K12: *F^- endA1 recA1 galE15 galK16 nupG rpsL Δ lacX74Φ 80lacZΔ M15 araD139 Δ (ara,leu)7697mcrAΔ (mrr-hsdRMS-mcrBC)λ^-*

Yeast

***Saccharomyces cerevisiae* strains** Unless otherwise stated, all yeast strains used in this work were derived from a W303 strain expressing only one G1 cyclin (Cln2) under the control of a methionine repressible promoter (RWS 116). All strains used in this study were haploids.

Table 4.1: Yeast strains

STRAIN	GENOTYPE	SOURCE
RWS116	MATa *cln1*Δ::HisG *cln2*Δ *cln3*Δ ::HisG YipLac204- MET-CLN2::TRP1 ura3 his3-11,15 ade2-1 can1-100	Gulli et al., 2000
RWS119	pGal-myc-GFP-CDC42::URA3 (RWC21)	Wedlich-Soldner et al. 2004
RWS1421	pCDC42-myc-GFP-CDC42::URA3 (RWC108)	this study
RWS794	pCDC24-CDC24-GFP::hphNT1	lab collection
RWS1017	*bem3*Δ::G418pCDC42-myc-GFP-CDC42::URA3 (RWC108)	this study
RWS1018	*bem1*Δ::G418	this study
RWS1020	*bni1*Δ::G418	this study
RWS1021	*bni1*Δ::G418 pCDC42-myc-GFP-CDC42::URA3 (RWC108)	this study
RWS1023	pCDC42-myc-GFP-CDC42^{D57Y}::URA3 (RWC686)	this study
RWS1024	pCDC42-myc-GFP-CDC42^{R66E}::URA3 (RWC689)	this study
RWS1026	*bem1*Δ::G418 pCDC42-myc-GFP-CDC42::URA3 (RWC108)	this study

Table 4.1: Yeast strains (continued)

STRAIN	GENOTYPE	SOURCE
RWS1028	*bem2*Δ::G418	this study
RWS1029	*bem1*Δ::G418pCDC24-CDC24-GFP::LEU2 (RWC153)	this study
RWS1030	*bem1*Δ::G41 pCDC24-CDC24-GFP::LEU2 (RWC153) pCDC24-CDC24-GFP::URA(RWC146)	this study
RWS1031	*bem2*Δ::G418pCDC42-myc-GFP-CDC42::URA3(RWC108) p42-GFP-Cdc42::LEU2 (RWC151)	this study
RWS1422	pCDC24-CDC24::LEU2(RWC153)	lab collection
RWS1034	pCDC42-GFP-CDC42::cloNAT	this study
RWS1423	*rdi1*Δ::LEU2pCDC42-myc-GFP-CDC42::URA3 (RWC108)	this study
RWS1035	*bem2*Δ::G418pCDC42-myc-GFP-CDC42::URA3 (RWC108)	this study
RWS1042	*bem3*Δ::G418pCDC42-myc-GFP-CDC42::URA3 (RWC108)	this study
RWS1035	*rga2*Δ::G418pCDC42-myc-GFP-CDC42::URA3 (RWC108)	this study
RWS1038	*vps27*Δ::G418pCDC42-myc-GFP-CDC42::URA3 (RWC108)	lab collection
RWS1039	*rdi1*Δ::LEU2 *vps27*Δ::G418 pCDC42-myc-GFP-CDC42::URA3 (RWC108)	lab collection
RWS1047	*myo2-16* pCDC42-myc-GFP-CDC42::URA3 (RWC108)	lab collection
RWS1048	*rdi1*Δ::LEU2pCDC42-myc-GFP-CDC42::URA3 (RWC108)	lab collection
RWS1036	pCDC42-myc-GFP-CDC42^{G60A}::URA3(RWC688)	this study
RWS1037	pCDC42-myc-GFP-CDC42^{G12V}::URA3(RWC687)	this study
RWS1040	pCDC24-CDC24-GFP::LEU2(RWC153)pCDC24-CDC24-GFP::URA(RWC146)	this study
RWS1029	*bem2*Δ::G418pCDC24-CDC24-GFP::LEU2(RWC153)	this study
RWS1041	*bem2*Δ::G418pCDC24-CDC24-GFP::LEU2 (RWC153) pCDC24-CDC24-GFP::URA (RWC146)	this study
RWS1045	pBem1-Bem1-GFP::URA3(RWC138)	lab collection
RWS1046	pBem2-GFP-Bem2::cloNAT	this study
RWS786	pBem1-GFP-Bem1::cloNAT	this study
RWS1091	*bem2*Δ::G418pBem1-GFP::URA3 (RWC138)	this study
RWS1094	*bem1*Δ::G418 pBEM2-GFP-BEM2::LEU2 (RWC706)	this study
RWS1096	pCDC24-CDC24-GFP::URA(RWC146)pBEM2-mRFP-Ruby-BEM2::LEU2 (RWC707)	this study

Table 4.1: Yeast strains (continued)

STRAIN	GENOTYPE	SOURCE
RWS1097	pCDC42-myc-GFP-CDC42::URA(RWC108) pBEM2-mRFP-Ruby-BEM2::LEU2 (RWC707)	this study
RWS1099	pCDC42-myc-GFP-CDC42::URA3 (RWC108) p42-GFP-Cdc42::LEU2 (RWC151)	this study
RWS1110	pGal-myc-GFP-CDC42^{G12V}::URA3 (RWC127)	this study
RWS1135	pCDC42-myc-GFP-CDC42F28L::URA3 (RWC790)	this study
RWS1136	*bem2*Δ::G418pCDC42-myc-GFP-CDC42F28L::URA3 (RWC790)	this study
RWS1088	pCDC42-myc-GFP-CDC42::URA(RWC108)pCdc24Cdc24mRFP-Ruby::LEU2 (RWC723)	this study
RWS1424	pCDC42-myc-GFP-CDC42::URA(RWC108)pCdc24Cdc24mRFP-Ruby::LEU2 (RWC723)	this study

4.1.2 Kits

Agarose Gel Extraction Kit (Jena Bioscience) for DNA-fragment isolation

Agarose Gel Extraction Kit (Promega) for DNA-fragment isolation

ClonJET™ (Fermentas) for PCR product cloning

TOPO TA cloning® (Invitrogen) for PCR product cloning

EZNA™ (Omega Bio-Tek) Plasmid Mini Kit for plasmid minipreparation

QiAGEN® Plasmid Mini Kit (QIAGEN) for plasmid minipreparation

4.1.3 Enzymes and proteins

Table 4.2: Enzymes

ENZYME	SOURCE
Bovine Serum Albumin	Sigma
Concanavalin A	Roth
Pfu DNA Polymerase	Fermentas
Phusion DNA Polymerase	Finzymes
Restriction enzymes	New England Biolabs
RNAse A	Amersham
Taq DNA Polymerase	Biolabs
T4 DNA Ligase	Biolabs
Vent® (exo-) DNA Poymerase	Biolabs
Zymolyase	Biomolecule

4.1.4 Nucleic acids

Salmon sperm carrier DNA (Invitrogen) was used for plasmid and PCR product transformation of yeast.

GenRulers™ 1 kb DNA Ladder and GeneRuler™ DNA ladder mix were used as size standards for agarose gel-electrophoresis.

Table 4.3: Primer

NAME	5′-3′ SEQUENCE	DESCRIPTION
RWS650	AGCAAAACTTATAAAACAAGAAATAAACGTATTAGCTCTTCC ACAAAATGcgtacgctgcaggtcgac	Cdc42 genomic GFP integration
RWS651	CACGTTTTCCCAACAGCACCATCACCGACAACAACACACT TTAGCGTTTGCatcgatgaattctctgtcg	Cdc42 genomic GFP integration
RWS618	TCCGGATTTGTGGAAGAGCTAATACGTTTATTTC	Cdc42 promoter with BspEI
RWS617	GAGCTCCAGGCCGGAACTCAAAAGG	Cdc42 promoter with SacI
RWS655	AAGAAATGTTGGCGGAAAACAATGAGAAATTCTTGAACATTC GTCTGTATcgtacgctgcaggtcgac	Cdc24 genomic GFP integration
RWS654	GTTTTTTTCTTGAATTATTTAGTATTTGCTGTATACTAGTTTTA TTTATCAatcgatgaattcgagctcg	Cdc24 genomic GFP integration

Table 4.3: Primer (continued)

NAME	5′-3′ SEQUENCE	DESCRIPTION
RWS1112	GAGCGCAACGCAATTAATG	Cdc42 amplification from RWC 21
RWS73	CTGCCCTTTCGAAAGATC	Cdc42 amplification from RWC 21
RWS1110	GATATGACAAGGGTCTCAATTCATCGTAATCTTC TTGACCG	R66E mutation primer
RWS1109	GAAGATTACGATGAATTGAGACCC TTGTCATATC	R66E mutation primer
RWS1112	GAGCGCAACGCAATTAATG	Cdc42 amplification from RWC 21
RWS73	CTGCCCTTTCGAAAGATC	Cdc42 amplification from RWC 21
RWS1540	GGAACATAGTCGGCTGGCAATTGA TTCGTTGTATAG	F28L mutation primer
RWS1539	CTATACAACGAATCAATTGCCAGCCGA CTATGTTCC	F28L mutation primer
RWS677	TCCGGATTATATGGCTTTCTTGACAA TTTC	Bem1 promoter with BspEI
RWS676	GAGCTCCGAGAACGGCATCACATC	Bem1 promoter with SacI
RWS670	CTGCCCTTCGACCCATTACTATCTCTT TTTG AGAGTTTGAAGTTTTTTCAGCatcgatgaattctctgtcg	Bem1 genomic GFP integration
RWS669	CACGTTGAAAGCACTGTGTGAAAAGAATTGT CAAGAAAGCCATATAAATGcgtacgctgcaggtcgac	Bem1 genomic GFP integration
RWS1030	GGATCCTAGACTCCTGCTTCGTT ATTTG	Bem2 promoter with BamHI
RWS1029	CTCGAGCACAAGATATCAGACG GCTC	Bem2 promoter with XhoI
RWS1038	GCGGCCGCTTATTGCTTGAAATAAT CATTTGG	Bem2 with NotI
RWS1037	ACGCGTATGAAAGGTCTTCTCT GGTC	Bem2 with MluI
RWS679	TCCGGATAGACTCCTGCTTCGTT ATTTG	Bem2 promoter with BspEI
RWS678	GAGCTCCTTCACAGACTCTTCTG GTG	Bem2 promoter with SacI
RWS271	CTAGCACTGGCCGTTGAAGATTTCCTGTTCT TAGACCAGAGAAGACCTTTCatcgatgaattctctgtcg	Bem2 genomic GFP integration
RWS270	CTTTTCTGGATAGACACAAAAAAAACAAATA ACGAAGCAGGAGTCTAATGcgtacgctgcaggtcgac	Bem2 genomic GFP integration
RWS962	GGTACCCAACTTTACATTTG	Bem1 deletion primer
RWS961	GTTATTCGACATTCTTCCCG	Bem1 deletion primer
RWS104	GAGAAAGTATCTTTGGGCTG	Bem1 deletion test primer
RWS134	GTTACAGGTGAACATTCATG	Bem1 deletion test primer

Table 4.3: Primer (continued)

NAME	5′-3′ SEQUENCE	DESCRIPTION
RWS989	GAAGTTTGAGATGCTGTTGC	Bem1 deletion test primer
RWS988	CAGCAGCAGCAGCAATCC	Bem1 deletion test primer
RWS347	AGGCAAGAGATCAGGCGGAAAGA	Bem2 deletion primer
RWS346	AGAAGCAAGCTACGTTGCAGCCA	Bem2 deletion primer
RWS885	CAGGTTTCATTGGAGGTGC	Bem2 deletion test primer
RWS265	GGTGCTCAACAATTCAGTTCT	Bem2 deletion test primer
RWS352	GCACCAACATACCGTTTTGC	Bem2 deletion test primer
RWS351	TGATGGTAAATCCCGTCCTGC	Bem2 deletion test primer
RWS626	CCTTCTTTATCTCAGCTCTTC	Bem3 deletion primer
RWS1058	TCAAGATTGTTAAATACATCAAC	Bem3 deletion primer
RWS1142	GTAAAGTACCAGATAAGAACC	Bem3 deletion test primer
RWS625	GTTGTACTTGAGAAAGTTGC	Bem3 deletion test primer
RWS295	TTTTATTATTACAAATATAT	Bem3 deletion test primer
RWS297	ACATACATATCCAGTAACAA	Rga1 deletion primer
RWS296	AAATTTTTAAGAAACTGAAA	Rga1 deletion primer
RWS1204	ACTGGCTAATTCATTGAACG	Rga1 deletion test primer
RWS1203	GTAGAGCCTCTTTCATAGAC	Rga1 deletion test primer
RWS1202	CAAGTGAATTGTTGACCTCG	Rga1 deletion test primer
RWS630	GCCTAAGAGATTAAGTGGG	Rga2 deletion primer
RWS629	CTACCATTAAACAACGACAAG	Rga2 deletion primer
RWS292	ACCTTTTCACACCCTGAACT	Rga2 deletion primer
RWS291	CTTTGCATACTTGGCGTTTG	Rga2 deletion test primer
RWS1081	TGCTACAGCTGCAAGTGAC	Bni1 deletion primer
RWS1080	CTTCCTACAGATAAGAGGAC	Bni1 deletion primer
RWS418	CTGAAGATTTACCATCGCCATC	Bni1 deletion test primer
RWS417	GCTGTTGTTGGGATGCATAGGTC	Bni1 deletion test primer
RWS416	CCCGACATCGGTTAGAGGAAG	Bni1 deletion test primer
RWS98	CACGGAGCCTACCTTTTAG	Vps27 deletion test primer
RWS97	GTTCGTGTGGTTAGACAAC	Vps27 deletion test primer
RWS207	TGATGCTTTGTAGCTGTTGCTC	Vps27 deletion test primer
RWS206	AGAGAAGCTGAAGAAGCGAAGC	Vps27 deletion test primer

Table 4.3: Primer (continued)

NAME	5′-3′ SEQUENCE	DESCRIPTION
RWS343	TGAAATGCTTCTGAGCGAAGC	Vps27 deletion test primer
RWS342	TCAAATGCCTTGCTGACCACT	Vps27 deletion test primer
RWS48	GTATTCTGGGCCTCCATG	KanMX test primer
RWS47	GATACTAACGCCGCCATC	KanMX test primer
RWS1247	TGAGCTGCGCACGTCAAG	KanMX test primer
RWS1246	TGGTCGCTATACTGCTGTC	KanMX test primer
	CGACTCACTATAGGGAGAGCGGC	Sequencing
	AAGAACATCGATTTTCCATGGCAG	Sequencing

Table 4.4: Plasmids

NAME	ORIGIN	DESCRIPTION	SOURCE
RWC21	pRS306	GFP-CDC42 under the control of Gal promoter in a pRS306 backbone for integration into the URA3 locus after linearization	Wedlich-Soldner et al, 2004
RWC108	pRS306	GFP-CDC42 under the control of the endogenous CDC42-promoter in a pRS306 backbone for integration into the URA3 locus after linearization	Wedlich-Soldner et al, 2004
RWC127	pRS306	GFP-CDC42^{G12V} under the control of Gal promoter in a pRS306 backbone for integration into the URA3 locus after linearization	lab collection
RWC138	pRS306	Bem1-GFP under the control of the endogenous Bem1-promoter in a pRS306 backbone for integration into the URA3 locus after linearization	M.Peter
RWC146	pRS316	CDC24-GFP under the control of the endogenous CDC24-promoter in a pRS316 backbone URA3-CEN plasmid	lab collection
RWC148	pRS305	pRS305 backbone for integration into the LEU2 locus after linearization	lab collection
RWC151	pRS305	GFP-CDC42 under the control of the endogenous CDC42-promoter in a pRS305 backbone for integration into the LEU2 locus after linearization	lab collection

Table 4.4: Plasmids (continued)

NAME	ORIGIN	DESCRIPTION	SOURCE
RWC153	pRS305	CDC24-GFP under the control of the endogenous CDC24-promoter in a pRS305 backbone for integration into the LEU2 locus after linearization	Wedlich-Soldner et al, 2004
RWC233	pYM-25	plasmid for C-terminal direct tagging, hphNT1,	Janke et al, 2004
RWC257	pYM-N4	plasmid for N-terminal direct tagging, cloNAT,	Janke et al, 2004
RWC550	pYM-N4	plasmid for N-terminal direct tagging, cloNAT under the control of the endogenous CDC42 promoter	Janke et al, 2004
RWC582	pYM-N4	plasmid for N-terminal direct tagging, cloNAT under the control of the endogenous Bem1 promoter	Janke et al, 2004
RWC583	pYM-N4	plasmid for N-terminal direct tagging, cloNAT under the control of the endogenous Bem2 promoter	Janke et al, 2004
RWC686	pRS306	GFP-CDC42^{D57Y} under the control of the endogenous CDC42-promoter in a pRS306 backbone for integration into the URA3 locus after linearization	this study
RWC687	pRS306	GFP-CDC42^{G12V} under the control of the endogenous CDC42-promoter in a pRS306 backbone for integration into the URA3 locus after linearization	this study
RWC688	pRS306	GFP-CDC42^{G60A} under the control of the endogenous CDC42-promoter in a pRS306 backbone for integration into the URA3 locus after linearization	this study
RWC689	pRS306	GFP-CDC42^{R66E} under the control of the endogenous CDC42-promoter in a pRS306 backbone for integration into the URA3 locus after linearization	this study
RWC706	pRS315	GFP-Bem2 under the control of the endogenous Bem2-promoter in a pRS315 backbone LEU2 CEN plasmid	this study
RWC707	pRS315	mRFP-Ruby-Bem2 under the control of the endogenous Bem2-promoter in a pRS315 backbone LEU2 CEN plasmid	this study

Table 4.4: Plasmids (continued)

NAME	ORIGIN	DESCRIPTION	SOURCE
RWC723	pRS305	CDC24-mRFP under the control of the endogenous CDC24-promoter in a pRS305 backbone for integration into the LEU2 locus after linearization	this study
RWC790	pRS306	GFP-CDC42F28L under the control of the endogenous CDC42-promoter in a pRS306 backbone for integration into the URA3 locus after linearization	this study

4.1.5 Chemicals and reagents

Table 4.5: Chemicals

DESCRIPTION	SOURCE
Acetic acid	Sigma
Agarose	Invitrogen
Ampicilin	Carl Roth GmbH
L-Alanin	VWR
Alexa Fluor 568 Phalloidine	Invitrogen
Ammonium chloride	Alfa Aesar
Ammonium hydrogen carbonate	Alfa Aesar
Ammonium nitrate	Carl Roth
Ampicillin sodium salt	Carl Roth
L-Arginin	VWR
L-Asparagin-Monoydrate	VWR
L-Aspartic acid	Sigma
Calcium chloride	Serva
ClonNAT	Werner
Chloroform	Carl Roth
Concavalin A	Carl Roth
L-Cysteine	VWR
Demethyl sufoxide (DMSO)	Sigma

Table 4.5: Chemicals (continued)

DESCRIPTION	SOURCE
Deoxynucleotide Solution mix	New England Biolabs
Difco Bacto Agar	Becton Dickinson
Difco Bacto Peptone	Becton Dickinson
Difco Bacto Tryptone	Becton Dickinson
Difco Yeast Extract	Becton Dickinson
dNTP Set, 100 mM Solution	Fermentas
DTT	Fermentas
EDTA (Titriplex)	Merck
EGTA	Roth
Genticin	Roth
D(+)-Glucose	VWR
L-Glutamine	PAA
Glycerin 86 % (w/v) p.a.	Roth
Hygromycin B	Merck
Kanamycin Sulfate	Invitrogen
Latrunculin B	Merck
Lectin from concanavalin A	Sigma
L-Leucin	VWR
Lipofectamine 2000	Invitrogen
Lithium acetate dihydrate	SIGMA
L-Lysin-Monohydrat	VWR
Magnesium chloride-Hexahydrate	Roth
Magnesium sulfate-Heptahydrate	Roth
2-Mercaptoethanol	Sigma
L-Methionine	VWR
Sodium azide	Sigma
Sodium chloride	Merck
Sodium dihydrogenphosphate	Roth
Sodium fluoride	Sigma
di-Sodium hydrogenphosphate	Sigma

Table 4.5: Chemicals (continued)

DESCRIPTION	SOURCE
Nicotinic acid	Alfa Aesar
dNTP Set, 100 mM solutions	GE Healthcare
N-(3-triethylammoniumpropyl)-4-(4-(dibutylamino) - styryl) pyridinium dibromide	Invitrogen
Paraformaldehyd 37 % (w/v)	Alfa Aesar
L-Phenylalanine	VWR
Pimaricin, streptomyces chattanoogensis	Merck
Polyethyleneglycol (PEG2000)	SIGMA
Potassium hydride	Alfa Aesar
Rhodamine phalloidine	Invitrogen
ROTI-Phenol/Chloroform/Isoamyl	Carl Roth
Rubidiumchloride	Sigma
Salmon Sperm DNA	Invitrogen
SDS	Roth
L-Serine	VWR
Salmon Sperm DNA	Eppendorf AG
Sodium azide	Sigma
Sodium bicarbonate solution	Sigma
Sodium carbonate	Sigma
Sodium hydride	Sigma
Sodium sulfate anhydrous	Alfa
D(-)-Sorbitol	VWR
L-Threonine	VWR
Tris, HCl	Merck
Triton X-100	Roth
L-Tryptophan	VWR
L-Tyrosine	VWR
L-Valine	VWR

Table 4.5: Chemicals (continued)

DESCRIPTION	SOURCE
Yeast Nitrogen Base Becton	Dickinson

4.1.6 Buffers and solutions

Table 4.6: Buffers and Solutions

DESCRIPTION	RECIPE
Ampicilin solution	10 mg/ml Ampicilin In double distilled sterile H_2O
clonNAT solution	20 % (w/v) clonNAT In double distilled sterile H_2O
Concavalin A coating solution	0.5 mg/ml Concanavalin A 10 mM Potassium Phosphate buffer pH 6.0 1 mM $CaCl_2$ 0.02 % NaN_3
6x DNA Loading buffer	50 % (w/v) sucrose 0.25 % (w/v) bromophenol-blue in TE buffer
DNA precipitation buffer	3_2M NaOAc pH 4.8
EDTA solution pH 8.0	0.5 M EDTA Na_2EDTA x $2H_2O$ pH 8.0
Geneticin solution	200 mg/ml Geneticin In double distilled sterile H_2O
Hygromycin B solution	50 mg/ml Hygromycin In sterile PBS
10x Ligase buffer	50 mM $MgCl_2$ 660 mM Tris-HCl 10 mM DTT 10 mM ATP pH 7.5
Lysis buffer	2 % (v/v) Triton X-100 1 % (w/v) SDS 100 mM NaCl 10 mM Tris-HCl 1 mM EDTA
MOPS	20 mM MOPS 8 mM NaOAc 1 mM EDTA pH 6.8
Sodium phosphate buffer	1 M NaH_2PO_4 1 M NaH_2PO_4 pH 7.0
10x PBS buffer	92 mM NaH_2PO_4 147 mM K_2PO_4 27 mM KCl 1.39 M NaCl pH 7.2
10x Pfu buffer	200 mM Tris-HCl 100 mM KCl 100 mM $(NH4)_2SO_4$ 20 mM $MgSO_4$ 1 % Triton X-100 1 mg/ml BSA pH 8.8
PEG mix	100 mM LiOAc 10 mM Tris-HCl pH 8 1 mM EDTA 40 % (v/v) PEG 3350
Phenol chloroform	50 % Phenol 50 % Chloroform
Potassium phosphate buffer (10x)	1 M KH_2PO_4 1 M K_2PO_4 pH 7.0

Table 4.6: Buffers and Solutions (continued)

DESCRIPTION	RECIPE
RF1	100 mM RbCl 50 mM $MnCl_2$ 30 mM KOAc 10 mM $CaCl_2$ 15 % (w/v) Glycerol pH 5.8
RF2	10 mM MOPS 10 mM RbCl 75 mM $CaCl_2$
Rhodamine-Phalloidine staining solution	6.6 µM Rhodamine Phalloidine In Methanol
SORB	100 mM LiOAc 10 mM Tris-HCl 1 mM EDTA 1 M Sorbitol
50x TAE buffer	2 M Tris-Base 2 M Acetic Acid 50 mM EDTA pH 8.0
10x TBE buffer	440 mM Tris Base 440 mM Boric Acid 10 mM EDTA pH 8.0
10x TBS buffer	50 mM Tris-HCl 150 mM NaCl pH 7.5
10x TE buffer	10 mM Tris Base 1 mM EDTA pH 8.0
10x Thermopol buffer	500 mM KCl 15 mM $MgCl_2$ 100 mM Tris-HCl pH 8.3
1 M Tris buffer	619 mM Tris-HCl 38 mM Tris Base pH 8.0
VALAP	33 % Valine (w/w) 33 % Lanoline (w/w) 33 % Parafin (w/w)

4.1.7 Media

Table 4.7: Media

DESCRIPTION	RECIPE
YPD-Medium (liquid)	2 % (w/v) Bacto peptone 1 % (w/v) Bacto yeast extract 2 % (w/v) D(+)- Glucose
SD-Medium (liquid)	0.67 % (w/v) Bacto-yeast nitrogen base without amino acid 0.2 % (w/v) drop-out powder
Sporulation medium	0.1 % (w/v) Bacto yeast extract 1 % (w/v) KCl 0.05 % (w/v) D(+)- Glucose
YPD plates	2 % (w/v) Bacto peptone 1 % (w/v) Bacto yeast extract 2 % (w/v) D(+)- Glucose 0.8 % (w/v) Bacto agar
YPD plates + Geneticin	YPD plates 300 µg/ml Geneticin
YPD plates + Hygromycin B	YPD plates 300 µg/ml Hygromycin B
YPD plates + clonNAT	YPD plates 100 µg/ml clonNAT
SD-plate	0.67 % (w/v) Bacto-yeast nitrogen base without amino acid 0.2 % (w/v) drop-out powder 0.8 % (w/v) Bacto agar

Different combinations of drop-out powder were added to the synthetic drop-out (SD)

mix. To obtain the required amino acid concentration in the synthetic complete (SC) medium, the following amounts of amino acids were added:

Table 4.8: Amino acids

AMINO ACID	AMOUNT
Adenine sulfate	20 mg/l
Uracil	20 mg/L
L-tryptophan	20 mg/l
L-histidine	20 mg/l
L-arginine	40 mg/l
L-methionine	20 mg/l
L-tyrosine	50 mg/l
L-leucine	60 mg/l
L-isoleucine	60 mg/l
L-lycine	50 mg/l
L-phenylalanine	50mg/l
L-aspartic	100 mg/l
L-glutamic acid	100 mg/l
L-valine	150 mg/l
L-threonine	200 mg/l
L-serine	400 mg/l

4.1.8 Other materials

4.2 Microbiological and genetic methods

4.2.1 *Escherichia coli*

Culturing

E. coli strains were cultured either on YT plates or shaking in liquid at 200 rpm at 37 °C. For plasmid extraction, *E. coli* was grown shaking overnight in YT medium. Strains were stored at 4 °C on YT plates or -80 °C in 50 % glycerol.

Table 4.9: Other materials

DESCRIPTION	SOURCE
Coverslip	Menzel Gläser
Filter paper 3 MM	Whatman
Glassbeads	Sigma
Glassbottom dishes	MatTek
Glass slides	Menzel Gläser
Lense paper	Assistent
Petri dishes	Greiner
Plastic cuvettes	Brand
Pipet Tips	Qiagen

OD measurement

E. coli density of liquid cultures was determined photometrically at 600 nm wavelength using plastic cuvettes an a GeneSys spectrophotometer (Thermo Electron Corporation). YT medium was used as reference.

Preparation of competent *E. coli* using rubidium chloride

DH10B *E. coli* cultures were grown overnight in 5-10 ml LB medium at 37 °C and then transferred to 500 ml LB medium. Inoculated cultures were grown to OD600 0.5, and were cooled on ice for 15 min. The *E. coli* cultures were centrifuged at 4500 rpm in a Biofuge Primo R (Thermo Scientific) for 10 min. Supernatants were discarded and the pellets were resuspended in 30 µl RF1 (Tab. 4.6). The suspension was incubated on ice for 15 min, and then centrifuged at 4000rpm for 5 min. The pellets were resuspended in RF2 (table 4.6) on ice and aliquoted into 100 µl tubes and stored at -80 °C.

Chemical transformation of competent *E. coli*

50 µl-100 µl competent *E. coli* cells were thawed on ice before 1-10 µl of Plasmid (1-5 ng DNA) or ligation mix were added. The mixture was incubated on ice for 20-25 min followed by heat shock at 42 °C for 2 min. The cells were transferred on ice for 2 min. 150 µl YT or LB medium was added to cells and then plated out on YT or LB plates containing 100 µg/ml ampicillin. Plates were incubated overnight at 37 °C.

4.2.2 *S. cerevisiae*

Culturing

S. cerevisiae strains were cultured at 30 °C or RT either in liquid with 200 rpm shaking or on plates. Overnight cultures were grown in SD liquid medium to stationary phase and then diluted and grown to log phase for storage or experiments. Strains could be either stored longterm in 25 % glycerol at -80 °C or shorterm (2-3 weeks) on plates at RT.

OD measurement

The cell densities of liquid *S. cerevisiae* cultures were determined photometrically at 600 nm wavelength using plastic cuvettes and a GeneSys spectrophotometer (Thermo Electron Corporation). Culture medium was used as reference.

Transformation

S. cerevisiae strains were cultured overnight in 2-6 ml appropriate medium at 30 °C . The cultures were then transferred into 50 ml medium and grown at 30 °C until OD600 0.4 - 0.8. Cells were centrifuged at 1000 rpm for 5 min in a Biofuge Primo R (Thermo Scientific) and the pellets were first washed in 25 ml ddH_2O and then in 10 ml SORB solution. The pellets were resuspended in 360 µl SORB solution, aliquoted in 45 µl vials and either stored at -80 °C or directly used for transformation reactions.

For transformations salmon sperm carrier DNA was heated at 95 °C for 5 min and then added to the 45 µl competent cells. For transformation of PCR products 12 µl of reaction mix was added to the cells, for transformation of CEN plasmids 2-5 µl were added. Integrating plasmids were linearized in the selection marker region before 12 µl of the reaction mix were added to the cells. Then 300 µl PEG Mix was added and reactions were incubated for 30-60 min at 30 °C. Then 35 µl DMSO was added and the transformation mix was incubated at 42 °C for 15 min. Cells were centrifuged at 2000 rpm for 20 s and pellets were resuspended in 150 µl appropriate medium and plated on SD plates. When cells were transformed with an antibiotic-resistance cassette, 600 µl appropriate medium was added and cells were incubated overnight at RT. Cells were sedimented and resuspended in appropriate medium and plated on antibiotic containing SD plates.

Genetic manipulation

The ability of *S. cerevisiae* to undergo homologous recombination during DNA replication can be exploited to genetically manipulate a gene of interest. Therefore, PCR methods are used to either tag or delete the gene of interest. In order to manipulate a gene, primers were designed to generate fragments that include flanking regions of a target gene together with promoters, selection markers and tags. For C- and N-terminal tagging we used a commercially available toolbox (Janke et al. 2004), which allows the amplification of different combinations of promoters, selection markers and tags with a set of only four primers. For C-terminal tagging Primers were designed to flank the sequence around the STOP codon including the tag and the selection marker. For N-terminal tagging, first the endogenous promoter had to be amplified with the respective restriction sites and cloned into the required N-terminal tagging vector. Then primers were designed on flanking sequences around the start codon of the target ORF, selection marker, promoter and the tag. For gene knockouts, deletion cassettes were amplified by PCR from the gene deletion library. Primers were designed to amplify the cassette with 300-500 bp flanking regions upstream and downstream to facilitate homologous recombination. To that end, PCR was either performed on yeast colonies or on extracted genomic DNA (see 4.3.1) bearing the respective gene deletion. For site-directed mutagenesis, primers were designed complementary to the gene of interest bearing the desired mutation. Primers should have 12-15 bp on each site of the mutation. A second pair of primers is needed upstream and downstream of the fragment amplified with the first set of primers.

Transformant selection and testing

Colonies were selected 2-4 days after transformation, streaked on fresh selective plates, and incubated for 1-2 days at 30 °C. To screen for positive clones expressing a fluorescent tag, cells were cultured in liquid medium over night at 30 °C, diluted and grown to log phase. Cells were checked for correct localization of the fluorescent protein under a Zeiss Axio Imager A1 microscope. Gene deletions were tested by PCR using primers that bind to the flanking regions as well as inside the knockout cassette.

Sporulation and tetrad dissection

Diploid cells were transferred onto sporulation plates in thick spots and incubated at 30 °C for 2-5 days. A few colonies were resuspended in ddH_2O and tetrad formation was confirmed under a Zeiss Axio Imager A1 microscope. A small amount of cells was resuspended in 10 µl 0.1 M potassium phosphate buffer. 10 µl zymolyase (5 µg/ml) was added and cells were incubated at 30 °C for 5-10 mins. 100 µl of the digested cells were pipetted onto a YPD plate in one line. A dissecting microscope was used to isolate tetrads. The plate containing tetrads was incubated at 30 °C for 1-2 days before replica plating to determine the segregation of selection markers.

4.3 Molecular biological and genetic techniques

4.3.1 Handling nucleic acids

DNA precipitation

DNA was concentrated and purified from aqueous solutions by adding DNA precipitation buffer (3 M NaOAc, pH 4.8) in 1/10 of sample volume. 2x sample volume 100 % ethanol was added and the sample was transferred on ice for 1-2 hr, before being centrifuged at 14000 rpm in a table centrifuge (Galaxy 16DH, VWR) for 10-15 min. Supernatant was discarded and pellet was washed two times with 70 % ethanol. Ethanol was removed and pellet was air-dried at RT. Pellet was resuspended in 50-100 µl TE buffer.

Mini-preparation of plasmid DNA from *E. coli*

The mini-preparation of plasmid DNA was carried out according to the instructions provided in QIAGEN® Plasmid Mini Kit and EZNA™ Plasmid Mini Kit.

Isolation of genomic DNA from *S. cerevisiae*

Cells were grown overnight at 30 °C in 5-8 ml liquid SD medium. Cells were sedimented at 2000 rpm for 2 min and pellets were washed 1x with ddH_2O. Pellets were resuspended in 200 µl lysis buffer. 200 µl of TE buffer and 200 µl of phenol/chloroform were added, followed by an equal volume of glass-beads. Cells were vortexed for 5-10 min. The mixture was

centrifuged at 14000 rpm in a table centrifuge for 10 min resulting in three distinct layers. After transferring the aqueous top layer to a new 1.5 ml tube, 1 ml 100 % ethanol was added to precipitate DNA. After centrifugation for 2 min at 14000 rpm, the pellet was washed with 700 µl 70 % ethanol. Pellets were air dried and then dissolved in 50-100 µl TE buffer containing 10 µg/ml RNAse A.

4.3.2 *In vitro* modification of DNA

Restriction digestion of DNA

For Restriction digest of double stranded DNA Type II restriction endonucleases (New England Biolabs) were used in combination with recommended buffers. Digests were incubated at 37 °C for 1-2 hr before being subjected to TBE-Agarose gel electrophoresis.

Ligation of DNA fragments

Double-stranded DNAs were covalently linked using T4 DNA ligase. All ligation reactions in this study were carried out in order to introduce a linear insert into a digested vector. Molar ratios between insert and vector were either 1: 3 or 1: 6. A ligation reaction contained:
100 ng linearized vector
3 times of equal molar amount of insert DNA
1 U T4 DNA ligase
1 µl 10x ligase buffer
add sterile ddH_2O to a total volume of 10 µl
The reaction was incubated either 1 hr at RT or overnight at 4 °C before transformation into competent *E. coli*.

4.3.3 Analyses of DNA

Agarose electrophoresis

Separation of DNA fragments according to their sizes was achieved by applying an electric field. Percentage of the agarose gel depends on the fragment size: 1.5 % agarose gels were used for fragments below 500 bp, 1 % agarose gels for fragments above 500 bp and below 1.5 kb, 0.8 % agarose gels for fragments above 1.5 kB length. The gels were prepared with 1x TBE buffer and 1:2000 ethidiumbromide or SybrGreen. DNA samples were mixed with 0.2 volumes of 6x DNA loading buffer and pipetted into the pockets of the agarose gel. The DNA was separated horizontally at 90-120 V. Gel bands were visualized and photographed using a GeneFlash gel imaging system (Syngene Bio Imaging)

DNA sequencing

DNA was sequenced using sequencing primers, ABI Big Dye 3.1 sequencing chemistry and an ABI-3730 (Perkin Elmers) sequencer. The reactions were carried out by the Core Facility of Max Planck Institute of Biochemistry.

Table 4.10: Sequencing setup

REAGENT	VOLUME	FINAL CONCENTRATION
Plasmid	3.0 µl	300 ng
Primer 1:10	1.0 µl	5 pM
ddH_2O	3.5 µl	-
Total	7.5 µl	

4.3.4 Polymerase chain reaction (PCR)

Polymerase chain reaction was used to amplify DNA fragments. PCR products were used for validation purposes, as plasmid inserts, integration cassettes or deletion and mutation constructs. One PCR reaction requires two primers that bind to the 5' and 3' end of the amplification target. The reaction was carried out using a PXE 0.2 Thermal Cycler (Thermo Electro Corporation). PCR products were analyzed by agarose gel electrophoresis. Bands

of interest were excised and extracted.

Standard PCR

Standard PCR reactions were carried out to validate integrated or deleted DNA and to amplify DNA fragments used as plasmid inserts. Depending on the used polymerase (Taq, Pfu or Phusion) the reaction mix and cycling program had to be accordingly.

Table 4.11: Taq/Pfu PCR reaction setup

REAGENT	VOLUME	FINAL CONCENTRATION
10x Thermo Buffer	5.0 µl	-
dNTPs	1.0 µl	0.2 mM
Primer 5′ FW	0.5 µl	1.0 µM
Primer 3′ RV	0.5 µl	1.0 µM
Template DNA (genomic or plasmid)	1.0 µl	approx. 1.0 ng
Taq/Pfu-Polymerase	0.5 µl	2 U
ddH_2O	42.5 µl	-
Total	50.0 µl	

Table 4.12: Taq/Pfu PCR reaction cycle

STEP	CYCLES	TIME	TEMPERATURE
Initial denaturation	1x	10 min	95 °C
Denaturation	32x	30 s	95 °C
Annealing		30 s	56 °C
Elongation		1 min - 2.5 min	72 °C
Final elongation	1x	10 min	72 °C
Storage	1x	hold	4 °C

Table 4.13: Phusion® PCR reaction setup

REAGENT	VOLUME	FINAL CONCENTRATION
5x Phusion® HF Reaction Buffer	10.0 µl	-
dNTPs	1.0 µl	0.2 mM
Primer 5′ FW	0.5 µl	1.0 µM
Primer 3′ RV	0.5 µl	1.0 µM
Template DNA (genomic or plasmid)	1.0 µl	approx. 1.0 ng
Phusion® Polymerase	1.0 µl	2 U
ddH_2O	36.0 µl	-
Total	50.0 µl	

Table 4.14: Phusion® PCR reaction cycle

STEP	CYCLES	TIME	TEMPERATURE
Initial denaturation	1x	5 min	95 °C
Denaturation	32x	60 s	95 °C
Annealing		30 s	56 °C
Elongation		30 s - 90 s	72 °C
Final elongation	1x	10 min	72 °C
Storage	1x	hold	4 °C

Amplification of integrative cassettes

PCR reactions to amplify integrative cassettes were performed as described by Janke et al 2004. PCR products were analyzed by agarose gel electrophoresis (4.3.3). The PCR product was directly used for yeast transformations 4.2.2).

Colony control PCR

Taq Polymerase was used to validate cassette integration. Four different primers were used to validate correct gene deletion. One fragment was amplified with primers binding upstream and downstream of the ORF of interest. The size of the product either confirmed integration of the deletion cassette or the remaining ORF of interest. Then primers binding inside the deletion cassette and upstream or downstream of the target ORF were used to amplify fragments confirming correct insertion of the deletion cassette. The samples were prepared as listed below (Tab. 4.15). Polymerase was added after 10 min at 96 °C.

Table 4.15: *Taq* colony PCR reaction setup

REAGENT	VOLUME	FINAL CONCENTRATION
10x *Taq* reaction buffer	10.0 µl	-
dNTPs	1.0 µl	0.2 mM
Primer 5' FW	0.5 µl	1.0 µM
Primer 3' RV	0.5 µl	1.0 µM
Taq Polymerase	2.0 µl	approx. 4 U
ddH_2O inoculated with colony tip	36.0 µl	-
Total	50.0 µl	

Table 4.16: *Taq* colony PCR reaction cycle

STEP	CYCLES	TIME	TEMPERATURE
Initial denaturation	1x	20 min	96 °C
Denaturation	32x	60 s	96 °C
Annealing		30 s	56 °C
Elongation		1 min - 2.5 min	72 °C
Final elongation	1x	10 min	72 °C
Storage	1x	hold	4 °C

4.4 Microscopy

4.4.1 ConA coating of coverslips

Concanavalin A (ConA) is a lectin that binds to polysaccharide molecules on the yeast cell walls, which physically fixes cells on a coverslip, allowing long-term fluorescent imaging of the same cell. For coating 3 µl ConA was pipetted on coverslip, distributed evenly and air dried.

4.4.2 Sample preparation

S. cerevisiae cultures were grown in SD medium overnight at 30 °C and diluted to OD600 0.2 the next morning. Diluted cultures were grown 2-3 hrs to OD600 0.5-0.8 before being transferred into arrest medium (see 4.5.1). For mounting, 2.5-3 µl of liquid sample was added in the centre of a glass slide. A ConA coated coverslip was carefully placed on top of the liquid drop, avoiding bubble formation.

4.4.3 FM4-64 staining

For FM4-64 staining, cells were incubated with a final concentration of 0.32 µM FM4-64 for 2 min at RT. Cells were visualized after briefly washing cells with ddH_2O.

4.4.4 Drug treatment

To disrupt all actin structures, cells were released from G1 arrest in medium containing 450 µM LatB.

4.4.5 Epifluorescence microscopy

Epifluorescence microscopy was used to determine protein localization and to perform polarization assays (see 4.5.1). Samples were mounted onto a glass slide and covered with a coverslip. For live cell imaging and quantification of cells, camera gain was set to minimum and the exposure time was 300-500 ms depending on the intensity of the fluorescent marker. The microscope is equipped with a filter set with allow the excitation and

detection of green, red, blue and yellow fluorescence. For image aquisition, exposure time was between 300 ms and 1000 ms. The following setup was used (Tab. 4.17).

Table 4.17: Epifluorescence microscope setup

COMPONENT	SUPPLIER	DESCRIPTION
Microscope	Zeiss	Epifluorescence microscope
Objective	Zeiss	100x Oil Immersion Objective, NA of 1.40 and DIC
Camera	Andor Technology	iXon EM+ DU-897ECS
Lamp	Xcite	Xenon lamp
Lamp	Andor Technology	HBO-lamp
Imager	Axio	Imager
Table	Applied Precision	xy-motorized table

4.4.6 TIRF microscopy

Table 4.18: TIRF microscope setup

COMPONENT	SUPPLIER	DESCRIPTION
Microscopic unit	TiLL photonics	iMIC standing unit
Objective lense	Olympus	Olympus 1.45 NA 100x
Control unit	TiLL photonics	ICU
TIRF angle control	TiLL photonics	Galvanometer-drive 2-axis scan head
Excitation laser 1	Coherent Saphire	DPSS laser with 75 mW at 488 nm
Excitation laser 2	Cobolt Jive	DPSS laser with 7 5mW at 56 nm
Light source for DIC imaging	TiLL photonics	LED lamp
Lamp source for epifluorescence	TiLL photonics	Polychrome unit
Laser shutter	TiLL photonics	AOTF unit
Camera 1	TiLL photonics	Imago QE CCD
Camera 2	Andor	Andor iXON DU-897 EM CCD
Climate control	Workshop in MPI of Biochemistry	Temperature control unit with heating block
Software	TiLL photonics	Live-Acquisition

FRAP experiments and dynamics of polarity regulators were conducted using a custom-made TIRFM set-up based on an iMIC modular microscopic unit The setup in (Tab. 4.18) was used .

Samples were mounted onto the microscope in an inverted manner. Target cells for imaging were first identified using live streaming with DIC imaging. For FRAP experiments and time-lapse microscopy of polarity regulators the TIRF angles were set slightly below the critical angle for total reflection, resulting in an excitation light passing through the sample with an extremely low angle (oblique illumination). Oblique illumination allows illumination of an increased area of the sample but does not cause as much photo-bleaching as wide-field imaging (Tokunaga et al. 2008). For surface imaging of GFP-Cdc42^{G12V} TIRF angles were adjusted to total reflection.

4.4.7 Spinning disc microscopy

Table 4.19: Spinning disc microscope setup

COMPONENT	SUPPLIER	DESCRIPTION
Microscopic unit	Andor Technology/Till	iMIC standing unit
CSU22 spinning disk	Yokogawa, Amersfoort	confocal scanner
Objective lense	Olympus	Olympus 1.45 NA 100x
TIRF angle control	TiLL photonics	Galvanometer-drive 2-axis scan head
Excitation laser 1	Andor Technology	DPSS laser with 75 mW at 488 nm
Excitation laser 2	Andor Technology	DPSS laser with 75 mW at 561 nm
FRAPPA module	Andor Technology	Galvanometer-drive 2-axis scan head
Camera	Andor	Andor iXON D-977 EM CCD
Software	Andor	iQ Live Cell Imaging

Samples were mounted onto the microscope in an inverted manner. Target cells for imaging were first identified using live streaming with DIC imaging. For 4D timelapse microscopy of polarity regulators, cells were excited with 60 % laser intensity and exposed for 60-100 ms with 60 s frame rate. A stack of 4 frames was taken with a 40 nm increment

for each time point. A maximum projection of 2 or 3 frames was made.

4.4.8 FRAP

To quantify protein recovery during FRAP experiments, automatic MATLAB (MathWorks. 2010a) routines were implemented. Intensities in the bleached region were corrected for background fluorescence (using intensities in a cell free area) and photobleaching (using a reference cell in the same image that was not bleached). The recovery curve was normalized to the intensities before (1) and after (0) the FRAP event and fitted with the function $y_{fit}(t) = a(1 - b(exp(-tc)) - d(exp(-te))$. We used a double exponential fit to represent two processes contributing to fluorescence recovery in the bleached region. Fast recovery of soluble Cdc42 that was bleached in the cytosol (by rapid diffusion) and slower recovery of the membrane-bound Cdc42 pool (through a combination of GDI- and actin-mediated mechanisms). The half-time for the slower component, $t_2 1/2 = -log(0.5)/e$ was used for further comparison. Time information was automatically extracted from the meta data provided by the acquisition software. Results were only included in the analysis, if the data could be reliably fitted (residual sum of squares > 0.95) and the residuals were randomly distributed below and above the curve. Means and SEMs were calculated from at least 10 independent FRAP experiments on different cells. (This method was developed by Nikola Müller)

4.5 Cell biological methods

4.5.1 Polarization assay

To arrest logarithmically growing cells in the G1 phase of the cell cycle, 3 mM methionine was added to the medium for 4 hr. Cells were then released from the cell cycle arrest by washing 2 times and resuspension in methionine free medium. Caps of at least 50 cells per time point were counted in at least three independent experiments

4.5.2 Washout assay

For washout experiments, LatB treatment was performed for 20 min or 40 min, respectively. The drug was removed by one wash step and polarization (number of buds) was monitored after an additional 40-60 min. Cells with single and double buds were counted from three independent experiments with at least 100 cells each.

4.5.3 Effect of Cdc42 expression levels on polarization probability

Cells expressing either GFP-Cdc42 under its endogenous or a galactose inducible promoter were grown over night in SC-methionine and 2 % glucose, washed 3 times with ddH_2O and then diluted in SC-methionine with 2 % raffinose. Cells were arrested for 3 hr in G1 in Sc-all supplemented with 2 % raffinose and 3 mM methionine. Cells expressing GFP-Cdc42 under the Gal promoter were induced for 30 min, 60 min, 90 min and 120 min by addition of 2 % galactose. Cells were treated with 150 µM LatA during G1 release. Polarized cells were counted after 30 min and 60 min after release. Expression levels of GFP-Cdc42 were determined by integrating fluorescence intensity for each cell.

4.5.4 SGA screen

We used the following set of query proteins: Cdc42, its GEF Cdc24, its GAPs Bem2, Bem3, Rga1 and Rga2, and its GDI Rdi1. We also included the Cdc42 effectors Bem1 and Cla4. Physical and genetic interaction partners were collected from public databases (BioGRID (Breitkreutz et al. 2010), DIP (Salwinski et al. 2004) and MPACT (Mewes et al. 2011) and the literature. Physical interactions included data from affinity purification, co-crystallization, FRET, gel-retardation, PCA, protein-peptide interaction, reconstituted complexes and two hybrid interactions. Genetic interactions included synthetic growth defects, haploinsufficiencies and synthetic lethality. We only included negative interactions from synthetic genetic array (SGA) screens to focus on the redundancy of pathways We also performed an SGA screen with Rdi1 as described elsewhere (Costanzo et al. 2010) and identified two additional actin related interaction partners, Gos1 and Bem2. These were verified by random spore analysis (Tong & Boone 2007) and included in the final list. All interac-

tion partners involved in actin-related processes were grouped in four sub categories: actin general (involved in formation of actin patches or cables), early secretion (ER-Golgi transport), late secretion (Golgi-plasma membrane transport) and endocytic recycling. All identified genetic and physical interactions are listed in Tables A.3 and A.4, respectively. For each query protein the number of interactions to each functional group was extracted. This strength of interaction with a functional group (determined by the number of unique interaction partners) was colour-coded in a heat map. (The heat map was generated by Nikola Müller)

4.6 Image processing and analyses

4.6.1 Image analysis

Unless otherwise specified, images presented in this work were raw images. For better visualization cells were background-subtracted and contrast-enhanced.

4.6.2 Cap/cytosol intensity ratio

Average intensity of cap and cytosol were measured manually with ImageJ software (U. S. National Institutes of Health, Bethesda, Maryland, USA, http://rsb.info.nih.gov/ij/, 1997-2008.)

4.6.3 Cap intensity profile

Cap intensity profiles were determined by measuring the average intensities along the circumference of a cell with ImageJ software, (U. S. National Institutes of Health, Bethesda, Maryland, USA, http://rsb.info.nih.gov/ij/, 1997-2008.)

4.6.4 Statistical analysis

Curve fitting for polarization curves was done using Prism 4 (GraphPad Software, La Jolla) using a sigmoidal dose response equation: $Y = Bottom + (Top - Bottom)/(1 + 10^{(}LogEC50 - x) * Hillslope$. All averages are given as either geometric mean $\pm$ SD or geometric mean $\pm$ SEM. Unpaired two-tailed t-tests were performed to validate significance of differences.

4.7 Biochemistry

This part was provided by Jared Johnson, Cornell University

4.7.1 Protein purification

Cdc42 was purified as His_6-tagged protein from baculovirus infected Sf21 insect cells. All purification steps were performed at 4 °C. One liter stirred cultures of Sf21 cells were infected for 48 h by Kinnakeet Biotechnology (Midlothian, VA). Cell pellets were resuspended in 40 ml of hypotonic buffer (20 mM sodium borate pH 10.2, 5 mM $MgCl_2$, 200 µM PMSF, 1 µg/ml aprotinin and leupeptin) and disrupted by dounce homogenization. The membrane-containing components of the lysate were spun down at 150,000 x g in a Ti70 rotor (Beckman Coulter) for 20 min, after which the supernatant containing non-prenylated Cdc42 was discarded and the pellet was resuspended in 50 ml of TBSM (50 mM Tris, pH 7.5, 150 mM NaCl, and 5 mM $MgCl_2$). The procedure was repeated twice and the final pellet was resuspended in TBSM containing 1 % Triton-X 100. The lysate was further homogenized and agitated for 30 min on a rotisserie, resulting in the solubilization of the geranylgeranylated Cdc42. The remaining insoluble fraction was pelleted in a tabletop centrifuge at 9,000 x g for 20 min at 4 °Cand discarded. The supernatant containing detergent-solubilized, isoprenylated His_6-tagged Cdc42 was incubated for 30 min with chelating Sepharose beads (Qiagen) charged with Ni^{2+}. Beads were washed with 400 ml of high salt buffer (50 mM Tris pH 7.5, 700 mM NaCl, 5 mM $MgCl_2$, 0.1 % CHAPS, and 20 mM imidazole) and protein was eluted with 1 ml of elution buffer (50 mM Tris, pH 7.5, 150 mM NaCl, 5 mM $MgCl_2$, 0.1 % CHAPS, 500 mM imidazole). The fractions containing Cdc42 were pooled and concentrated to a volume of 2 ml. His_6-tagged prenylated Rac1 was purified in the same manner as Cdc42. RhoGDI (human) and the limit GAP domain of Cdc42-GAP (human, residues 234-462) were purified from *E. coli* cells harbouring plasmids encoding N-terminal GST fused to each construct. The limit guanine nucleotide exchange domain of Dock180 (DHR2C domain, human) was purified from *E. coli* cells harbouring plasmids encoding it as an N-terminal His_6-tagged construct. Cells were grown at 37 °Cto OD 0.8. Protein expression was induced by 1 mM isopropyl 1-thio-β-D-galactopyranoside for 3 hr before pelleting at 6,000 x g for 10 min. Cell pellets were

homogenized in TBSM and lysed by sonication. Cell debris was centrifuged at 20,000 x g for 30 min, and the supernatant was used for purification. Supernatants containing GST-tagged proteins were incubated with glutathione beads (Amersham Biosciences) and equilibrated with TEDA buffer (20 mM Tris pH 8.0, 1 mM EDTA, 1 mM DTT, and 1 mM sodium azide) for 30 min at 4 °C. The beads were then washed with several column volumes of TEDA-containing 500 mM NaCl. After a final rinse with TBSM, the protein was eluted with 10 mM glutathione in TBSM. The His_6-tagged DHR2 domain was purified on chelating Sepharose beads (Qiagen) charged with Ni^{2+}, as described above. All proteins were concentrated in a 10 MWC Amicon Ultra concentrator (Fisher). Protein concentrations were determined using the Bio-Rad Protein Assay Kit with bovine serum albumin as standard.

4.7.2 Liposome binding assays

All liposome vesicles were prepared by extrusion using the Avanti mini-extruder. For fluorescence experiments smaller liposomes were prepared with 1 µm diameter membrane. For pelleting experiments larger liposomes were prepared using 8 µm membranes, followed by centrifugation at 16,000 x g for 10 min and resuspension of pellets in TBSM. All lipids used were purchased from Avanti Polar Lipids, unless stated otherwise. The standard lipid composition in molar percentages was 35 % PE, 25 % PS, 5 % PI, and 35 % cholesterol (Nu Chek Preps).For radioactive assays of Rac1-liposome association, Rac1 (40 nM) was preloaded with $\alpha^{(32P)}$GTP (2300 cpm/pmol, 10 µM) by EDTA (8 mM)-stimulated nucleotide exchange in the presence of 8 µm liposomes (1 mg/ml). Rac1 was then allowed to hydrolyze its bound nucleotide to $\alpha^{(32P)}$)GDP by incubation fro 30 min on ice in the presence of excess magnesium (14 mM). This also prevented further EDTA-stimulated nucleotide exchange. The protein was then incubated with 45 nM GDI for 10 min, followed by a 10 min treatment with the DHR2 domain of Dock180 (500 nM), in the presence of 100 µM unlabelled GTPγS. The mixture was pelleted by centrifugation for 10 min at 16,000 x g. Radioactivity levels in the supernatant and pellet fractions were measured separately. For fluorescence-based assays of Cdc42-liposome association a Varian Cary Eclipse fluorimeter was used in the counting mode. Excitation and emission wavelengths were 365 and 440 nm, respectively. Samples were stirred continuously at 25 °C in TBSM. To prepare HAF (hexdecanoylaminofluorescein)-labelled lipids for FRET assays, 1.25 nmol of HAF

(Molecular Probes) was vortexed with 50 µl of lipids (1 mg/ml). In order to monitor the release of Cdc42 from liposomes, Cdc42 was preloaded with a methylanthaniloyl-modified (Mant)-nucleotide (GTP, GDP or GMP-PNP) and incubated with 30 µl of HAF-containing liposomes at RT for 5 min. The mixture was added to the cuvette, bringing Cdc42 concentration to 40 nM. At the indicated timepoints, 50 nM RhoGDI and 10 nM Cdc42GAP were added, and fluorescence was recorded for 20 min. Traces monitored the changes in Mant fluorescence due to changes in FRET between Mant-nucleotide-bound Cdc42 and liposomes containing HAF.

4.7.3 Nucleotide exchange assay

Competition between GDI and the guanine nucleotide exchange factor Dock180 was measured with prenylated Rac1. Rac1 was preloaded with Mant-GDP in a 25 µl volume in the presence of 20 µl of unlabelled 1 µm liposomes. After transferring the mixture to the cuvette (final concentration Rac1, 60 nM; Mant GDP, 500 nM), unlabelled GTP (10 µM) and GDI (80 nM) were added for 10 min. At the indicated times, different concentrations of the DHR2 domain of Dock180 were added. Traces monitored the loss of Mant fluorescence due to nucleotide exchange.

4.8 Stochastic model

This part was provided by Ben Klünder, LMU: To further elucidate the roles of Rdi1 and actin-dependent recycling pathways in polarization we built a stochastic particle-based model, and simulated the emergence of polarity in budding yeast. Our model explicitly includes as model variables the active (T) and inactive (D) forms of Cdc42, which can be recruited to the plasma membrane and accumulate in caps. A pool of Cdc42 (T_{IM}, D_{IM}) can be found on internal membranes (IM) and is allowed to shuttle between plasma membrane and internal membranes via endocytosis and exocytosis. Cdc42 can also be extracted from the plasma membrane into a well-mixed pool of cytosolic Cdc42-GDP (D_{cyt}) by interaction with its GDI, Rdi1. We considered a two-dimensional model of a circular shaped cell with radius R.

The membrane was split into n = 100 segments where reactions take place between par-

ticles on the same segment i = 1,..., *n*. This approach allowed us to stochastically simulate the temporal evolution of the system using the Gillespie algorithm (Gillespie 1977). We fitted our model to recapitulate the emergence of Cdc42 caps in Latrunculin-treated and in *rdi1*Δ cells, and tested its reliability by comparing the predictions of the combined model with our experimental results on control cells and mutants altered in GTP hydrolysis.
Model Reactions: To achieve and maintain polarization, Cdc42 must be continuously returned to the cap, as diffusion in the plasma membrane acts to flatten any inhomogeneities in protein distribution. We incorporated diffusion of Cdc42 in the plasma membrane by jumps between neighbouring segments with the stochastic rate constant D_k. The rate can be calculated from $k_D = (2\pi R/n)^2$, where D is the diffusion constant and R the cell radius (Bernstein 2005). The intrinsic GTPase activity of Cdc42 is markedly increased by its only GEF, Cdc24, which is delivered to already active Cdc42 on the membrane by the effector Bem1 (Irazoqui et al. 2003; Butty et al. 2002). However, recruitment of Cdc24 and Bem1 to the cap is bounded through depletion of the available molecules (Wedlich-Soldner et al. 2004). We employed an effective description of this bounded positive feedback such that the activation rate for the process

$$D_i \xrightarrow{b_1 F(\{T_i\})} T_i\,, \tag{4.1}$$

is given by a Michaelis-Menten law $F(\{T_i\}) = T_i/(c_{th} + \sum_i T_i)$ with amplitude b_1. Here D_i and T_i denote the number of passive and active Cdc42 respectively at site i. The denominator of $F(\{T_i\})$ effectively limits GEF recruitment if the total amount of active Cdc42 substantially exceeds the threshold t_{hc}. Moreover, we used the functional form $F(\{T_i\})$ to account for GEF-mediated recruitment of Cdc42 from the cytosol with subsequent nucleotide-exchange

$$D_{cyt} \xrightarrow{c_1 F(\{T_i\})} T_i\,. \tag{4.2}$$

to take into account our results (Fig. 2.11, Fig. 2.12) and other evidence (Gibson & Wilson-Delfosse 2001; Schoebel et al. 2009; Ugolev et al. 2008) that GEFs can displace GTPases from their GDI. In the absence of GEF, nucleotide-exchange and membrane attachment of Cdc42-GDP are taken to occur with background rates $2b_b$ and $2b_c$. Extraction of Cdc42-GDP from the plasma membrane is facilitated by interaction with its GDI Rdi1

(Fig. 2.9 and Slaughter et al. 2009; Koch et al. 1997). We assumed that Rdi1 is present in large excess and diffuses rapidly in the cytosol. Therefore the extraction of Cdc42-GDP into the well-mixed cytosolic pool of Cdc42 is taken to occur with a constant rate d. The last reaction necessary for Rdi1-dependent polarization is hydrolysis of Cdc42-GTP which we implemented as a first order reaction with rate a. The reactions of the Rdi1-dependent polarization pathway are shown in Fig. 2.12. A second mechanism for Cdc42 recycling and cell polarization is provided by actin-mediated transport of exocytic and endocytic vesicles (Wedlich-Soldner et al. 2003). A promising modelling approach has been published recently, in which vesicles were explicitly taken into account (Layton et al. 2011). However, as we were mainly interested in how the distribution of Cdc42 affected the reorganization of the cytoskeleton, we heuristically modelled the effective protein dynamics induced by endocytosis and exocytosis. Details of the model are shown in Fig. 2.23.

We assumed that Cdc42 caps are maintained by a dynamic balance of focused exocytosis, diffusive spread within the plasma membrane and endocytosis (Marco et al. 2007). We made the simplifying assumption that the total exocytic flux of Cdc42 remains the same before and after polarization for a given internal pool of cargo. The flux of Cdc42 from the internal membranes is equally spread over the whole plasma membrane in unpolarized cells but is slightly focused in polarized cells. We implemented this in our model by allowing the "nucleation" N_A = 2 sites of increased exocytosis on the plasma membrane similar to earlier models (Wedlich-Soldner et al. 2003). As actin reorganization is under control of Cdc42-GTP we modelled the nucleation of stable actin bundles as

$$A_{cyt} \xrightarrow{eT_i} A_i \,. \tag{4.3}$$

where A_{cyt} and A_i represent available and nucleated stable actin bundles, respectively, with $\sum A_i + A_{cyt} = N_A$. The exocytic flux is described by the reactions

$$T_{IM} \xrightarrow{f[A_i+G(A_i)]} T_i \,, \tag{4.4}$$

$$D_{IM} \xrightarrow{f[A_i+G(A_i)]} D_i \tag{4.5}$$

with $G(\{A_i\}) = (h - \sum_i A_i)/n$ describing the background exocytosis rate outside of caps.

This description allows for focused exocytosis towards nucleated actin bundles while keeping the total exocytosis constant. Finally, we approximated endocytosis of Cdc42 to internal membranes by a constant endocytosis rate g. All reactions of the agent-based model are summarized in Tab. 4.20.

Table 4.20: Model reactions

REACTION	FORMULA
membrane diffusion	$T_i \xrightarrow{k_D} T_{i\pm1}$, $D_i \xrightarrow{k_D} D_{i\pm1}$
hydrolysis	$T_i \xrightarrow{a} D_i$
nucleotide-exchange	$D_i \xrightarrow{b_1 T_i/(c_{th}+\sum_j T_j)+b_2} T_i$
recruitment	$D_{cyt} \xrightarrow{c_1 T_i/(c_{th}+\sum_j T_j)} T_i$
	$D_{cyt} \xrightarrow{c_2} D_i$
extraction	$D_i \xrightarrow{d} D_{cyt}$
actin bundle nucleation	$A_{cyt} \xrightarrow{eT_i} A_i$
exocytosis	$T_{IM} \xrightarrow{f[A_i+(h-\sum_j A_j)/n]} T_i$,
	$D_{IM} \xrightarrow{f[A_i+(h-\sum_j A_j)/n]} D_i$
endocytosis	$T_i \xrightarrow{g} T_{IM}$
	$D_i \xrightarrow{g} D_{IM}$

Parameter estimates: To fit our model we separately considered LatB-treated wild-type and *rdi1*Δ cells. The diffusion constant D of Cdc42, the total number N_{42} of Cdc42 and the intrinsic activation rate b_2 were taken from published data (Marco et al. 2007; Wedlich-Soldner et al. 2004; Ghaemmaghami et al. 2003; Zheng & Cerione 1994). The average cell radius R was determined to be 3.95 µm. As LatB-treated wild-type cells show a Cdc42 mobility (FRAP) rate of approximately 0.28/s, we estimated the extraction rate d to be 0.5/s. As initial conditions for LatB-treated cells we distributed on average 20 % of all Cdc42 to the plasma membrane, with the remaining Cdc42 was being split equally between internal membranes and cytosol (Wedlich-Soldner et al. 2004). In simulations of *rdi1*Δ cells the cytosolic fraction was redistributed to the membranes, with 1/3 located to the plasma membrane. To begin our simulation, we assumed that the GEF had just arrived at the plasma membrane, and started with an average fraction of active Cdc42 on all membranes determined by the ratio of intrinsic activation and hydrolysis. The activation threshold c_{th} limiting the total amount of active GEF was estimated to be 100, given that

roughly 300 Cdc42 molecules are localized to steady-state caps (Wedlich-Soldner et al. 2004; Ghaemmaghami et al. 2003). The remaining parameters were chosen such that the caps of LatB-treated and *rdi1*Δ cells satisfied a set of constraints over an average of 400 runs. We fitted the GEF-dependent activation and recruitment rates b_1 and c_1, and the hydrolysis and background insertion rates a and c_2 in LatB simulations assuming exocytosis and endocytosis to be zero. Using FRAP and fractionation experiments from (Wedlich-Soldner et al. 2004) we estimated the fraction of Cdc42 in the cap at steady state to be 10 % with the same amount spread over the remaining plasma membrane. From previous data (Marco et al. 2007; Slaughter et al. 2009) we estimated the height and width of Cdc42 caps to 10 times the background density and 10 % of the circumference, respectively. The fitting constraints were a Cdc42 FRAP time in steady-state LatB caps between 2 s and 3 s, a total amount of Cdc42 on the plasma membrane between 15-25 %, a cap height of 7-12 times the background, and a cap width of 8-12 %. Each simulation was terminated after t_{end} = 1300 s internal simulation time - comparable to the duration of our experiments and the time cells need to polarize after GEF release from the nucleus (Caviston et al. 2002; Shimada & Gulli 2000). A cap was detected if a spatially averaged profile of Cdc42 (over 5 % of the membrane) was higher than twice its average value. At the end of the simulation the number of caps and the particle density of Cdc42 were detected and a Gaussian distribution was fitted to the Cdc42 profile to quantify its shape. We defined the cap width as twice the distance between the turning points of the fit. To simulate FRAP values, at time t_{frap} = 1200 s the number of caps was determined. For simulations with a single cap Cdc42 in a region corresponding to 20 % of the plasma membrane and centered at the cap position was changed into a non-fluorescent version of Cdc42. The recovery of fluorescent Cdc42 into the cap was then monitored and the recovery half time t 1/2 was calculated by fitting with a single exponential function. After fitting the model to LatB-treated cells we used some of the parameters obtained to fit the actin nucleation rate e, the exocytosis parameters f and h, and the endocytosis rate g. Model parameters for *rdi1*Δ cells were chosen such that steady-state caps had a FRAP recovery time of 10-12 s, with 30-40 % of all Cdc42 on the plasma membrane, a cap height of 7-12 times background, 0-10 % cells with double caps and 90-100 % total polarization. The results shown in Fig. 2.24, Fig. 2.25, Fig. 2.26 were obtained from 400 runs

for each point in parameter space with the same simulation time and evaluation procedure as described for fitting the model above. Model parameters used in simulations are summarized in Tab. 4.21.

Table 4.21: Model parameters

PARAMETER	VALUE
N	100
R	3.95 µm
D	0.036 µm$_2$/s
k_D	0.585 /s
N_{42}	3000
N_A	2
a	2.74/s
b_1	63.1/s
b_2	0.0002/s
c_1	0.04472/s
c_2	0.0015/s
d	0.5/s
e	0.000139/s
f	0.02236/s
h	4
g	0.04472/s
c_{th}	100

5 Literature

Adams AE, Johnson DI, Longnecker RM, Sloat BF & Pringle JR (1990) CDC42 and CDC43, two additional genes involved in budding and the establishment of cell polarity in the yeast Saccharomyces cerevisiae. J Cell Biol 111: 131–142

Altschuler SJ, Angenent SB, Wang Y & Wu LF (2008) On the spontaneous emergence of cell polarity. Nature 454: 886–889

Amon A, Irniger S & Nasmyth K (1994) Closing the cell cycle circle in yeast: G2 cyclin proteolysis initiated at mitosis persists until the activation of G1 cyclins in the next cycle. Cell 77: 1037–1050

Arkowitz RA (1999) Responding to attraction: chemotaxis and chemotropism in Dictyostelium and yeast. Trends in Cell Biology 9: 20–27

Bender A (1993) Genetic Evidence for the Roles of the Bud-Site-Selection Genes BUD5 and BUD2 in Control of the Rsr1p (Bud1p) GTPase in Yeast. Proc Natl Acad Sci U S A 90: 9926–9929

Bernstein D (2005) Simulating mesoscopic reaction-diffusion systems using the Gillespie algorithm. Phys Rev E Stat Nonlin Soft Matter Phys 71: 041103

Bi E, Maddox P, Lew D & Salmon E (1998) Involvement of an actomyosin contractile ring in Saccharomyces cerevisiae cytokinesis. J. Cell Biol. 142:1301–1312

Bloom J & Cross FR (2007) Multiple levels of cyclin specificity in cell-cycle control. Nat. Rev. Mol. Cell Biol. 8: 149–160

Bokoch G (2003) Biology of the p21-activated kinases. Annu. Rev. Biochem. 72:743–81

Bos JL, Rehmann H & Wittinghofer A (2007) GEFs and GAPs: Critical elements in the control of small G proteins (vol 129, pg 865, 2007). Cell 130: 385–385

Bose II, Irazoqui JEJ, Moskow JJJ, Bardes ESE, Zyla TRT & Lew DJD (2001) Assembly of scaffold-mediated complexes containing Cdc42p, the exchange factor Cdc24p, and the effector Cla4p required for cell cycle-regulated phosphorylation of Cdc24p. J Biol Chem 276: 7176–7186

Breitkreutz A, Choi H, Sharom J & Boucher L (2010) A global protein kinase and phosphatase interaction network in yeast. Science 328: 1043–1046

Bretscher A (2003) Polarized growth and organelle segregation in yeast: the tracks, motors, and receptors. J Cell Biol 160: 811–816

Brown J, Jaquenoud M & Gulli M (1997) Novel Cdc42-binding proteins Gic1 and Gic2 control cell polarity in yeast. Genes Dev 11: 2972–2982

Brownlee C (1998) Polarity determination inFucus: From zygote to multicellular embryo. Semin. Cell. Dev. Biol. 9, 179 – 185

Bustelo X & Sauzeau V (2007) GTP-binding proteins of the Rho/Rac family: regulation, effectors and functions in vivo. Bioessays 29: 356–370

Butty A-CA, Perrinjaquet NN, Petit AA, Jaquenoud MM, Segall JEJ, Hofmann KK, Zwahlen CC & Peter MM (2002) A positive feedback loop stabilizes the guanine-nucleotide exchange factor Cdc24 at sites of polarization. Embo J 21: 1565–1576

Caviston J & Longtine M (2003) The role of Cdc42p GTPase-activating proteins in assembly of the septin ring in yeast. Mol Biol Cell 14: 4051–4066

Caviston J, Tcheperegine S & Bi E (2002) Singularity in budding: A role for the evolutionarily conserved small GTPase Cdc42p. Proc Natl Acad Sci USA 99: 12185–12190

Chant J (1991) Genetic control of bud site selection in yeast by a set of gene products that constitute a morphogenetic pathway. Cell 65, 1203–1212

Chant J (1995) Patterns of bud-site selection in the yeast Saccharomyces cerevisiae. J. Cell Biol. 129, 751–765

Chen G & Kim Y (1997) The Cdc42 GTPase-associated proteins Gic1 and Gic2 are required for polarized cell growth in Saccharomyces cerevisiae. Genes Dev. 11:2958–2971

Chuang TH, Xu X, Knaus UG, Hart MJ & Bokoch GM (1993) GDP dissociation inhibitor prevents intrinsic and GTPase activating protein-stimulated GTP hydrolysis by the Rac GTP-binding protein. J Biol Chem 268: 775–778

Chung C & Funamoto S (2001) Signaling pathways controlling cell polarity and chemotaxis. Trends Biochem Sci , 26:557-566

Cole K, Barbour J, Midkiff J & Marble B (2009) Multiple proteins and phosphorylations regulate Saccharomyces cerevisiae Cdc24p localization. FEBS Lett 583, 3339–3343

Costanzo M, Baryshnikova A, Bellay J, Kim Y, Spear ED, Sevier CS, Ding H, Koh JL, Toufighi K, Mostafavi S, Prinz J, St Onge RP, Vandersluis B, Makhnevych T, Vizeacoumar FJ, Alizadeh S, Bahr S, Brost RL, Chen Y, Cokol M, et al (2010) The Genetic Landscape of a Cell. Science 327: 425–431

DerMardirossian C & Bokoch G (2005) GDIs: central regulatory molecules in Rho GTPase

activation. Trends Cell Biol 15: 356–363

Drees BL (2001) A protein interaction map for cell polarity development. J Cell Biol 154: 549–576

Drubin DGD & Nelson WJW (1996) Origins of cell polarity. Cell 84: 335–344

Eby J, Holly S, van Drogen F & Grishin A (1998) Actin cytoskeleton organization regulated by the PAK family of protein kinases. Curr. Biol. 8:967–970

Eitzen G, Thorngren N & Wickner W (2001) Rho1p and Cdc42p act after Ypt7p to regulate vacuole docking. Embo J 20: 5650–5656

Enserink JM & Kolodner RD (2010) An overview of Cdk1-controlled targets and processes. Cell Div 5: 11

Etienne-Manneville S (2004) Cdc42–the centre of polarity. J Cell Sci 117: 1291–1300

Etienne-Manneville S & Hall A (2002) Rho GTPases in cell biology. Nature 420: 629–635

Evangelista M, Pruyne D, Amberg DC, Boone C & Bretscher A (2002) Formins direct Arp2/3-independent actin filament assembly to polarize cell growth in yeast. Nat Cell Biol 4: 32–41

Fairn GD, Hermansson M, Somerharju P & Grinstein S (2011) Phosphatidylserine is polarized and required for proper Cdc42 localization and for development of cell polarity. Nature Cell Biology 13: 1424–1430

Faure J & Dagher M (2001) Interactions between Rho GTPases and Rho GDP dissociation inhibitor (Rho-GDI). Biochimie 83: 409–414

Firtel R & Meili R (2000) Dictyostelium: a model for regulated cell movement during morphogenesis. Current Opinion in Genetics & Development 10: 421–427

Freisinger T & Wedlich-Soldner R (2011) Phosphatidylserine promotes polar Cdc42 localization. Nature Cell Biology 13: 1387–1388

Garcia-Mata R, Boulter E & Burridge K (2011) The "invisible hand": regulation of RHO GTPases by RHOGDIs. Nat. Rev. Mol. Cell Biol. 12: 493–504

Gerhart J, Danilchik M, Doniach T, Roberts S, Rowning B & Stewart R (1989) Cortical rotation of the Xenopus egg: consequences for the anteroposterior pattern of embryonic dorsal development. Development 107: 37

Ghaemmaghami S, Huh W-K, Bower K, Howson RW, Belle A, Dephoure N, O'shea EK &

Weissman JS (2003) Global analysis of protein expression in yeast. Nature 425: 737–741

Gibson RM & Wilson-Delfosse AL (2001) RhoGDI-binding-defective mutant of Cdc42Hs targets to membranes and activates filopodia formation but does not cycle with the cytosol of mammalian cells. Biochem J 359: 285–294

Gillespie DT (1977) Exact stochastic simulation of coupled chemical reactions. J. Phys. Chem. 81: 2340–2361

Goryachev AB & Pokhilko AV (2006) Computational model explains high activity and rapid cycling of Rho GTPases within protein complexes. PLoS Comput Biol 2: e172

Goryachev ABA & Pokhilko AVA (2008) Dynamics of Cdc42 network embodies a Turing-type mechanism of yeast cell polarity. FEBS Lett 582: 1437–1443

Gulli M, Jaquenoud M, Shimada Y, Niederhäuser G, Wiget P & Peter M (2000) Phosphorylation of the Cdc42 exchange factor Cdc24 by the PAK-like kinase Cla4 may regulate polarized growth in yeast. Molecular Cell 6: 1155–1167

Han B, Bogomolnaya L & Totten J (2005) Bem1p, a scaffold signaling protein, mediates cyclin-dependent control of vacuolar homeostasis in Saccharomyces cerevisiae. Genes Dev 19: 2606–2618

Hancock J & Hall A (1993) A Novel Role for Rhogdi as an Inhibitor of Gap Proteins. Embo J 12: 1915–1921

Hart MJ, Maru Y, Leonard D, Witte ON, Evans T & Cerione RA (1992) A GDP Dissociation Inhibitor That Serves as a GTPase Inhibitor for the Ras-Like Protein CDC42Hs. Science. New Series 258: 812–815

Hartwell L (1971) Genetic control of the cell division cycle in yeast 1:: IV. Genes controlling bud emergence and cytokinesis. Exp. Cell Res. 69:265– 276.

Hoffman GR, Nassar N & Cerione RA (2000) Structure of the Rho family GTP-binding protein Cdc42 in complex with the multifunctional regulator RhoGDI. Cell 100: 345–356

Holly S (1999) PAK-family kinases regulate cell and actin polarization throughout the cell cycle of Saccharomyces cerevisiae. J. Cell Biol. 147, 845–856

Howell AS, Savage NS, Johnson SA, Bose I, Wagner AW, Zyla TR, Nijhout HF, Reed MC, Goryachev AB & Lew DJ (2009) Singularity in Polarization: Rewiring Yeast Cells to Make Two Buds. Cell 139: 731–743

Ingmundson A, Delprato A, Lambright DG & Roy CR (2007) Legionella pneumophila pro-

teins that regulate Rab1 membrane cycling. Nature 450: 365–369

Irazoqui JE, Gladfelter AS & Lew DJ (2003) Scaffold-mediated symmetry breaking by Cdc42p. Nature Cell Biology 5: 1062–1070

Iwamoto KK, Kobayashi SS, Fukuda RR, Umeda MM, Kobayashi TT & Ohta AA (2004) Local exposure of phosphatidylethanolamine on the yeast plasma membrane is implicated in cell polarity. Genes Cells 9: 891–903

Jacobs CW, Adams AEM, Szansizlo PJ & Pringle JR (1988) Functions of microtubules in the Saccharomyces cerevisiae cell cycle. The Journal of Cell Biology 107

Janke C, Magiera MM, Rathfelder N, Taxis C, Reber S, Maekawa H, Moreno-Borchart A, Doenges G, Schwob E, Schiebel E & Knop M (2004) A versatile toolbox for PCR-based tagging of yeast genes: new fluorescent proteins, more markers and promoter substitution cassettes. Yeast 21: 947–962

Jilkine A & Edelstein-Keshet L (2011) A comparison of mathematical models for polarization of single eukaryotic cells in response to guided cues. PLoS Comput Biol 7: e1001121

Johnson DI & Pringle JR (1990) Molecular characterization of CDC42, a Saccharomyces cerevisiae gene involved in the development of cell polarity. J Cell Biol 111: 143–152

Johnson DI (1999) Cdc42: An essential Rho-type GTPase controlling eukaryotic cell polarity. Microbiology and Molecular Biology Reviews 63: 54–105

Johnson JL, Erickson JW & Cerione RA (2009) New insights into how the Rho guanine nucleotide dissociation inhibitor regulates the interaction of Cdc42 with membranes. J Biol Chem 284: 23860–23871

Kang PJ, Sanson A, Lee B & Park H-O (2001) A GDP/GTP exchange factor involved in linking a spatial landmark to cell polarity. Science 292: 1376–1378

Katzmann D, Stefan C, Babst M & Emr S (2003) Vps27 recruits ESCRT machinery to endosomes during MVB sorting. J Cell Biol 162: 413–423

Knaus M, Pelli-Gulli M-P, Van Drogen F, Springer S, Jaquenoud M & Peter M (2007) Phosphorylation of Bem2p and Bem3p may contribute to local activation of Cdc42p at bud emergence. Embo J 26: 4501–4513

Koch G, Tanaka K, Masuda T, Yamochi W, Nonaka H & Takai Y (1997) Association of the Rho family small GTP-binding proteins with Rho GDP dissociation inhibitor (Rho GDI) in Saccharomyces cerevisiae. Oncogene 15: 417–422

Kozubowski L, Saito K, Johnson JM, Howell AS, Zyla TR & Lew DJ (2008) Symmetry-Breaking Polarization Driven by a Cdc42p GEF-PAK Complex. Current Biology 18: 1719–1726

Layton AT, Savage NS, Howell AS, Carroll SY, Drubin DG & Lew DJ (2011) Modeling Vesicle Traffic Reveals Unexpected Consequences for Cdc42p-Mediated Polarity Establishment. Current Biology 1–11

Leonard D, Hart MJ, Platko JV, Eva A, Henzel W, Evans T & Cerione RA (1992) The identification and characterization of a GDP-dissociation inhibitor (GDI) for the CDC42Hs protein. Journal of Biological Chemistry 267: 22860–22868

Lew D (1993) Morphogenesis in the yeast cell cycle: regulation by Cdc28 and cyclins. J Cell Biol 120:1305-1320

Lin M, Unden H, Jacquier N, Schneiter R, Just U & Hoefken T (2009) The Cdc42 Effectors Ste20, Cla4, and Skm1 Down-Regulate the Expression of Genes Involved in Sterol Uptake by a Mitogen-activated Protein Kinase-independent Pathway. Mol Biol Cell 20: 4826–4837

Lin R, Bagrodia S, Cerione R & Manor D (1997) A novel Cdc42Hs mutant induces cellular transformation. Curr Biol 7: 794–797

Lippincott J (1998) Sequential assembly of myosin II, an IQGAP-like protein, and filamentous actin to a ring structure involved in budding yeast cytokinesis. J. Cell Biol. 140:355–366

Machner M (2006) Targeting of host Rab GTPase function by the intravacuolar pathogen Legionella pneumophila. Dev. Cell 11, 47–56

Marco E, Wedlich-Soldner R, Li R, Altschuler S & Wu L (2007) Endocytosis optimizes the dynamic localization of membrane proteins that regulate cortical polarity. Cell 129: 411–422

Marquitz A, Harrison J, Bose I, Zyla T, McMillan J & Lew D (2002) The Rho-GAP Bem2p plays a GAP-independent role in the morphogenesis checkpoint. Embo J 21: 4012–4025

Masuda T, Tanaka K, Nonaka H, Yamochi W, Maeda A & Takai Y (1994) Molecular-Cloning and Characterization of Yeast-Rho Gdp Dissociation Inhibitor. J Biol Chem 269: 19713–19718

McCusker DD, Denison CC, Anderson SS, Egelhofer Tat, Yates JRJ, Gygi SPS & Kellogg DRD (2007) Cdk1 coordinates cell-surface growth with the cell cycle. Nat Cell Biol 9: 506–515

Meinhardt H (1972) A theory of biological pattern formation. Kybernetik 12:30-39

Meinhardt H (2000) Pattern formation by local self-activation and lateral inhibition. Bioessays 22, 753–760

Mewes HW, Ruepp A, Theis F, Rattei T, Walter M, Frishman D, Suhre K, Spannagl M, Mayer KFX, Stümpflen V & Antonov A (2011) MIPS: curated databases and comprehensive secondary data resources in 2010. Nucleic Acids Res. 39: D220–4

Moffat J & Andrews B (2004) Late-G1 cyclin-CDK activity is essential for control of cell morphogenesis in budding yeast. Nat Cell Biol 6: 59–66

Moseley J (2006) The yeast actin cytoskeleton: from cellular function to biochemical mechanism. Microbiol. Mol. Biol. Rev. 70:605–645

Munemitsu S, Innis M & Clark R (1990) Molecular cloning and expression of a G25K cDNA, the human homolog of the yeast cell cycle gene CDC42. Mol. Cell. Biol. 10:5977-5982

Murata T, Delprato A, Ingmundson A, Toomre DK, Lambright DG & Roy CR (2006) The Legionella pneumophila effector protein DrrA is a Rab1 guanine nucleotide-exchange factor. Nat Cell Biol 8: 971–977

Nomanbhoy TK, Erickson JW & Cerione RA (1999) Kinetics of Cdc42 membrane extraction by Rho-GDI monitored by real-time fluorescence resonance energy transfer. Biochemistry 38: 1744–1750

Onsum MD & Rao CV (2009) Calling heads from tails: the role of mathematical modeling in understanding cell polarization. Curr Opin Cell Biol 21: 74–81

Ozbudak EM, Becskei A & Van Oudenaarden A (2005) A System of Counteracting Feedback Loops Regulates Cdc42p Activity during Spontaneous Cell Polarization. Developmental Cell 9: 565–571

Parent CA (2004) Making all the right moves: chemotaxis in neutrophils and Dictyostelium. Curr Opin Cell Biol 16: 4–13

Park H-O & Bi E (2007) Central Roles of Small GTPases in the Development of Cell Polarity in Yeast and Beyond. Microbiology and Molecular Biology Reviews 71: 48–96

Park HO, Chant J & Herskowitz I (1993) BUD2 encodes a GTPase-activating protein for Bud1/Rsr1 necessary for proper bud-site selection in yeast. Nature 365: 269–274

Perez P (2010) Rho GTPases: regulation of cell polarity and growth in yeasts. Biochem. J. 426: 243–253

Peterson J, Zheng Y, Bender L & Myers A (1994) Interactions between the bud emergence proteins Bem1p and Bem2p and Rho-type GTPases in yeast. J Cell Biol 127, 1395–1406

Pollard T (2003) Cellular motility driven by assembly and disassembly of actin filaments.

Cell 112:453-65

Pruyne D, Gao L, Bi E & Bretscher A (2004) Stable and dynamic axes of polarity use distinct formin isoforms in budding yeast. Mol Biol Cell 15: 4971–4989

Reinstein J, Schlichting I, Frech M, Goody RS & Wittinghofer A (1991) p21 with a phenylalanine 28—-leucine mutation reacts normally with the GTPase activating protein GAP but nevertheless has transforming properties. J Biol Chem 266: 17700–17706

Richman T & Johnson D (2000) Saccharomyces cerevisiae cdc42p GTPase is involved in preventing the recurrence of bud emergence during the cell cycle. Mol Cell Biol 20: 8548–8559

Robbe K, Otto-Bruc A, Chardin P & Antonny B (2003) Dissociation of GDP dissociation inhibitor and membrane translocation are required for efficient activation of Rac by the Dbl homology-pleckstrin homology region of Tiam. J Biol Chem 278: 4756–4762

Rodal A, Kozubowski L & Goode B (2005) Actin and septin ultrastructures at the budding yeast cell cortex. Mol. Biol. Cell 16, 372–384

Sagot I & Klee S (2001) Yeast formins regulate cell polarity by controlling the assembly of actin cables. Nat Cell Biol 4, 42–50

Saito K, Fujimura-Kamada K, Hanamatsu H, Kato U, Umeda M, Kozminski KG & Tanaka K (2007) Transbilayer phospholipid flipping regulates Cdc42p signaling during polarized cell growth via Rga GTPase-activating proteins. Dev Cell 13: 743–751

Salwinski L, Miller C, Smith A, Pettit F, Bowie J & Eisenberg D (2004) The Database of Interacting Proteins: 2004 update. Nucleic Acids Res. 32: D449–D451

Schoebel S, Oesterlin LK, Blankenfeldt W, Goody RS & Itzen A (2009) RabGDI Displacement by DrrA from Legionella Is a Consequence of Its Guanine Nucleotide Exchange Activity. Molecular Cell 36: 1060–1072

Shimada Y & Gulli M (2000) Nuclear sequestration of the exchange factor Cdc24 by Far1 regulates cell polarity during yeast mating. Nat. Cell Biol. 2: 117–124

Shimada Y, Wiget P, Gulli M & Bi E (2004) The nucleotide exchange factor Cdc24p may be regulated by auto-inhibition. EMBO ?J. 23:1051–1062

Slaughter BD, Das A, Schwartz JW, Rubinstein B & Li R (2009) Dual Modes of Cdc42 Recycling Fine-Tune Polarized Morphogenesis. Dev Cell 17: 823–835

Smith GR, Givan SA, Cullen P & Sprague GF (2002) GTPase-activating proteins for Cdc42.

Eukaryotic Cell 1: 469–480

Sopko R, Huang D, Smith J, Figeys D & Andrews B (2007) Activation of the Cdc42p GTPase by cyclin-dependent protein kinases in budding yeast. Embo J 26: 4487–4500

Stevenson B, Ferguson B, Devirgilio C, Bi E, Pringle J, Ammerer G & Sprague G (1995) Mutation of Rga1, Which Encodes a Putative Gtpase-Activating Protein for the Polarity-Establishment Protein Cdc42p, Activates the Pheromone-Response Pathway in the Yeast Saccharomyces-Cerevisiae. Genes Dev. 9:2949–2963

Tcheperegine SE, Gao X-D & Bi E (2005) Regulation of cell polarity by interactions of Msb3 and Msb4 with Cdc42 and polarisome components. Mol Cell Biol 25: 8567–8580

Tiedje C, Sakwa I, Just U & Höfken T (2008) The Rho GDI Rdi1 regulates Rho GTPases by distinct mechanisms. Mol Biol Cell 19: 2885–2896

Tjandra H & Compton J (1998) Control of mitotic events by the Cdc42 GTPase, the Clb2 cyclin and a member of the PAK kinase family. Curr. Biol. 8, 991–1000

Tokunaga M, Imamoto N & Sakata-Sogawa K (2008) Highly inclined thin illumination enables clear single-molecule imaging in cells. Nat Meth 5: 159–161

Tong A & Boone C (2007) Methods in Microbiology. 36: 369–707

Turing A (1952) The chemical basis of morphogenesis. Philos. Trans. R. Soc. Lond. B Biol. Sci. 237, 37–72

Ubersax JA, Woodbury EL, Quang PN, Paraz M, Blethrow JD, Shah K, Shokat KM & Morgan DO (2003) Targets of the cyclin-dependent kinase Cdk1. Nature 425: 859–864

Ugolev Y, Berdichevsky Y, Weinbaum C & Pick E (2008) Dissociation of Rac1(GDP)center dot RhoGDI complexes by the cooperative action of anionic liposomes containing phosphatidylinositol 3,4,5-trisphosphate, rac guanine nucleotide exchange factor, and GTP. J Biol Chem 283: 22257–22271

Vetter I (2001) The guanine nucleotide-binding switch in three dimensions. Science 294, 1299–1304

Wai S & Gerber S (2009) Multisite phosphorylation of the guanine nucleotide exchange factor Cdc24 during yeast cell polarization. PLoS ONE 4, e6563

Wedlich-Soldner R & Li R (2004) Closing the loops: new insights into the role and regulation of actin during cell polarization. Exp Cell Res 301: 8–15

Wedlich-Soldner R, Altschuler S, Wu L & Li R (2003) Spontaneous cell polarization through actomyosin-based delivery of the Cdc42 GTPase. Science 299: 1231–1235

Wedlich-Soldner R, Wai SC, Schmidt T & Li R (2004) Robust cell polarity is a dynamic state established by coupling transport and GTPase signaling. J Cell Biol 166: 889–900

Weiner OD, Neilsen PO, Prestwich GD, Kirschner MW, Cantley LC & Bourne HR (2002) A PtdInsP3- and Rho GTPase-mediated positive feedback loop regulates neutrophil polarity. Nat Cell Biol 4: 509–513

Wu Y, Oesterlin L, Tan K & Waldmann H (2010) Membrane targeting mechanism of Rab GTPases elucidated by semisynthetic protein probes. Nat Chem Biol. 2010;6:534–540

Yeung T, Gilbert GE, Shi J, Silvius J, Kapus A & Grinstein S (2008) Membrane phosphatidylserine regulates surface charge and protein localization. Science 319: 210–213

Yu JH, Crevenna AH, Bettenbuehl M, Freisinger T & Wedlich-Soeldner R (2011) Cortical actin dynamics driven by formins and myosin V. J Cell Sci 124: 1533–1541

Zenke FT, Kapp L & Breunig KD (1999) Regulated phosphorylation of the Gal4p inhibitor Gal80p of Kluyveromyces lactis revealed by mutational analysis. Biol. Chem. 380: 419–430

Zheng Y & Cerione R (1994) Control of the yeast bud-site assembly GTPase Cdc42. Catalysis of guanine nucleotide exchange by Cdc24 and stimulation of GTPase activity by Bem3. J Biol Chem 269, 2369–2372

Ziman M, O'Brien J, Ouellette L, Church W & Johnson D (1991) Mutational analysis of CDC42Sc, a Saccharomyces cerevisiae gene that encodes a putative GTP-binding protein involved in the control of cell polarity. Mol Cell Biol 11: 3537–3544

A Annex

A.1 Tables

Table A.1: FRAP recovery half-time

STRAIN	N	t 1/2 (s)	SEM
Cdc42 (1x)	24	2.0	0.15
Cdc42 (2x)	56	2.2	0.08
Cdc42 (3x)	10	2.3	0.16
Cdc42 (1x)+LatB	11	2.8	0.12
Cdc42 (2x)+LatB	14	2.7	0.09
Cdc42 (3x)+LatB	12	3.3	0.25
*rdi1*ΔCdc42 (2x)	20	10.6	0.45
$Cdc42^{R66E}$	11	9.1	0.66
$Cdc42^{R66E}$+Cdc24OE	10	11.0	0.57
*vps27*Δ Cdc42 (2x)	15	2.4	0.13
*rdi1*Δ *vps27*ΔCdc42 (2x)	10	13.5	0.54
*bem2*ΔCdc42 (2x)	20	6.6	0.39
*bem2*ΔCdc42 (2x)+LatB	12	9.6	0.57
*bem2*ΔCdc42 (3x)	10	7.0	0.47
*bem2*ΔCdc42(3x)+LatB	17	9.3	0.40
*bem3*ΔCdc42 (2x)	14	2.7	0.25
*rga2*ΔCdc42 (2x)	11	3.3	0.23
$Cdc42^{G60A}$	11	6.8	0.40
$Cdc42^{G60A}$+Cdc24OE	10	5.4	0.22
$Cdc42^{G12V}$	16	33.4	2.20
$Cdc42^{D57Y}$	16	11.9	0.68
$Cdc42^{F28L}$	13	2.1	0.07
Cdc24 (1x)	10	2.1	0.14
Cdc24 (2x)	20	2.1	0.15
Cdc24 (3x)	11	2.2	0.14

N = cell number

Table A.1: FRAP recovery half-time (continued)

STRAIN	N	T 1/2 (S)	SEM
Cdc24 (2x)+LatB	14	2.2	0.12
Cdc24 (3x)+LatB	17	2.0	0.09
*bem2*ΔCdc24 (2x)	10	2.1	0.15
*bem2*ΔCdc24 (3x)	10	2.3	0.18
Cdc42(2x)+Cdc24OE	17	2.0	0.09
Cdc42(2x)+Cdc24OE+latB	16	2.6	0.13
*bem2*ΔCdc42 (2x)+Cdc24OE	17	4.8	0.32
*bem2*ΔCdc42 (2x)+Cdc24OE+LatB	11	6.7	0.35
*bem2*ΔCdc42^{F28L}	11	4.8	0.18
GFP-Bem1 (1x)	14	2.0	0.17
GFP-Bem2 (1x)	12	2.2	0.18

N = cell number

Table A.2: Cells with two buds

STRAIN	EXPERIMENT	N	2 BUDS(%)	SEM
GFP-Cdc42 (integr. Plasmid)	/	300	0.0	0.0
	a	300	0.0	0.0
	b	300	0.7	0.6
2x GFP-Cdc42 (2x integr. Plasmid)	/	500	0.0	0.0
	a	300	0.0	0.0
	b	300	0.3	0.6
GFP-Cdc42+Cdc24OE	/	900	0.0	0.0
	a	300	0.0	0.0
	b	300	0.0	0.0
Cdc42^{F28L}	/	500	0.0	0.0
	a	300	0.0	0.0
	b	300	0.0	0.0
*bem1*Δ GFP-Cdc42	/	500	3.3	0.9

N = cell number; / = no LatB treatment; a = 20 min LatB treatment; b = 40 min LatB treatment

Table A.2: Cells with two buds (continued)

STRAIN	EXPERIMENT	N	2 BUDS (%)	SEM
	a	300	3.0	1.0
	b	300	2.7	1.2
*rdi1*Δ GFP-Cdc42	/	400	2.3	0.5
	a	300	13.0	1.0
	b	300	23.0	0.6
*bem2*Δ (no tag)	/	200	7.0	1.4
	a	300	14.0	1.5
	b	300	25.0	1.5
*bem2*Δ GFP-Cdc42	/	600	8.7	0.8
	a	300	13.0	1.5
	b	300	25.0	0.6
*bem2*Δ 2x GFP-Cdc42	/	500	9.8	1.5
	a	300	17.0	1.2
	b	300	26.0	1.5
*bem2*Δ GFP-Cdc42+Cdc24OE	/	900	12.0	1.3
	a	300	24.0	1.5
	b	300	30.0	2.6
*bem2*ΔCdc42^{F28L}	/	500	25.0	1.5
	a	300	55.0	0.6
	b	300	63.0	3.1
Cdc24-GFP (integr. Plasmid)	/	700	0.0	0.0
	a	300	0.0	0.0
	b	300	0.0	0.0
2xCdc24-GFP (integr.+CEN Plasmid)	/	700	0.0	0.0
	a	300	0.0	0.0
	b	300	0.0	0.0
*bem2*Δ Cdc24-GFP	/	1000	10.0	1.3
	a	300	21.0	1.0
	b	300	28.0	2.0
*bem2*Δ 2xCdc24-GFP	/	600	19.0	1.5

N = cell number; / = no LatB treatment; a = 20 min LatB treatment; b = 40 min LatB treatment

Table A.2: Cells with two buds (continued)

STRAIN	EXPERIMENT	N	2 BUDS (%)	SEM
	a	300	26.0	1.0
	b	300	26.0	2.1

N = cell number; / = no LatB treatment; a = 20 min LatB treatment; b = 40 min LatB treatment

Table A.3: Genetic interactions

QUERY	INTERACTOR	EXPERIMENT	INTERACTOR CATEGORY
BEM1	RSR1	(This study)	CDC42 SIGNALLING
BEM1	VPS9	(This study)	ENDOCYTIC RECYCLING
RDI1	GOS1	(This study)	EARLY SECRETION
BEM2	RDI1	(This study)	CDC42 MODULE
CDC42	MSB3	SYNTHETIC GROWTH DEFECT	LATE SECRETION
CDC42	CAP1	SYNTHETIC GROWTH DEFECT	ENDOCYTIC RECYCLING
CDC42	BUD6	SYNTHETIC GROWTH DEFECT	ACTIN GENERAL
CDC42	GIC2	SYNTHETIC GROWTH DEFECT	CDC42 SIGNALLING
CDC42	CAP2	SYNTHETIC GROWTH DEFECT	ACTIN GENERAL
BEM2	PXL1	SYNTHETIC GROWTH DEFECT	ACTIN GENERAL
CLA4	RGA1	SYNTHETIC GROWTH DEFECT	CDC42 MODULE
CLA4	RGA2	SYNTHETIC GROWTH DEFECT	CDC42 MODULE
BEM2	GET2	SYNTHETIC GROWTH DEFECT	EARLY SECRETION
BEM2	GET1	SYNTHETIC GROWTH DEFECT	EARLY SECRETION
BEM2	BEM3	SYNTHETIC GROWTH DEFECT	CDC42 MODULE
CLA4	RVS161	SYNTHETIC GROWTH DEFECT	ACTIN GENERAL
CLA4	PEA2	SYNTHETIC GROWTH DEFECT	ACTIN GENERAL
RGA1	RIC1	SYNTHETIC GROWTH DEFECT	ENDOCYTIC RECYCLING
CLA4	RVS167	SYNTHETIC GROWTH DEFECT	ACTIN GENERAL
CLA4	ICE2	SYNTHETIC GROWTH DEFECT	EARLY SECRETION
CDC42	SPA2	SYNTHETIC GROWTH DEFECT	ACTIN GENERAL
CDC42	RSR1	SYNTHETIC GROWTH DEFECT	CDC42 SIGNALLING

Table A.3: Genetic interactions (continued)

QUERY	INTERACTOR	EXPERIMENT	INTERACTOR CATEGORY
CLA4	CHS6	SYNTHETIC GROWTH DEFECT	LATE SECRETION
CLA4	CHS5	SYNTHETIC GROWTH DEFECT	LATE SECRETION
BEM1	ACT1	SYNTHETIC HAPLOINSUFFICIENCY	ACTIN GENERAL
BEM2	ACT1	SYNTHETIC HAPLOINSUFFICIENCY	ACTIN GENERAL
BEM2	SMY1	SYNTHETIC LETHALITY	LATE SECRETION
CLA4	CHS5	SYNTHETIC LETHALITY	LATE SECRETION
CLA4	SMY1	SYNTHETIC LETHALITY	LATE SECRETION
CLA4	EDE1	SYNTHETIC LETHALITY	ENDOCYTIC RECYCLING
CLA4	CHS6	SYNTHETIC LETHALITY	LATE SECRETION
CLA4	BNI1	SYNTHETIC LETHALITY	ACTIN GENERAL
CLA4	BEM4	SYNTHETIC LETHALITY	CDC42 SIGNALLING
CLA4	ARP2	SYNTHETIC LETHALITY	ACTIN GENERAL
BEM1	BBC1	SYNTHETIC LETHALITY	ACTIN GENERAL
BEM2	TPM1	SYNTHETIC LETHALITY	ACTIN GENERAL
CLA4	BUD6	SYNTHETIC LETHALITY	ACTIN GENERAL
CLA4	RVS167	SYNTHETIC LETHALITY	ACTIN GENERAL
CLA4	RVS161	SYNTHETIC LETHALITY	ACTIN GENERAL
CLA4	VAC14	SYNTHETIC LETHALITY	ENDOCYTIC RECYCLING
BEM2	CHS5	SYNTHETIC LETHALITY	LATE SECRETION
CLA4	SPA2	SYNTHETIC LETHALITY	ACTIN GENERAL
CLA4	MYO2	SYNTHETIC LETHALITY	LATE SECRETION
BEM2	SAC6	SYNTHETIC LETHALITY	ACTIN GENERAL
CLA4	FAB1	SYNTHETIC LETHALITY	ENDOCYTIC RECYCLING
BEM2	MYO2	SYNTHETIC LETHALITY	LATE SECRETION
BEM1	ARP2	SYNTHETIC LETHALITY	ACTIN GENERAL
CLA4	PEA2	SYNTHETIC LETHALITY	ACTIN GENERAL
CDC42	PEA2	SYNTHETIC LETHALITY	ACTIN GENERAL
CDC24	SEC15	SYNTHETIC LETHALITY	LATE SECRETION
CDC42	MSB3	SYNTHETIC LETHALITY	LATE SECRETION
CDC42	SEC10	SYNTHETIC LETHALITY	LATE SECRETION
CDC42	RSR1	SYNTHETIC LETHALITY	CDC42 SIGNALLING

Table A.3: Genetic interactions (continued)

QUERY	INTERACTOR	EXPERIMENT	INTERACTOR CATEGORY
BEM1	BNI1	SYNTHETIC LETHALITY	ACTIN GENERAL
CDC42	BUD6	SYNTHETIC LETHALITY	ACTIN GENERAL
CDC42	BEM4	SYNTHETIC LETHALITY	CDC42 SIGNALLING
CDC42	BNI1	SYNTHETIC LETHALITY	ACTIN GENERAL
CDC42	GIC2	SYNTHETIC LETHALITY	CDC42 SIGNALLING
CDC42	CAP2	SYNTHETIC LETHALITY	ACTIN GENERAL
CDC42	SEC8	SYNTHETIC LETHALITY	LATE SECRETION
CDC42	SEC66	SYNTHETIC LETHALITY	EARLY SECRETION
CDC42	SEC5	SYNTHETIC LETHALITY	LATE SECRETION
CLA4	ARC40	SYNTHETIC LETHALITY	ACTIN GENERAL
CDC42	SPA2	SYNTHETIC LETHALITY	ACTIN GENERAL
CDC42	SEC9	SYNTHETIC LETHALITY	LATE SECRETION
CDC42	SEC2	SYNTHETIC LETHALITY	LATE SECRETION
CDC42	SEC15	SYNTHETIC LETHALITY	LATE SECRETION
CDC42	CAP1	SYNTHETIC LETHALITY	ENDOCYTIC RECYCLING
CDC24	BEM4	SYNTHETIC LETHALITY	CDC42 SIGNALLING
CDC42	SEC3	SYNTHETIC LETHALITY	LATE SECRETION
CDC42	SEC4	SYNTHETIC LETHALITY	LATE SECRETION
BEM2	BNI1	SYNTHETIC LETHALITY	ACTIN GENERAL
BEM2	ARC40	SYNTHETIC LETHALITY	ACTIN GENERAL
RGA1	RIC1	SYNTHETIC LETHALITY	ENDOCYTIC RECYCLING
BEM2	CDC24	SYNTHETIC LETHALITY	CDC42 MODULE
BEM2	RGA1	SYNTHETIC LETHALITY	CDC42 MODULE
BEM2	ARP2	SYNTHETIC LETHALITY	ACTIN GENERAL
BEM2	CLA4	SYNTHETIC LETHALITY	CDC42 MODULE
BEM1	ARC40	SYNTHETIC LETHALITY	ACTIN GENERAL
BEM1	CDC42	SYNTHETIC LETHALITY	CDC42 MODULE
BEM1	CDC24	SYNTHETIC LETHALITY	CDC42 MODULE
BEM1	BEM2	SYNTHETIC LETHALITY	CDC42 MODULE
BEM2	ACT1	SYNTHETIC LETHALITY	ACTIN GENERAL
BEM1	SMY1	SYNTHETIC LETHALITY	LATE SECRETION

Table A.3: Genetic interactions (continued)

QUERY	INTERACTOR	EXPERIMENT	INTERACTOR CATEGORY
BEM1	CLA4	SYNTHETIC LETHALITY	CDC42 MODULE
BEM3	CDC24	SYNTHETIC LETHALITY	CDC42 MODULE
CDC24	CDC42	SYNTHETIC LETHALITY	CDC42 MODULE
CDC42	CLA4	SYNTHETIC LETHALITY	CDC42 MODULE
BEM1	MYO2	SYNTHETIC LETHALITY	LATE SECRETION
CDC24	CDC42	SYNTHETIC LETHALITY (CONDITIONAL)	CDC42 MODULE
BEM1	RDI1	Costanzo et al. 2010	CDC42 MODULE
BEM1	CDC42	Costanzo et al. 2010	CDC42 MODULE
BEM1	BOI1	Costanzo et al. 2010	CDC42 SIGNALLING
BEM1	CAP2	Costanzo et al. 2010	ACTIN GENERAL
BEM1	CHS6	Costanzo et al. 2010	LATE SECRETION
CDC42	SRO7	Costanzo et al. 2010	LATE SECRETION
CDC42	TPM1	Costanzo et al. 2010	ACTIN GENERAL
BEM1	ACT1	Costanzo et al. 2010	ACTIN GENERAL
CLA4	RGA1	Costanzo et al. 2010	CDC42 MODULE
BEM1	BEM4	Costanzo et al. 2010	CDC42 SIGNALLING
CDC42	SPA2	Costanzo et al. 2010	ACTIN GENERAL
BEM1	AIP1	Costanzo et al. 2010	ACTIN GENERAL
BEM2	CLA4	Costanzo et al. 2010	CDC42 MODULE
CDC42	GIC2	Costanzo et al. 2010	CDC42 SIGNALLING
BEM3	RGA1	Costanzo et al. 2010	CDC42 MODULE
BEM2	RGA1	Costanzo et al. 2010	CDC42 MODULE
BEM1	BUD6	Costanzo et al. 2010	ACTIN GENERAL
BEM2	BEM3	Costanzo et al. 2010	CDC42 MODULE
CDC42	CAP1	Costanzo et al. 2010	ENDOCYTIC RECYCLING
BEM1	ARC18	Costanzo et al. 2010	ACTIN GENERAL
BEM1	CAP1	Costanzo et al. 2010	ENDOCYTIC RECYCLING
BEM2	CDC42	Costanzo et al. 2010	CDC42 MODULE
CDC42	CAP2	Costanzo et al. 2010	ACTIN GENERAL
CLA4	SHE4	Costanzo et al. 2010	LATE SECRETION

Table A.3: Genetic interactions (continued)

QUERY	INTERACTOR	EXPERIMENT	INTERACTOR CATEGORY
RDI1	YCK2	Costanzo et al. 2010	ENDOCYTIC RECYCLING
CLA4	RVS161	Costanzo et al. 2010	ACTIN GENERAL
RDI1	VRP1	Costanzo et al. 2010	ACTIN GENERAL
BEM1	ARF1	Costanzo et al. 2010	EARLY SECRETION
CLA4	PEA2	Costanzo et al. 2010	ACTIN GENERAL
CLA4	CHS5	Costanzo et al. 2010	LATE SECRETION
RGA1	ACT1	Costanzo et al. 2010	ACTIN GENERAL
BEM1	ARF3	Costanzo et al. 2010	ENDOCYTIC RECYCLING
CLA4	YEL1	Costanzo et al. 2010	ENDOCYTIC RECYCLING
CLA4	TPM1	Costanzo et al. 2010	ACTIN GENERAL
RDI1	TOS2	Costanzo et al. 2010	CDC42 SIGNALLING
RDI1	BEM4	Costanzo et al. 2010	CDC42 SIGNALLING
RDI1	PEA2	Costanzo et al. 2010	ACTIN GENERAL
CLA4	SMY1	Costanzo et al. 2010	LATE SECRETION
CLA4	SLA1	Costanzo et al. 2010	ACTIN GENERAL
CLA4	SPA2	Costanzo et al. 2010	ACTIN GENERAL
RDI1	VPS27	Costanzo et al. 2010	ENDOCYTIC RECYCLING
RGA1	SRO7	Costanzo et al. 2010	LATE SECRETION
CLA4	BUD6	Costanzo et al. 2010	ACTIN GENERAL
CLA4	CAP2	Costanzo et al. 2010	ACTIN GENERAL
CLA4	CAP1	Costanzo et al. 2010	ENDOCYTIC RECYCLING
RGA2	GET1	Costanzo et al. 2010	EARLY SECRETION
CLA4	BEM4	Costanzo et al. 2010	CDC42 SIGNALLING
RGA1	VPS9	Costanzo et al. 2010	ENDOCYTIC RECYCLING
RGA1	VRP1	Costanzo et al. 2010	ACTIN GENERAL
RGA1	BUD14	Costanzo et al. 2010	ACTIN GENERAL
BEM1	ATG8	Costanzo et al. 2010	EARLY SECRETION
CLA4	EDE1	Costanzo et al. 2010	ENDOCYTIC RECYCLING
RGA1	CMD1	Costanzo et al. 2010	ACTIN GENERAL
CLA4	ICE2	Costanzo et al. 2010	EARLY SECRETION
RGA1	SLA1	Costanzo et al. 2010	ACTIN GENERAL

Table A.3: Genetic interactions (continued)

QUERY	INTERACTOR	EXPERIMENT	INTERACTOR CATEGORY
RGA1	SLY41	Costanzo et al. 2010	EARLY SECRETION
BEM1	BBC1	Costanzo et al. 2010	ACTIN GENERAL
CLA4	CHS6	Costanzo et al. 2010	LATE SECRETION
BEM2	CCZ1	Costanzo et al. 2010	ENDOCYTIC RECYCLING
BEM2	BUL1	Costanzo et al. 2010	ENDOCYTIC RECYCLING
BEM2	BUD6	Costanzo et al. 2010	ACTIN GENERAL
BEM2	BUD14	Costanzo et al. 2010	ACTIN GENERAL
BEM2	CCZ1	Costanzo et al. 2010	ENDOCYTIC RECYCLING
BEM2	CAP2	Costanzo et al. 2010	ACTIN GENERAL
BEM2	CAP1	Costanzo et al. 2010	ENDOCYTIC RECYCLING
BEM2	BST1	Costanzo et al. 2010	EARLY SECRETION
BEM2	APL1	Costanzo et al. 2010	ENDOCYTIC RECYCLING
BEM2	ACT1	Costanzo et al. 2010	ACTIN GENERAL
BEM1	SEC61	Costanzo et al. 2010	LATE SECRETION
BEM2	BNI1	Costanzo et al. 2010	ACTIN GENERAL
BEM2	ARF1	Costanzo et al. 2010	EARLY SECRETION
BEM2	APS2	Costanzo et al. 2010	ENDOCYTIC RECYCLING
CDC24	RIC1	Costanzo et al. 2010	ENDOCYTIC RECYCLING
BEM1	FAR10	Costanzo et al. 2010	CDC42 SIGNALLING
BEM1	GIC1	Costanzo et al. 2010	CDC42 SIGNALLING
BEM2	GCS1	Costanzo et al. 2010	EARLY SECRETION
BEM2	MYO2	Costanzo et al. 2010	LATE SECRETION
BEM2	ICE2	Costanzo et al. 2010	EARLY SECRETION
BEM2	GIC1	Costanzo et al. 2010	CDC42 SIGNALLING
BEM2	ERV14	Costanzo et al. 2010	EARLY SECRETION
BEM2	CLC1	Costanzo et al. 2010	ENDOCYTIC RECYCLING
BEM2	CHS6	Costanzo et al. 2010	LATE SECRETION
BEM2	CHS5	Costanzo et al. 2010	LATE SECRETION
BEM2	COG7	Costanzo et al. 2010	EARLY SECRETION
BEM2	COG6	Costanzo et al. 2010	EARLY SECRETION
BEM2	CMD1	Costanzo et al. 2010	ACTIN GENERAL

Table A.3: Genetic interactions (continued)

QUERY	INTERACTOR	EXPERIMENT	INTERACTOR CATEGORY
BEM1	RVS167	Costanzo et al. 2010	ACTIN GENERAL
BEM1	RVS161	Costanzo et al. 2010	ACTIN GENERAL
BEM1	RUD3	Costanzo et al. 2010	EARLY SECRETION
BEM1	SEC3	Costanzo et al. 2010	LATE SECRETION
BEM1	SEC15	Costanzo et al. 2010	LATE SECRETION
BEM1	SEC10	Costanzo et al. 2010	LATE SECRETION
BEM1	KES1	Costanzo et al. 2010	EARLY SECRETION
BEM1	PEA2	Costanzo et al. 2010	ACTIN GENERAL
BEM1	MYO2	Costanzo et al. 2010	LATE SECRETION
BEM1	KIN1	Costanzo et al. 2010	LATE SECRETION
BEM1	RHB1	Costanzo et al. 2010	EARLY SECRETION
BEM1	RGP1	Costanzo et al. 2010	ENDOCYTIC RECYCLING
BEM1	PXL1	Costanzo et al. 2010	ACTIN GENERAL
BEM1	YPT31	Costanzo et al. 2010	LATE SECRETION
BEM1	VPS74	Costanzo et al. 2010	EARLY SECRETION
BEM1	VPS51	Costanzo et al. 2010	ENDOCYTIC RECYCLING
BEM1	VPS17	Costanzo et al. 2010	ENDOCYTIC RECYCLING
BEM1	YEL1	Costanzo et al. 2010	ENDOCYTIC RECYCLING
BEM1	VRP1	Costanzo et al. 2010	ACTIN GENERAL
BEM1	GIC2	Costanzo et al. 2010	CDC42 SIGNALLING
BEM1	TPM1	Costanzo et al. 2010	ACTIN GENERAL
BEM1	SHE4	Costanzo et al. 2010	LATE SECRETION
BEM1	SEC72	Costanzo et al. 2010	EARLY SECRETION
BEM1	SEC63	Costanzo et al. 2010	LATE SECRETION
BEM1	SYT1	Costanzo et al. 2010	LATE SECRETION
BEM1	SPA2	Costanzo et al. 2010	ACTIN GENERAL
BEM1	SMY1	Costanzo et al. 2010	LATE SECRETION
CDC24	CAP2	Costanzo et al. 2010	ACTIN GENERAL
CDC24	CAP1	Costanzo et al. 2010	ENDOCYTIC RECYCLING
CDC24	BUD6	Costanzo et al. 2010	ACTIN GENERAL
CDC24	PEA2	Costanzo et al. 2010	ACTIN GENERAL

Table A.3: Genetic interactions (continued)

QUERY	INTERACTOR	EXPERIMENT	INTERACTOR CATEGORY
CDC24	GIC2	Costanzo et al. 2010	CDC42 SIGNALLING
CDC24	COG7	Costanzo et al. 2010	EARLY SECRETION
CDC24	BEM4	Costanzo et al. 2010	CDC42 SIGNALLING
BEM3	EDE1	Costanzo et al. 2010	ENDOCYTIC RECYCLING
BEM3	CHS5	Costanzo et al. 2010	LATE SECRETION
BEM2	SPA2	Costanzo et al. 2010	ACTIN GENERAL
BEM3	SMY1	Costanzo et al. 2010	LATE SECRETION
BEM3	SLA1	Costanzo et al. 2010	ACTIN GENERAL
BEM3	SHE4	Costanzo et al. 2010	LATE SECRETION
CDC42	BEM4	Costanzo et al. 2010	CDC42 SIGNALLING
CDC24	VPS41	Costanzo et al. 2010	ENDOCYTIC RECYCLING
CDC24	VAM7	Costanzo et al. 2010	ENDOCYTIC RECYCLING
CDC24	VAM6	Costanzo et al. 2010	ENDOCYTIC RECYCLING
CDC24	YPT7	Costanzo et al. 2010	ENDOCYTIC RECYCLING
CDC24	YPT32	Costanzo et al. 2010	LATE SECRETION
CDC24	YJL206C-A	Costanzo et al. 2010	LATE SECRETION
CDC24	VAM3	Costanzo et al. 2010	ENDOCYTIC RECYCLING
CDC24	SPA2	Costanzo et al. 2010	ACTIN GENERAL
CDC24	SNX41	Costanzo et al. 2010	ENDOCYTIC RECYCLING
CDC24	RSR1	Costanzo et al. 2010	CDC42 SIGNALLING
CDC24	TPM1	Costanzo et al. 2010	ACTIN GENERAL
CDC24	TLG2	Costanzo et al. 2010	EARLY SECRETION
CDC24	SPH1	Costanzo et al. 2010	LATE SECRETION
BEM2	SHE4	Costanzo et al. 2010	LATE SECRETION
BEM2	SEC72	Costanzo et al. 2010	EARLY SECRETION
BEM2	SEC66	Costanzo et al. 2010	LATE SECRETION
BEM2	SNC2	Costanzo et al. 2010	LATE SECRETION
BEM2	SMY1	Costanzo et al. 2010	LATE SECRETION
BEM2	SHE4	Costanzo et al. 2010	LATE SECRETION
BEM2	SEC3	Costanzo et al. 2010	LATE SECRETION

Table A.3: Genetic interactions (continued)

QUERY	INTERACTOR	EXPERIMENT	INTERACTOR CATEGORY
BEM2	RSR1	Costanzo et al. 2010	CDC42 SIGNALLING
BEM2	PXL1	Costanzo et al. 2010	ACTIN GENERAL
BEM1	ERV41	Costanzo et al. 2010	EARLY SECRETION
BEM2	SEC15	Costanzo et al. 2010	LATE SECRETION
BEM2	SEC10	Costanzo et al. 2010	LATE SECRETION
BEM2	RUD3	Costanzo et al. 2010	EARLY SECRETION
BEM3	BNI1	Costanzo et al. 2010	ACTIN GENERAL
BEM2	YCK1	Costanzo et al. 2010	ENDOCYTIC RECYCLING
BEM2	VPS74	Costanzo et al. 2010	EARLY SECRETION
BEM2	VPS51	Costanzo et al. 2010	EARLY SECRETION
BEM3	ARC15	Costanzo et al. 2010	ACTIN GENERAL
BEM2	YPT32	Costanzo et al. 2010	LATE SECRETION
BEM2	YCK2	Costanzo et al. 2010	ENDOCYTIC RECYCLING
BEM2	VPS30	Costanzo et al. 2010	ENDOCYTIC RECYCLING
BEM2	SYT1	Costanzo et al. 2010	LATE SECRETION
BEM2	SSO2	Costanzo et al. 2010	LATE SECRETION
BEM2	SSO1	Costanzo et al. 2010	LATE SECRETION
BEM2	VPS21	Costanzo et al. 2010	ENDOCYTIC RECYCLING
BEM2	VAC14	Costanzo et al. 2010	ENDOCYTIC RECYCLING
BEM2	TPM1	Costanzo et al. 2010	ACTIN GENERAL

Table A.4: Physical interations

QUERY	INTERACTOR	EXPERIMENT	INTERACTOR CATEGORY
BEM1	ACT1	AFFINITY CAPTURE-WESTERN	ACTIN GENERAL
BEM1	ACT1	AFFINITY PRECIPITATION	ACTIN GENERAL
BEM1	ACT1	PHYSICAL INTERACTION	ACTIN GENERAL
BEM1	ACT1	TWO HYBRID	ACTIN GENERAL
BEM1	LAS17	AFFINITY CAPTURE-WESTERN	ACTIN GENERAL
BEM1	LAS17	PHYSICAL INTERACTION	ACTIN GENERAL
BEM2	BUD14	AFFINITY CAPTURE-MS	ACTIN GENERAL
BEM2	BUD14	PHYSICAL INTERACTION	ACTIN GENERAL
BEM2	SPA2	AFFINITY CAPTURE-MS	ACTIN GENERAL
CDC42	BNI1	PHYSICAL INTERACTION	ACTIN GENERAL
CDC42	BNI1	TWO HYBRID	ACTIN GENERAL
CLA4	ABP1	PHYSICAL INTERACTION	ACTIN GENERAL
CLA4	ABP1	TWO HYBRID	ACTIN GENERAL
CLA4	SLA2	PHYSICAL INTERACTION	ACTIN GENERAL
CLA4	SLA2	TWO HYBRID	ACTIN GENERAL
RGA1	CMD1	AFFINITY CAPTURE-MS	ACTIN GENERAL
BEM1	BOI1	AFFINITY CAPTURE-MS	CDC42 SIGNALLING
BEM1	BOI1	AFFINITY PRECIPITATION	CDC42 SIGNALLING
BEM1	BOI1	PCA	CDC42 SIGNALLING
BEM1	BOI1	PHYSICAL INTERACTION	CDC42 SIGNALLING
BEM1	BOI1	TWO HYBRID	CDC42 SIGNALLING
BEM1	BOI2	AFFINITY CAPTURE-MS	CDC42 SIGNALLING
BEM1	BOI2	PHYSICAL INTERACTION	CDC42 SIGNALLING
BEM1	BOI2	RECONSTITUTED COMPLEX	CDC42 SIGNALLING
BEM1	BOI2	TWO HYBRID	CDC42 SIGNALLING
BEM1	FAR1	AFFINITY CAPTURE-WESTERN	CDC42 SIGNALLING
BEM1	FAR1	AFFINITY CHROMATOGRAPHY	CDC42 SIGNALLING
BEM1	FAR1	PHYSICAL INTERACTION	CDC42 SIGNALLING
BEM1	FAR1	RECONSTITUTED COMPLEX	CDC42 SIGNALLING
BEM1	FAR1	TWO HYBRID	CDC42 SIGNALLING
BEM1	RSR1	AFFINITY CHROMATOGRAPHY	CDC42 SIGNALLING

Table A.4: Physical interations (continued)

QUERY	INTERACTOR	EXPERIMENT	INTERACTOR CATEGORY
BEM1	RSR1	PHYSICAL INTERACTION	CDC42 SIGNALLING
BEM1	RSR1	RECONSTITUTED COMPLEX	CDC42 SIGNALLING
BEM3	BEM4	PHYSICAL INTERACTION	CDC42 SIGNALLING
BEM3	BEM4	TWO HYBRID	CDC42 SIGNALLING
CDC24	BEM4	PHYSICAL INTERACTION	CDC42 SIGNALLING
CDC24	BEM4	TWO HYBRID	CDC42 SIGNALLING
CDC24	BOI1	AFFINITY CAPTURE-MS	CDC42 SIGNALLING
CDC24	BOI1	AFFINITY CAPTURE-WESTERN	CDC42 SIGNALLING
CDC24	BOI2	AFFINITY CAPTURE-MS	CDC42 SIGNALLING
CDC24	BOI2	AFFINITY CAPTURE-WESTERN	CDC42 SIGNALLING
CDC24	BOI2	PHYSICAL INTERACTION	CDC42 SIGNALLING
CDC24	FAR1	AFFINITY CAPTURE-WESTERN	CDC42 SIGNALLING
CDC24	FAR1	AFFINITY PRECIPITATION	CDC42 SIGNALLING
CDC24	FAR1	PHYSICAL INTERACTION	CDC42 SIGNALLING
CDC24	FAR1	RECONSTITUTED COMPLEX	CDC42 SIGNALLING
CDC24	FAR1	TWO HYBRID	CDC42 SIGNALLING
CDC24	RSR1	AFFINITY CAPTURE-WESTERN	CDC42 SIGNALLING
CDC24	RSR1	AFFINITY PRECIPITATION	CDC42 SIGNALLING
CDC24	RSR1	PHYSICAL INTERACTION	CDC42 SIGNALLING
CDC24	RSR1	RECONSTITUTED COMPLEX	CDC42 SIGNALLING
CDC24	RSR1	TWO HYBRID	CDC42 SIGNALLING
CDC24	TOS2	PHYSICAL INTERACTION	CDC42 SIGNALLING
CDC24	TOS2	TWO HYBRID	CDC42 SIGNALLING
CDC42	BEM4	AFFINITY CAPTURE-MS	CDC42 SIGNALLING
CDC42	BEM4	PHYSICAL INTERACTION	CDC42 SIGNALLING
CDC42	BEM4	TWO HYBRID	CDC42 SIGNALLING
CDC42	BOI1	PHYSICAL INTERACTION	CDC42 SIGNALLING
CDC42	BOI1	TWO HYBRID	CDC42 SIGNALLING
CDC42	BOI2	PHYSICAL INTERACTION	CDC42 SIGNALLING
CDC42	BOI2	TWO HYBRID	CDC42 SIGNALLING
CDC42	FAR1	PHYSICAL INTERACTION	CDC42 SIGNALLING

Table A.4: Physical interations (continued)

QUERY	INTERACTOR	EXPERIMENT	INTERACTOR CATEGORY
CDC42	FAR1	TWO HYBRID	CDC42 SIGNALLING
CDC42	GIC1	AFFINITY CAPTURE-WESTERN	CDC42 SIGNALLING
CDC42	GIC1	PHYSICAL INTERACTION	CDC42 SIGNALLING
CDC42	GIC1	RECONSTITUTED COMPLEX	CDC42 SIGNALLING
CDC42	GIC1	TWO HYBRID	CDC42 SIGNALLING
CDC42	GIC2	AFFINITY CAPTURE-WESTERN	CDC42 SIGNALLING
CDC42	GIC2	PHYSICAL INTERACTION	CDC42 SIGNALLING
CDC42	GIC2	RECONSTITUTED COMPLEX	CDC42 SIGNALLING
CDC42	GIC2	TWO HYBRID	CDC42 SIGNALLING
CDC42	RSR1	AFFINITY CAPTURE-WESTERN	CDC42 SIGNALLING
CDC42	RSR1	RECONSTITUTED COMPLEX	CDC42 SIGNALLING
CDC42	SKM1	PHYSICAL INTERACTION	CDC42 SIGNALLING
CLA4	BOI2	PHYSICAL INTERACTION	CDC42 SIGNALLING
CLA4	BOI2	TWO HYBRID	CDC42 SIGNALLING
CLA4	GIC1	PHYSICAL INTERACTION	CDC42 SIGNALLING
CLA4	GIC1	TWO HYBRID	CDC42 SIGNALLING
CLA4	GIC2	PHYSICAL INTERACTION	CDC42 SIGNALLING
CLA4	GIC2	TWO HYBRID	CDC42 SIGNALLING
CLA4	SKM1	AFFINITY CAPTURE-MS	CDC42 SIGNALLING
RGA1	GIC2	PHYSICAL INTERACTION	CDC42 SIGNALLING
RGA1	GIC2	TWO HYBRID	CDC42 SIGNALLING
RGA2	RSR1	TWO HYBRID	CDC42 SIGNALLING
BEM3	APL6	PHYSICAL INTERACTION	EARLY SECRETION
CLA4	SEC23	AFFINITY CAPTURE-MS	EARLY SECRETION
CDC24	ENT2	PHYSICAL INTERACTION	ENDOCYTIC RECYCLING
CDC24	ENT2	TWO HYBRID	ENDOCYTIC RECYCLING
RGA1	ENT1	AFFINITY CAPTURE-WESTERN	ENDOCYTIC RECYCLING
RGA2	ENT1	AFFINITY CAPTURE-WESTERN	ENDOCYTIC RECYCLING
BEM1	SEC10	RECONSTITUTED COMPLEX	LATE SECRETION
BEM1	SEC15	AFFINITY CAPTURE-WESTERN	LATE SECRETION
BEM1	SEC15	PHYSICAL INTERACTION	LATE SECRETION

Table A.4: Physical interations (continued)

QUERY	INTERACTOR	EXPERIMENT	INTERACTOR CATEGORY
BEM1	SEC15	RECONSTITUTED COMPLEX	LATE SECRETION
BEM1	SEC15	TWO HYBRID	LATE SECRETION
BEM1	SEC5	PCA	LATE SECRETION
BEM1	SEC5	RECONSTITUTED COMPLEX	LATE SECRETION
BEM1	SEC8	AFFINITY CAPTURE-WESTERN	LATE SECRETION
CDC24	SEC15	PHYSICAL INTERACTION	LATE SECRETION
CDC24	SEC15	TWO HYBRID	LATE SECRETION
CDC42	MSB3	RECONSTITUTED COMPLEX	LATE SECRETION
CDC42	MSB4	RECONSTITUTED COMPLEX	LATE SECRETION
CDC42	SEC3	PHYSICAL INTERACTION	LATE SECRETION
CDC42	SEC3	RECONSTITUTED COMPLEX	LATE SECRETION
CLA4	SEC23	AFFINITY CAPTURE-MS	LATE SECRETION
RGA1	MLC1	AFFINITY CAPTURE-MS	LATE SECRETION
BEM1	CDC24	AFFINITY CAPTURE-MS	CDC42 MODULE
BEM1	CDC24	AFFINITY CAPTURE-WESTERN	CDC42 MODULE
BEM1	CDC24	AFFINITY PRECIPITATION	CDC42 MODULE
BEM1	CDC24	PCA	CDC42 MODULE
BEM1	CDC24	PHYSICAL INTERACTION	CDC42 MODULE
BEM1	CDC24	PROTEIN-PEPTIDE	CDC42 MODULE
BEM1	CDC24	RECONSTITUTED COMPLEX	CDC42 MODULE
BEM1	CDC24	TWO HYBRID	CDC42 MODULE
BEM1	CDC42	AFFINITY CAPTURE-WESTERN	CDC42 MODULE
BEM1	CDC42	PHYSICAL INTERACTION	CDC42 MODULE
BEM1	CDC42	RECONSTITUTED COMPLEX	CDC42 MODULE
BEM1	CDC42	TWO HYBRID	CDC42 MODULE
BEM1	CLA4	AFFINITY CAPTURE-WESTERN	CDC42 MODULE
BEM1	RGA2	AFFINITY CAPTURE-MS	CDC42 MODULE
BEM3	CDC42	TWO HYBRID	CDC42 MODULE
BEM3	CLA4	PHYSICAL INTERACTION	CDC42 MODULE
BEM3	CLA4	TWO HYBRID	CDC42 MODULE
CDC24	CDC42	AFFINITY CAPTURE-WESTERN	CDC42 MODULE

Table A.4: Physical interations (continued)

QUERY	INTERACTOR	EXPERIMENT	INTERACTOR CATEGORY
CDC24	CDC42	AFFINITY PRECIPITATION	CDC42 MODULE
CDC24	CDC42	PHYSICAL INTERACTION	CDC42 MODULE
CDC24	CDC42	RECONSTITUTED COMPLEX	CDC42 MODULE
CDC24	CDC42	TWO HYBRID	CDC42 MODULE
CDC24	CLA4	AFFINITY CAPTURE-WESTERN	CDC42 MODULE
CDC24	RGA2	AFFINITY CAPTURE-MS	CDC42 MODULE
CDC24	RGA2	AFFINITY CAPTURE-WESTERN	CDC42 MODULE
CDC42	CDC24	AFFINITY CAPTURE-WESTERN	CDC42 MODULE
CDC42	CDC24	AFFINITY PRECIPITATION	CDC42 MODULE
CDC42	CDC24	PHYSICAL INTERACTION	CDC42 MODULE
CDC42	CDC24	RECONSTITUTED COMPLEX	CDC42 MODULE
CDC42	CDC24	TWO HYBRID	CDC42 MODULE
CDC42	CLA4	AFFINITY CAPTURE-WESTERN	CDC42 MODULE
CDC42	CLA4	PHYSICAL INTERACTION	CDC42 MODULE
CDC42	CLA4	RECONSTITUTED COMPLEX	CDC42 MODULE
CDC42	CLA4	TWO HYBRID	CDC42 MODULE
CDC42	RDI1	AFFINITY CAPTURE-WESTERN	CDC42 MODULE
CDC42	RDI1	AFFINITY PRECIPITATION	CDC42 MODULE
CDC42	RDI1	FRET	CDC42 MODULE
CDC42	RDI1	PHYSICAL INTERACTION	CDC42 MODULE
CDC42	RDI1	TWO HYBRID	CDC42 MODULE
CDC42	RGA1	PHYSICAL INTERACTION	CDC42 MODULE
CDC42	RGA1	RECONSTITUTED COMPLEX	CDC42 MODULE
CDC42	RGA1	TWO HYBRID	CDC42 MODULE
CDC42	RGA2	TWO HYBRID	CDC42 MODULE
CLA4	RGA1	PHYSICAL INTERACTION	CDC42 MODULE
CLA4	RGA1	TWO HYBRID	CDC42 MODULE

A.2 Abbreviations

aa	Amino acid
ADP	Adenosine-5'-diphosphate
ATP	Adenosine-5'-triphosphate
ATPase	Adenoisine triphosphate hydrolase
bp	Base pair(s)
C-terminal	Carboxyl terminal
CCD	Charge-coupled device
Cdc	Cell division cycle
CDK	Cyclin-dependent kinase
CEN plasmid	Centromeric plasmid
ConA	Concanavalin A
CRIB domain	Cdc42/Rac-interactive binding domain
DAD domain	Diaphanous autoregulatory domain
ddH_2O	Double distilled water
DIC	Differential interference contrast microscopy
DID	diaphanous inhibitory domain
DMSO	Dimethylsulfoxide
DNA	Deoxyribonucleic acid
DRF	Diaphanous related formin
EDTA	Ethylenediaminetetraacetic acid
EGFP	Enhanced green fluorescent protein
EGTA	Ethylene glycol tetraacetic acid
EM	Electron microcopy
ER	Endoplasmic reticulum
F-actin	Filamentous actin
FCCS	Fluorescence correlation spectroscopy
FH	Formin homology
Fig.	Figure
FRAP	Fluorescence recovery after photobleaching

G-actin	Globular actin
G1	GAP phase 1
G2	GAP phase 2
GAP	GTPase-activating protein
GDF	GDP dissociation factor
GDI	GDP dissociation inhibitors
GDP	Guanosine-5'-biphosphate
GEF	Guanine-nucleotide-exchange factor
GEN	Geneticin
GFP	Green fluorescent protein
GTP	Guanosine-5'-triphosphate
GTPase	Guanosine triphosphate hydrolase
HAF	Hexdecanoylaminofluorescei
HYG	Hygromycin B
KAN	Kanamycin
LatB	Latrunculin B
LB	Luri-Bertani medium
M	Mitosis
Mant	Methylanthaniloyl-modified
MAPK	Mitogen-activated protein kinase
MOPS	3-(N-morpholino) propanesulfonic acid
N	Sample size
N-terminal	Amino terminal
Nat	Nourseothricin
ORF	Open-reading frame
PAK	p21-activated kinase
PBS	Phosphate-buffered saline
PCR	Polymerase chain reaction
PE	Phosphatidylethanolamine
PEG	Polyethylenglycol

PH domain	Pleckstrin homology domain
PI3 Kinase	Phosphatidyl-3-Kinase
Pi	Phosphate
PIP2	Phosphatidylinositol 4,5-bisphosphate
PIP3	Phosphatidylinositol(3,4,5)-triphosphate
PM	Plasma membrane
PS	Phosphatidylserine
PTEN	Phosphatase and tensin homolog
RFP	Red fluorescent protein
RNA	Ribonucleic acid
rpm	Rounds per minute (centrifugation)
RT	Room temperature
S phase	Synthesis phase
SC	Synthetic complete
SD	Standard deviation
SD	Synthetic drop-out
SDS	Sodium dodecyl sulfate
SEM	Standard error of mean
TAE	Tris-acetate-EDTA
TBE	Tris-Borate-EDTA
TE	Tris-EDTA
TIRFM	Total internal reflection microscopy
Tris	Tris(hydroxymethyl)aminomethane
ts	Temperature sensitive
U	Unit (enzyme activity unit)
v/v	Volume over volume
w/v	Weight over volume
WASp	Wiscott-Aldrich Syndrome
YPD	Yeast extract (Y)-peptone (P)- Glucose (D)
YT	Yeast extract (Y)-tryptone (T)

A.3 Declaration

Declaration according to the "Promotionsordnung der LMU München für die Fakultät Biologie"

Hiermit erkläre ich, dass die vorgelegte Arbeit in der Zeit vom 8.10.2007 bis März 2012 in der Arbeitsgruppe zelluläre Dynamik und Musterbildung von Dr. Roland Wedlich-Söldner am Max-Planck-Institut für Biochemie in Martinsried entstanden ist. Die Arbeit wird erstmalig einer Prüfungskommission vorgelegt und weiterhin habe ich weder an einem anderen Ort eine Promotion angestrebt noch angemeldet noch versucht eine Doktorprüfung abzulegen.

Ich versichere hiermit an Eides statt, dass die vorgelegte Dissertation von mir selbständig und ohne unerlaubte Hilfe angefertigt wurde.

München, den 12. März 2012

Tina Freisinger

A.4 Contributions

All FRAP analyses were conducted with a Matlab GUI developed by Nikola Müller.

Results 3.2.1: The synthetic lethal screen was performed in collaboration with Prof. Dr. Charles Boone's lab at the University of Toronto. While members of the Boone lab conducted the screening and computational analysis, I performed random spore analysis and tetrad dissection to verify genetic interactions of interest. Nikola Müller collected genetic and physical interactions from our own experiments, literature and databases to compare genetic and physical interactions in the heat map and interaction map depicted in Figure 3.4 B.

Results 3.3: The biochemical *in vitro* experiments in Figure 3.9, 3.11 and 3.12 were contributed by Jared Johnson from Prof. Dr. Eric Cerione's lab at Cornell University.

Results 3.6: The stochastic model was developed and contributed by Ben Klünder from Prof. Dr. Erwin Frey's group at the LMU.